Investigating aging hallmarks: From identifying accelerated senescence signature using machine learning, to discovering taurine's lifespan extension mechanisms

Dissertation

Zur Erlangung des Grades

Doktor der Naturwissenschaften

(Dr. rer. nat.)

Am Fachbereich Biologie

der Johannes Gutenberg-Universität Mainz

Iosif Rodolfos Danalatos

Geboren am 9 Januar 1995 in Athens, Griechenland

Mainz, April 2026

Dekan: Prof. Dr. Eckhard Thines

1. Berichterstatter:

2. Berichterstatter:

Datum der mündlichen Prüfung: 07.04.2026

Acknowledgements

During the interviews for this position, I said that working on telomeres and ageing was a childhood dream of mine. I would like to thank my supervisor for catalyzing the materialization of this dream, his guidance and support throughout this PhD as well as for giving me a chance during the lockdown, while other labs were canceling their invitations. I would also like to thank my TAC committee for their critical view on my work and for taking the time to read and follow my progress. Of course I would like to thank all collaborators leading the bioinformatics part of this work, allowing me to focus on the biology, the IMB imaging core facility, flow cytometry core facility and the media lab for allowing me to use their equipment and help me focus on the science rather than the preparation of buffers. I also want to thank the people who read my thesis and advised me on changes, who took their own time to help me write, and in the absence of them this text would be much more difficult to follow.
I would also like to thank Fabio, not only for his expert opinion whenever I asked, but also for improving the lab atmosphere and making sure that I have a smoother start. Because it is always better to have people watching your back on a professional but also personal level, I want to thank the inner circle for helping me deal with various challenges, for stepping in and helping when needed and for not only being an example of professionalism but also of human values.

I thank my family, especially my mother and my father for all they unconditional love they offered but also for being excellent examples of persistence, my grandparents whom most of them I unfortunately cannot thank in person, for all the support and inspiration they provided throughout not only this step, but the whole journey before it. Nothing would have been possible if they have not raised me to be the man I am, so I cannot thank you enough.

I also want to thank the people that although we are not blood related I consider them family (they know who they are), who stayed by me through the good times, while making the hard ones easier. They have acted as a harbor for me to weather the rough seas of the PhD, and were crucial from the beginning of this journey all the way to the very end. Without them this would not have been the same or as memorable. To all those I will be forever grateful.

To lighten up, I also thank all of my friends, the ones here but also the ones in the motherland, who with their mere presence lightened the load of the thesis. A special thanks however goes to Konstantinos, who always offered his critical views on both professional and personal matters, and for whenever I was wondering through dark paths, he was there to show me the light.

“Ain't nothin' but a peanut”

-Ronnie Coleman

Contents

Zusammenfassung

Das Altern ist ein komplexer und facettenreicher Prozess, der Wissenschaftler seit Jahrzehnten und die Menschheit seit Jahrhunderten beschäftigt. Trotz Fortschritten im Verständnis des Alterns und der zellulären Seneszenz fehlen noch zentrale Puzzleteile. In dieser Arbeit verfolge ich zwei Ansätze. Erstens konzentriere ich mich auf die Identifikation der Schlüsselakteure des beschleunigten Seneszenz-Phänotyps (AS). Anschließend enthülle ich die Mechanismen, die eine Lebensdauerverlängerung bei Taurin-Supplementierung auslösen.

Meine Arbeit basiert auf einer bereits veröffentlichten Studie, die die Existenz von 200 Gen-Deletion-Mutanten beschreibt, die nach Entfernung der Telomerase rasch in Seneszenz verfallen. Um zu klären, ob es gemeinsame Merkmale unter diesen Mutanten gibt, die das Auftreten von replizierender Seneszenz begünstigen, nutzte mein Kollaborator öffentlich zugängliche mRNA-Datensätze einzelner KO-Mutanten mit Telomerase-positivem Genotypen und trainierte ein maschinelles Lernmodell. Dieses Modell identifizierte gemeinsame Expressionsmuster, die die Zellen für eine schnelle Seneszenz nach Telomerase-Deletion prädisponieren könnten. Nach Feststellung einer potenziellen mRNA-Expressionssignatur wurde diese zur Vorhersage und Identifikation neuer, schnell seneszierender Mutanten verwendet, basierend auf dem Expressionsprofil ihrer nicht seneszierenden (Telomerase-positiven) Gegenstücke.

Neben der Identifikation neuer AS-Mutanten wurde kürzlich publiziert, dass bei mehreren Organismen die Supplementierung von Taurin die Lebensdauer signifikant erhöht. Die zugrundeliegenden Mechanismen bleiben weitgehend unbekannt; daher haben wir die primären Alterungsmarker unter Verwendung des leistungsstarken genetischen Modellorganismus *Saccharomyces cerevisiae* untersucht, um festzustellen, welche davon durch Taurin beeinflusst werden. Meine Arbeit konzentriert sich vorwiegend auf die Proteostase. Die Verlängerung der Lebensdauer durch Taurin wurde bei Telomerase-positiven Hefezellen nicht beobachtet, daher untersuchten wir die Wirkung in Telomerase-negativen Hintergrund. Obwohl es keine Unterschiede im replizierenden Lebenszyklus gab, stellte ich fest, dass Taurin-Supplementierung die In-Vivo-Stabilisierung verschiedener Temperatur-sensitiver (TS) Proteine bewirkt. Ähnliche stabilisierende Effekte lassen sich mit anderen Osmolyten replizieren, jedoch variiert die Stabilisierung je nach Protein-Osmolyt-Paar. Zusammengefasst ist es wahrscheinlich, dass der Grund, warum Taurin in einigen Modellorganismen so stark die Lebensdauer beeinflusst, die Proteinstabilisierung ist. Dies stimmt mit dem Befund übereinstimmt, dass seneszente oder ältere Zellen häufig durch Ansammlungen falsch gefalteter Proteine und den daraus entstehenden Stress charakterisiert sind. Die Entdeckung der Rolle von Taurin bei der Lebensdauerverlängerung eröffnet einen potenziellen therapeutischen Ansatz zur Verbesserung der menschlichen Leben-/Gesundheitsdauer und ebnet den Weg für die Entwicklung von Therapien gegen das Altern.

therapeutischen Ansatz zur Verbesserung der menschlichen Leben-/Gesundheitsdauer und ebnet den Weg für die Entwicklung anti-alterungs-Therapien.

Abstract

Ageing is a complex and multifaceted process that has puzzled scientists for decades and humanity for ages. Although progress has been made to better understand ageing and cellular senescence, pieces of this puzzle are still missing. In this study, I advance in two routes. First, I focus on the identification of key players in the accelerated senescence (AS) phenotype. Subsequently I unveil the mechanisms underlying lifespan extension upon taurine supplementation.

I based my work on a previously published study reporting the existence of 200 gene deletion mutants that senesce rapidly upon telomerase deletion. In order to understand if there are any commonalities among these mutants that may drive the onset of replicative senescence, we utilized publicly available mRNA datasets of single KO mutants in telomerase positive conditions and trained a machine-learning model to identify common expression patterns that might predispose these cells to senesce rapidly upon telomerase deletion. Following the identification of a putative mRNA expression signature, said signature was used in order to predict and identify novel fast senescing mutants, based on the mRNA expression profile of their non-senescing (telomerase proficient) counterparts.

In addition to the aforementioned identification of novel accelerated senescence mutants, it was recently published that in several organisms that taurine supplementation significantly increases their lifespan. The mechanisms underlying this phenomenon remain largely unknown, so we decided to dissect the primary hallmarks of ageing using the powerful genetic model organism, *S. cerevisiae*, to see which one is affected by taurine. My work is predominantly focused on the proteostasis hallmark, whereas members of the team are investigating the rest. Taurine's lifespan extension results were not present in the telomere positive budding yeast; hence, we decided to investigate that in telomerase negative conditions, to better mimic the rest of the organisms in the original publication. Although there was no difference in the replicative lifespan, I found out that taurine supplementation leads to in vivo stabilization of various TS (temperature sensitive) proteins. Similar stabilizing effects can be replicated with other osmolytes, however the degree of stabilization depends on the protein-osmolyte pair. In short, I suggest that the

reason taurine has such an impact on the lifespan of the models used in the original publication, is protein stabilization, which is in line with the fact that senescent or older cells are often characterized by accumulation of missfolding proteins and UPR stress. The discovery of taurine's role in lifespan extension provides a potential therapeutic target for improving human life-health span and paves the way to developing anti-ageing therapies.

Introduction

1.1 Replicative Senescence

Replicative senescence is a stable proliferative arrest that occurs after a finite number of cell divisions, as first reported by L. Hayflick in 1961. He discovered that serial cultivation of mammalian cells leads to them entering a state in which they stop dividing[1]. Senescence is semi-permanent, and can be triggered upon exposure of the cells to several stimuli such as excessive DNA damage, mitochondrial malfunction, activation of oncogenes in mammalian cells and telomeric attrition, to name a few[2,3]. The accumulation of senescent cells, is the cause for a plethora of deleterious phenotypes associated with aged organisms and is one of the hallmarks of ageing[4]. Recent medical advancements have led to a significant increase in the elderly population, posing challenges to healthcare systems in Western societies. This highlights the significance of understanding the mechanisms responsible for the onset, and progression of cellular senescence. Targeted elimination of senescent cells in mice, can lead to noticeable improvements in the life of these animals, as well as an increase in overall lifespan[5]. Paradoxically, senescence also serves beneficial, context-dependent functions: it acts as a potent tumor-suppressive mechanism[6] by halting the proliferation of damaged or pre-malignant cells[7], while transient senescent states can facilitate wound healing, embryonic development, and tissue remodeling[8]. It is now evident, that cellular senescence is a double-edged sword, and its balance is key to normal cell function. While our understanding of senescence has improved considerably, it remains incomplete as many mechanisms underlying it are still not understood.

S. cerevisiae is an ideal and broadly used model to study replicative senescence due to its ease of manipulation, upscaling potential and similarities of core mechanisms with mammalian cells, while maintaining a shorter lifespan. It is a very well characterized model, offering a variety of tools including but not limited to genome-wide libraries, allowing for high-throughput assays and screenings. Telomerase inactivation allows controlled induction of telomere attrition, mimicking replicative exhaustion and senescence in mammalian systems[9]. Overall, *S. cerevisiae's* mechanism conservation,

experimental tractability and available resources make it an excellent choice for dissecting genetic and molecular determinants of senescence[10].

1.2 Senescence and Ageing

Cellular senescence is a stable proliferative arrest that links molecular damage to organismal ageing. Senescent cells accumulate in tissues over time and contribute to functional decline. The cells remain metabolically active and secrete pro-inflammatory cytokines, growth factors, and proteases, a phenomenon known as the senescence-associated secretory phenotype (SASP). The SASP not only reinforces chronic inflammation, but also promotes secondary senescence in neighboring cells and disrupts tissue architecture and extracellular matrix[11], leading to impaired regeneration and tumor-permissive environments. Senescence therefore acts as both a protective mechanism and a source of age-related pathology: its beneficial and detrimental effects depend on timing and persistence, underscoring its significance in aging research and its potential as a therapeutic target to ameliorate age-related diseases[2,3,6].

In multicellular organisms, aged counterparts are characterized by the accumulation of senescent cells. Ageing itself is a multifactorial process driven by the progressive accumulation of cellular damage. In order for a process to be classified as a hallmark of ageing, three criteria must be met: (1) the time dependent manifestation of alterations accompanying the aging process, (2) the possibility to accelerate aging by experimentally triggering the hallmark, and—most decisively—(3) the opportunity to decelerate, halt, or reverse aging by therapeutic interventions on the hallmark[4]. Beyond telomere attrition and replicative exhaustion, mechanisms such as genomic instability, epigenetic drift, loss of proteostasis, and defective autophagy contribute to the systemic deterioration of function. These pathways are interconnected, amplify one another’s effects, and together form a complex biological network that drives the progressive decline in tissue and organ function.

In the updated conceptual framework proposed by López-Otín and colleagues (2022), the hallmarks are organized into three functional tiers: primary, antagonistic, and integrative. The primary hallmarks (genomic instability, telomere attrition, epigenetic alterations, loss

of proteostasis, and disabled macroautophagy) are designated “primary” because they represent the initial, causative sources of molecular damage that arise in virtually all cells, tissues, and organs as they age. These damage-initiating events are universal across species and organ systems, and outline the foundational mechanisms driving the ageing process on a cellular level (figure 3), providing a common mechanistic foundation for the biology of ageing. In contrast, the antagonistic hallmarks (e.g., deregulated nutrient sensing, mitochondrial dysfunction, cellular senescence) are primarily responses to this initial damage; they can be protective in the short term but become deleterious when chronically activated. Finally, the integrative hallmarks (e.g., stem cell exhaustion, altered intercellular communication, chronic inflammation, dysbiosis) reflect the cumulative impact of both primary and antagonistic processes, ultimately determining the functional decline and vulnerability to disease that characterize late-life physiology. Thus, while ageing manifests with organ- and tissue-specific features, the primary hallmarks are shared initiating mechanisms present in all aged systems. Recognizing this hierarchy is crucial, as it not only clarifies the causal relationships between different ageing processes but also highlights the most upstream targets for interventions aimed at extending health span.

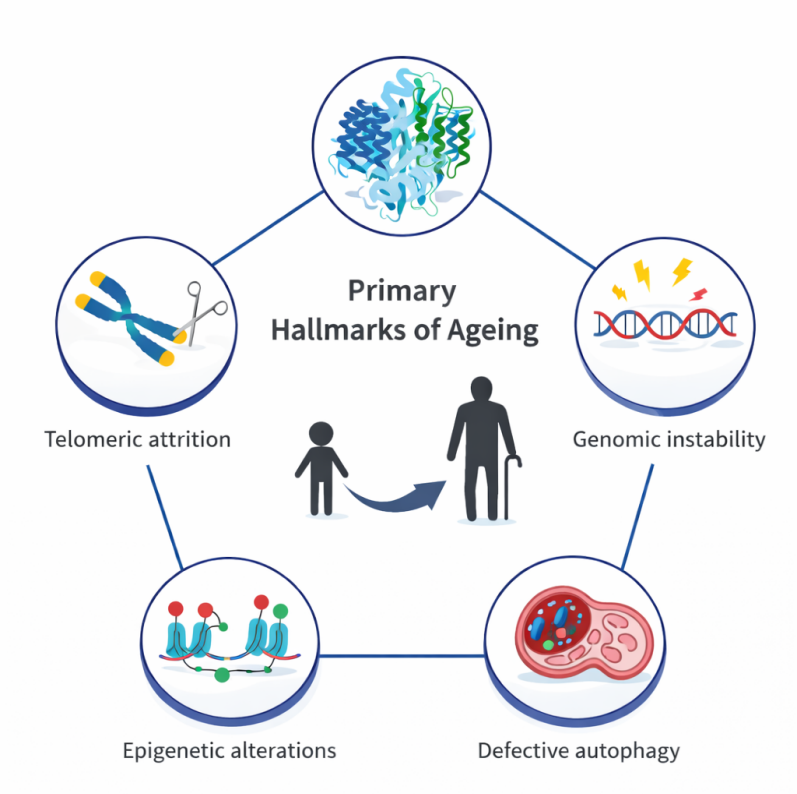

Figure 1: The five primary Hallmarks of ageing. Loss of proteostasis and accumulation of misfolded proteins, genomic instability, critically short telomeres leading to their recognition as sites of DNA damage, epigenetic alterations and malfunctioning autophagy machinery are the five primary Hallmarks of Ageing. Adapted from López-Otín et al. 2022[4].

1.3 Telomeres

1.3.1 Telomeres safeguard genomic integrity

Telomeres are specialized nucleoprotein structures located at the ends of eukaryotic chromosomes, playing a critical role in maintaining genome stability. Beyond simply concealing ends, telomeres serve three core protective roles. First, they buffer against the end-replication problem as they get shorter, protecting the protein coding regions of the genome. Second, they prevent illegitimate end-to-end chromosome fusions that would otherwise trigger breakage–fusion–bridge cycles and gross genomic rearrangements. Third, they restrict inappropriate homologous recombination at non-telomeric loci, preserving sequence integrity throughout the genome[12].

1.3.2 Telomeric structure

Telomeric regions consist of repetitive DNA sequences along with associated proteins that protect chromosome ends from degradation, end-to-end fusions, and erroneous repair mechanisms. In *S. cerevisiae*, telomeric repeats are primarily (TG_{1-3}) n at an approximate length of 30-350bp and end with a G-rich 3' overhang of 10-14 nucleotides. A key telomeric protein associated with yeast telomeres is Rap1, which binds directly to the double stranded telomeric DNA and plays a central role in capping and transcriptional regulation. Furthermore, Rif1 and Rif2 interact with Rap1 to regulate telomere length and prevent excessive elongation[13]. The 3' overhang is recognized and bound by the CST complex, which is essential for telomere replication and stability. The CST complex comprises of three proteins: Cdc13, Stn1 and Ten1, which is responsible for binding single-stranded telomeric DNA, as shown on Figure 2, protecting it from degradation and facilitating the recruitment of telomerase. Disruption of any component exposes single-stranded DNA, triggers checkpoint activation, and precipitates accelerated shortening or uncapping phenotypes.

Telomeres are also transcribed into the long noncoding RNA named TERRA (telomeric repeat–containing RNA), which hybridizes with telomeric DNA to form RNA–DNA hybrids, or R-loops. TERRA accumulates at shortened telomeres and regulate telomerase, linking elevated TERRA levels to telomere dysfunction and senescence. Additionally, TERRA-derived R-loops can promote recombination-based telomere elongation in the absence

of telomerase, integrating RNA-mediated processes into telomere maintenance[14,15]. The CST complex, Rap1, Rif1, Rap2, work in coordination along with TERRA, to maintain the integrity and functionality of yeast telomeres[16,17].

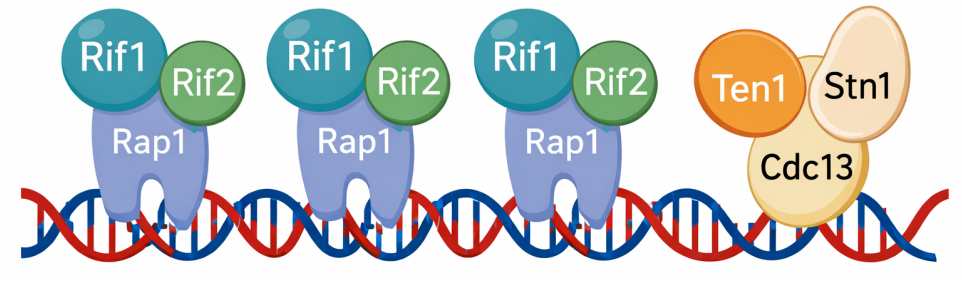

Figure 2: Visual representation of S. Cerevisiae telomeres adapted from Wellinger et al.[16]. Schematic showing the CST complex associating with the 3' telomeric overhang along with Rap1, Rif1 and Rif2 on telomeres in *S. cerevisiae*.

1.3.3 Telomere shortening

Telomeres get progressively shorter with every cell cycle. Their replication is more challenging for the cell due to the guanine-rich telomeric repeats, which result in higher thermodynamic stability. Telomeres are also susceptible to oxidative lesions or formation of secondary structures which slow down or even stall forks eventually leading to reducing the repeats of the telomere[16]. In addition, cells are unable to fully replicate the extreme ends of linear DNA molecules, termed the "end-replication problem". Polymerases are unable to replicate the ends of chromosomes due to their inherent biochemical limitations. DNA polymerases can only synthesize DNA in the 5' to 3' direction and require a primer to initiate replication. While the leading strand can be continuously synthesized, the lagging strand is replicated in short fragments, called Okazaki fragments, which are initiated by RNA primers. When the replication machinery reaches the very end of the lagging strand, there is no upstream DNA template available to provide a starting point for the final primer. As a result, the terminal portion of the chromosome cannot be replicated, leaving a gap at the end. On the leading strand, the replication naturally leads to a blunt end, which is transformed to the telomeric 3' overhang by 5' resection, significantly contributing to shortening. DNA end resection is a 5′→3′ exonucleolytic process that generates single-stranded G-rich overhangs at double-strand breaks (DSBs)

and telomeres. In S. cerevisiae, resection is initiated by the MRX complex (Mre11–Rad50–Xrs2) in conjunction with Sae2, followed by extensive degradation by Exo1 and/or the Sgs1. At telomeres, controlled resection is essential for generating the 3′ overhang required for telomerase action and t-loop formation. However, excessive or unregulated resection can accelerate telomere shortening by removing terminal repeats beyond the minimal processing requirement.

Nucleases involved in DNA end resection significantly influence telomere shortening rates. In telomerase-deficient cells, deletion of EXO1 slows telomere erosion, indicating that Exo1-mediated long-range resection contributes to the loss of telomeric DNA. Telomere-binding proteins modulate this process to balance the generation of the 3′ overhang with the risk of excessive degradation. The CST complex, particularly Cdc13, binds the G-rich overhang to shield it from nucleolytic attack, and loss of Cdc13 function results in extensive Exo1-dependent resection and rapid telomere loss, which can lead to checkpoint activation.

Defects in telomere capping or replication factors can similarly expose chromosome ends to resection, demonstrating that controlled processing is essential for stability, whereas unregulated activity accelerates attrition.

1.3.4 Telomere length maintenance

To overcome this consecutive shortening of the telomeres with each cell cycle, cells use telomerase. Telomerase, a ribonucleoprotein complex, is an enzyme with reverse transcriptase capabilities mediated by its integrated RNA motif. Telomerase is expressed and active during development and silenced/non-expressed in post-mitotic cells. Human stem cells maintain telomerase activity and tumor cells can regain telomerase activity to overcome the Hayflick limit; however, in yeast it is constitutively expressed. Therefore, in order to make yeast into a suitable model to study replicative senescence, telomerase needs to be inactivated. This inactivation is commonly facilitated by the deletion of one of its components, leading to telomere attrition. In yeast, telomerase is comprised of four components. It features the template RNA motif, *TLC1*, the catalytic subunit Est2p and two accessory subunits, Est1p and Est3p. As mentioned above, telomerase is active in *S. cerevisiae* therefore telomeres are being maintained. In normal conditions, telomeres

get progressively shorter but telomerase restores them to their normal length. In the absence of telomerase however, telomeres are not repaired and become critically short, as shown on Figure 3.

A very small subset of cells however, manages to re-elongate their telomeres by activating recombination-based pathways to re-elongate their telomeres independently of telomerase. These cells are called survivors or ALT mutants, and were initially divided into mainly two categories, based on the telomere maintenance mechanisms they employ. Type I Survivors rely on Rad51-dependent homologous recombination, leading to the amplification of subtelomeric Y' elements. Type II Survivors utilize Rad50-dependent recombination, resulting in heterogeneous telomeric repeats. However, more recent evidence indicates that these categories are not strictly separable, as both survivor types share extensive mechanistic overlap in homologous recombination–based telomere maintenance, and can utilize multiple recombination pathways in parallel. Despite this controversy, survivors have become a valuable tool to gain insights into ALT cancer biology.

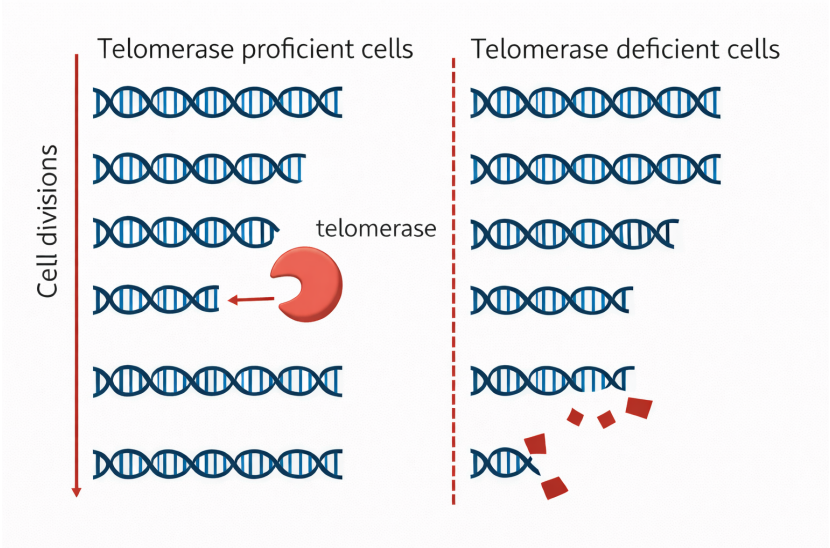

Figure 3: Schematic representation of how telomerase prevents telomeres from getting critically short. In the presence of telomerase, shortening telomeres will be elongated back to normal lengths to avoid telomeric attrition. In the absence of telomerase, telomeres get progressively shorter with each cell cycle until becoming critically short, triggering replicative senescence.

1.3.5 Checkpoint activation and senescence

Telomeres will progressively shorten with each S-phase until a critical length is reached, typically less than 100 bp in yeast. Once repeats fall below this threshold, the protective T-loop cannot form efficiently and key binding factor Cdc13 dissociate, uncovering single-stranded DNA overhangs and triggering a DNA damage checkpoint response (DDR). Upon sensing the ssDNA that resulted from the telomere uncapping, Mec1 is activated, which phosphorylates adaptor proteins such as Rad9 and Mrc1. These adaptors in turn activate downstream effector kinases Chk1 and Rad53 enforcing a durable G2/M arrest. In S. cerevisiae, even one critically short telomere is sufficient to lead to a G2 arrest. This cascade ensures the translation of a short telomere into DNA damage signal, halting cell-cycle progression and ultimately leading to replicative senescence if repair or elongation cannot occur. In mammalian cells, critically short telomeres also engage ATM and p53 pathways, leading to senescence or apoptosis depending on cellular context. In both yeast and higher eukaryotes, this checkpoint-mediated arrest prevents propagation of unstable genomes, but chronic activation contributes to tissue aging and compromises regenerative potential. In budding yeast, although all telomeres get progressively shorter in the absence of telomerase, only one critically short telomere is sufficient to trigger the cell's arrest.

1.4 Accelerated Senescence phenotype

A tool to prevent malignant transformation in cells, is senescence. As already mentioned, senescence is a semi-permanent cell cycle arrest that cells enter when they have accumulated damage beyond repair. In the case of replicative senescence, this is in form of critically short telomeres. In spite of the extensive research that has been done towards understanding senescence and the mechanisms underlying it, there are still core aspects of its onset that remain elusive. To better understand what additionally pathways are involved in the onset of replicative senescence, Chang et al. 2011, conducted a genome wide screening in budding yeast, to identify KO mutants exhibiting an accelerated entry into replicative senescence. Yeast however, expresses telomerase to maintain healthy lengths among its telomeres. In order to allow the yeast cells to senesce, they deactivated telomerase by deleting *est1*. All of the mutants proceeded to senescence at different rates, and based on the individual rate they categorized the mutants into three

archetypes. The vast majority of the mutants had a normal senescence rate hence were assigned to the *his3 est1* archetype (*his3* leads to a “normal” senescence rate, and serves as a control). Three mutants exhibited a fast entry and exit from senescence (via survivor formation) and were assigned to the *rif1 est1* archetype (the archetype was named after *rif1* because its members senesce in a manner similar to *rif1*). Finally, around 200 mutants exhibited a rapid entry into senescence without survivor formation, and were assigned to the *rad52 est1* archetype (as members of this archetype senesced rapidly like *rad52* mutants).

There are several studies tying accelerated ageing in telomerase proficient yeast mother cells. Recombination at the rDNA locus produces extrachromosomal rDNA circles (ERCs) whose mother-cell accumulation shortens replicative lifespan and produces nucleolar enlargement; genetic manipulations that increase ERC formation accelerate aging while ERC suppression can extend lifespan. Loss of proteostasis and increased protein aggregation also drive premature mother-cell aging. Mutants that fail to segregate damaged or aggregated proteins (for example sir2 mutants) show accelerated senescence that can be suppressed by reducing protein aggregates. Mitochondrial dysfunction shortens replicative lifespan through disturbed respiration and elevated ROS and RAS-dependent signaling, linking organelle failure to accelerated senescence. Impaired DDR pathways can also provoke an early onset of senescence, which is further exacerbated in the absence of telomerase, confirming the impact of DDR malfunction in replicative senescence. Another important factor determining the rate of senescence is RNA-DNA hybrid formation at the telomeres. More specifically, short telomeres have elevated levels of RNA-DNA hybrids, which triggers HDR. This increase of HDR results in a delay of replicative senescence[14], whereas decreasing R-loops at the telomeres leads to an increase senescence rate.

In spite of several reports on genes and pathways accelerating senescence, Chang et al. 2011 reported multiple genes that had not yet been implicated or studied in this context, highlighting our lack of knowledge when it comes to this field. Aiming to identify commonalities among these mutants, the authors checked whether these mutants have been reported in the literature to have shorter than normal telomeres; however, there was

no particular enrichment in short telomere mutants. Additionally, GO term analysis did not yield any results either, so the mechanisms underlying this rapid entry into replicative senescence are still under investigation. The present study is based on this high throughput screening and takes it one step further by questioning the undiscovered commonalities between these fast senescing mutants, characterizing an mRNA expression signature of the AS phenotype and using it to discover even more AS mutants in an attempt to better understand the underlying mechanisms that drive this early onset of replicative senescence. Some of the AS mutants reported by Chang et al. 2011, have severe growth defects even in the presence of telomerase.

Although budding yeast might have certain differences with human cells regarding telomere biology; many mechanisms are highly conserved and it is one of the most characterized models to study senescence. By identifying novel mutants, we improve our understanding of not only how accelerated senescence is triggered, but also potentially uncover mechanisms underlying normal senescence. Therefore this research has the potential to benefit other areas such as longevity, or human diseases where cellular senescence is implicated, such as age-related diseases, neurodegeneration or even cancer.

1.5 Taurine in lifespan extension

The first part of this thesis focused on the genetic determinants that predispose cells to accelerated entry into replicative senescence, focusing on how specific transcriptional signatures and loss-of-function mutations lead to AS. While replicative senescence reflects the finite proliferative capacity of cells, recent studies suggest that environmental factors such as nutrient availability, metabolic state, osmotic conditions, or exposure to small molecules profoundly influence the rate at which cells lose proteostasis, accumulate damage, and ultimately progress toward senescence. Indeed, environmental modulation of ageing trajectories is well documented in diverse model organisms, where factors such as caloric restriction, osmotic stress, or metabolite supplementation can markedly extend or shorten lifespan.

Building on this perspective, the second part of this thesis shifts from intrinsic genetic determinants to extrinsic chemical modulators of ageing, with a particular focus on taurine. Taurine has gained attention following the report by Singh et al. who demonstrated that taurine supplementation markedly extended lifespan in multiple model organisms but not in Saccharomyces cerevisiae. This observation raises critical questions about the conserved and species-specific mechanisms through which taurine influences aging.

Singh et al. Identified taurine as a potential longevity factor through multi-species analyses. The authors first observed that circulating taurine concentrations decline markedly with age in humans and other animals, claim that however was later challenged, as taurine levels show high deviation among individuals, and even an increase in taurine levels as the organisms grow older. Finally, there was no clear association found between taurine levels and general health status, which underlines a more complicated relationship of taurine and ageing.

Despite the controversy, taurine supplementation significantly extended median lifespan in mice and improved health span indicators including bone density, glucose tolerance and most importantly muscle strength. Similar lifespan extension occurred in C. elegans and zebrafish, indicating a conserved effect across metazoans. Mechanistically, taurine treatment reduced markers of cellular senescence and inflammation, improved

mitochondrial respiration, and modulated nutrient-sensing pathways including insulin signaling. Transcriptomic data suggested enhanced proteostasis and suppression of pro-inflammatory gene expression. However, taurine supplementation did not prolong lifespan in yeast, implying that its longevity-promoting action requires pathways absent in unicellular eukaryotes. Collectively, these findings positioned taurine as a conserved modulator of aging with potential therapeutic relevance.

Taurine, or 2-aminoethanesulfonic acid, is a sulfur-containing-amino acid that plays a crucial role in various physiological processes. Unlike most amino acids, taurine is not incorporated into proteins but exists freely in tissues, particularly in the brain, heart, retina, and skeletal muscles. It is synthesized in the body from cysteine and methionine, primarily in the liver, but is preferentially obtained through dietary sources such as meat, fish, and dairy products, mediated by transporters. Taurine has been reported to have several functions in cells, ranging from osmoregulation and calcium signaling to protection against DNA damage, neuroprotection and regulation of the metabolism. Taurine might not be a proteinogenic amino acid, however it is deemed semi-essential due to its various other crucial roles. In contrast, *S. cerevisiae* lacks a known taurine biosynthesis pathway; nor are there any reported specific taurine transporters, although it is possible that transporters that act on similar amino acids such as Alanine, Glycin, GABA and so forth import it.

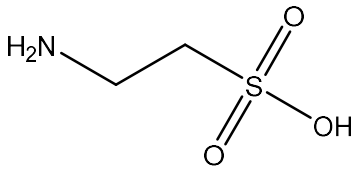

Figure 4 Structure of taurine: Taurine belongs in the aminoacid family as it contains an amino moiety, however instead of the common carboxyl group, it is a sulfonic acid.

The nutritional importance of taurine is exemplified in domestic cats, which cannot synthesize sufficient taurine endogenously and develop retinal degeneration and other pathologies without dietary taurine supplementation. The introduction of taurine supplementation in commercial pet foods effectively mitigated these health issues, thereby affirming taurine's essential role in feline nutrition and systemic function. In addition to felines, a lot of research has shown that taurine is also very important for other mammal neonates, with human babies not being an exception. In babies, taurine deficiency can lead to development issues such as retinal degeneration, delayed auditory maturation, and impaired fat absorption.

Although often associated with ergogenic use in sports, taurine's biological significance extends far beyond energy metabolism, as it is one of the most abundant amino acids in human tissues. In fact, taurine's concentration in human cells ranges from 0mM to 50mM, with example tissue concentrations being roughly 5mM for muscles, 1mM to 20mM for brain, 30 mM to 40mM for retina, 50 μM to 100uM for plasma and 4mM to 25mM for heart. Taurine supplementation ameliorates an increasing number of diverse pathologies, including hepatic, renal, and neurodegenerative disorders, though the underlying molecular mechanisms remain poorly defined.

There have been reports in a small number of studies that taurine might alter the expression of genes in some tissues such as in rat hippocampus, where it was shown to alter the expression and phosphorylation of ERK1/2, Akt, p53 and so forth. Another study analyzed hippocampal tissue from rats after four weeks of taurine supplementation. They observed altered expression and phosphorylation of proteins involved in neuronal signaling and stress regulation, including p53, Jun, PKC, and HDAC5. Although associative and limited to healthy tissue, the study showed that taurine broadly modulates intracellular signaling and gene expression, indicating functions extending beyond osmoregulation and redox balance. In pancreatic β-cells, taurine has been reported to suppress senescence and inflammation by modulating the p53 pathway. By binding CDKN2AIP, taurine disrupts its interaction with p53, inhibiting p53 expression and senescence induction. Despite numerous reports of taurine's beneficial effects, no comprehensive systems-level study has clarified how taurine modulates cellular

pathways. In particular, transcriptomic responses to taurine in mammalian cells—and in yeast, where lifespan extension is absent—remain unexplored. Addressing this gap may reveal conserved or divergent molecular mechanisms underlying taurine's effects on longevity.

Taurine has also been described to have some minor antioxidant capabilities *in vitro*, however it is unlikely that in physiological conditions taurine can scavenge free radicals. Taurine does not act as a classical free radical scavenger because its sulfur atom is already in a fully oxidized sulfonic acid form, making it incapable of behaving like an electron donor. This structural property limits taurine's direct radical-scavenging potential, which is likely relevant only in few tissues, such as the heart and eyes, where concentrations are very high. Nonetheless, taurine exhibits substantial indirect antioxidant activity. It can suppress oxidant production and enhance the activity of key endogenous defense enzymes, including glutathione-S-transferase (GST), glutathione peroxidase (GPx), superoxide dismutase (SOD), and catalase (CAT). A critical element of this protective role lies in its effects on mitochondria—the primary sites of reactive oxygen species (ROS) generation. Taurine deficiency impairs electron transport chain function and markedly elevates free radical production, whereas maintaining optimal mitochondrial taurine levels helps restrain excess ROS formation. This mitochondrial protection is especially important in mitochondria-rich tissues such as skeletal muscle and the heart, where taurine is present at very high concentrations and thus serves as the most abundant antioxidant. In fact, taurine has been reported to protect against cardiovascular diseases partially by limiting the oxidative stress, however this effect is again unlikely to be due to direct antioxidant capabilities as a weak ROS scavenger, and more likely indirectly by protecting antioxidant enzymes.

Evidence for covalent taurine incorporation into macromolecules remains limited, as there are only a few studies that report such findings. For instance, it has been experimentally shown that in avian erythrocytes, taurine is covalently incorporated into A-tubulin tails, as they exposed to the cytoplasm, and therefore site for many post translational modifications (PTM), such as the reversible de-tyrosination/re-tyrosination. It has been

reported that taurine is covalently bound on these tails as a PTM, requires the de-tyrosination and prevents the re-tyrosination.

Taurine has also been shown to be incorporated into some mitochondrial tRNAs in the form of two modified uridines. Interestingly, the authors discovered that these modifications were absent in two strains of pathogenic cells of mitochondrial encephalomyopathies, raising questions about the possible importance of taurine as a building block of biological macromolecules. Although evidence of taurine interacting with RNA or proteins is scare, taurine can form interactions through hydrogen bonds, electrostatic interactions and Van der Waals forces.

During normal ageing (in organisms like C. elegans, mice, and senescent cells), there is 1.3- to 2.5-fold increase in insoluble (misfolded/aggregated) proteins compared to young tissue. These accumulate in aggresomes, resist protease, and stain with amyloid dyes. Many of these aggregated proteins are normally soluble, essential in metabolism, synaptic function, or protein quality control. Their missfolding contributes to decline in tissue function.

Protein missfolding is a primary hallmark of ageing and underlies several late-onset degenerative diseases. Examples range from renal and liver disorders to neurodegenerative diseases such as Alzheimer's disease and Parkinson's disease, which are characterized by the accumulation of malfunctioning proteins which leads to cellular dysfunction and ultimately in neuronal death. In Alzheimer's disease, amyloid-β (Aβ) peptides aggregate into neuritic plaques, while hyper-phosphorylated tau forms neurofibrillary tangles, impairing synaptic transmission and inducing stress. α-Synuclein missfolding drives Parkinson's disease, where toxic oligomers form Lewy bodies that disrupt mitochondrial and proteasomal function. Polyglutamine expansion in huntingtin (mHtt) produces inclusion bodies characteristic of Huntington's disease (HD), overwhelming the cellular chaperone network and reducing proteasomal clearance leading to the proteostasis network failure.

Current therapeutic strategies include upregulation of heat-shock proteins (HSP70, HSP90), enhancement of autophagic and proteasomal degradation, inhibition of aggregation by small molecules or peptides, and stabilization of native protein

conformations through chemical chaperones or targeted immunotherapies. While several of these approaches show promise in preclinical models, clinical efficacy remains limited, underscoring the complexity of restoring proteostasis in ageing tissues. In recent years taurine has been getting a lot of interest from the scientific community, with the number of studies reporting taurine's benefits on various diseases is steadily increasing. Taurine has been reported to ameliorate the aggregation of amyloid-beta plaque buildup and an attenuation of Alzheimer's pathologies both in mice and in patient-derived cerebral organoids, however without suggesting any mechanisms of action. In HD, preliminary data shows taurine exhibiting neuroprotective effects in 3-nitropropionic acid-induced HD in rats, although the authors claim this is probably due to its indirect antioxidant effect and GABA agonistic action. In this study I demonstrate that, although taurine may confer benefits through antioxidant and osmoprotective mechanisms, the principal driver of its activity is its function as an osmolyte.

1.6 Osmolytes

1.6.1 Biological importance of osmolytes

Taurine belongs to a wide family of molecules called osmolytes. Osmolytes are small, highly soluble organic molecules that cells accumulate to maintain osmotic balance and protect cells from environmental stressors such as salinity, temperature, or pressure changes. In *S. cerevisiae*, osmolytes are central to the adaptive response to fluctuations in external osmolarity, particularly during hyperosmotic stress caused by elevated salt or sugar concentrations. Their accumulation counteracts water loss and restores turgor pressure. Osmolytes, also referred to as “compatible solutes” reach high intracellular concentrations without perturbing normal metabolism, or interfere with macromolecular function even at molar concentrations. Osmolytes are central to not only osmoadaptation strategies but also stabilize proteins, nucleic acid and cellular structures such as membranes. In membranes, osmolytes can influence lipid packing and phase behavior, thereby preserving membrane integrity during osmotic shrinkage or dehydration. For example, glycerol, due its small size and high polarity it can interact favorably with water molecules, contributing to the maintenance of intracellular hydration. Chemically, osmolytes encompass a diverse range of compounds, including methylamines (e.g., trimethylamine N-oxide), polyols, sugars (e.g., trehalose), amino acids (e.g., proline), and derivatives. Despite shared physicochemical roles, different organisms employ different osmolytes to counteract their most common stressors

This structural stabilization mechanism is evolutionarily conserved across bacteria, archaea, fungi, plants, and animals. In extremophiles, such as deep-sea organisms, common osmolytes include TMAO, polyols, and taurine derivatives among others, protecting proteins against pressure-induced unfolding and denaturation. Trehalose is also more prevalent in insects that have to endure sub-zero temperatures. In mammals, osmolytes such as taurine, betaine, and myo-inositol accumulate in cells to offset high osmolarity (e.g. in kidney) without disrupting cellular function, with taurine being the most dominant. In yeast, glycerol is the predominant osmolyte produced in response to hyperosmotic stress, while trehalose often functions as a secondary protectant, particularly under combined stress conditions such as heat shock and desiccation.. Glycerol is effective at balancing osmotic pressure because it is uncharged, highly

soluble, and does not perturb protein folding. Trehalose, although less directly involved in osmotic balance, contributes to stress tolerance by stabilizing proteins and membranes, reducing aggregation, and preserving enzyme activity during dehydration or thermal stress. Other osmolytes, such as taurine or betaine, are more prominent in other organisms but can still be relevant in budding yeast, employing the same protein stabilization mechanisms.

1.6.2 Biological mechanisms of osmolyte action

Naturally, osmolyte accumulation must be regulated by the cells, in order for them to survive different stressors. In *S. cerevisiae* this is tightly controlled by the High Osmolarity Glycerol (HOG) signaling pathway, a mitogen-activated protein kinase (MAPK) cascade that senses and responds to changes in external osmolarity. Two upstream branches, the Sln1 and Sho1 osmosensing systems, detect reductions in turgor pressure and activate a phosphorylation cascade culminating in the activation of the MAPK Hog1. Once activated, Hog1 translocates to the nucleus, where it modulates the transcription of numerous stress-responsive genes, including those encoding enzymes required for glycerol biosynthesis, such as GPD1 and GPP2. The coordinated induction of these genes increases the flux through the glycerol biosynthetic pathway, leading to rapid intracellular accumulation of glycerol. In parallel, the cell reduces glycerol efflux by regulating the activity of the Fps1 glycerol channel, which closes under hyperosmotic conditions to prevent loss of the newly synthesized osmolyte. Osmolytes often act synergistically or activate chaperones and heat-shock proteins, forming a multilayered defense system against proteotoxicity. Taurine additionally enables modulation of ion flux and membrane potential, protecting excitable tissues from osmotic and excitotoxic damage.

Osmolyte accumulation is integrated into a broader physiological program that includes metabolic reconfiguration and cell cycle regulation. Osmotic stress can transiently arrest the cell cycle, allowing time for osmolyte accumulation and restoration of homeostasis before growth resumes. The interplay between osmolyte metabolism and other stress responses is evident in the role of trehalose, which is induced not only by osmotic stress but also by heat shock, oxidative stress, and nutrient limitation. Additionally, trehalose

metabolism intersects with signaling pathways that regulate autophagy and longevity, suggesting broader roles in cellular physiology. This multifunctionality suggests that osmolytes serve as general stabilizing agents that protect cellular structures under a variety of adverse conditions. Beyond their regulation through cellular signaling pathways, osmolytes exert their protective roles at the molecular level, where their physicochemical interactions with proteins determine their stabilizing capacities. Reports of osmolytes forming covalent bonds with proteins are scarce; rather, their influence arises from two primary thermodynamic mechanisms: preferential exclusion and modulation of the hydration sphere.

1.6.3 Molecular mechanisms

Extensive in vitro and theoretical work has demonstrated that osmolytes can shift the equilibrium between folded and unfolded protein states, thereby influencing proteostasis beyond mere osmotic balance. Although the topic remains under investigation, they exert their effects *via* two main mechanisms:

Preferential exclusion

Predominantly small molecule osmolytes, such as taurine, are thermodynamically excluded from the immediate vicinity (hydration shell) of the protein surface. This exclusion of some osmolytes stabilizes the compact, folded conformation of the protein, as the unfolded state exposes a greater surface area that incurs more unfavorable interactions with the osmolyte, rendering unfolding energetically less favorable.

Hydration sphere

Apart of the direct interaction of the osmolytes with the protein, osmolytes also interact with the water molecules of the hydration sphere around the protein, indirectly affecting its stability. A hydrogen bond network reinforced by an osmolyte, modify the energetics of the solvation environment and can favor the native protein conformation, thus stabilizing it under stress. In contrast, an osmolyte that disrupts this hydrogen bond network and results in less structured or optimally organized hydration shell, has a negative impact on the protein conformation. A simplified schematic of how stabilizing and denaturing osmolytes function is depicted on Figure 5.

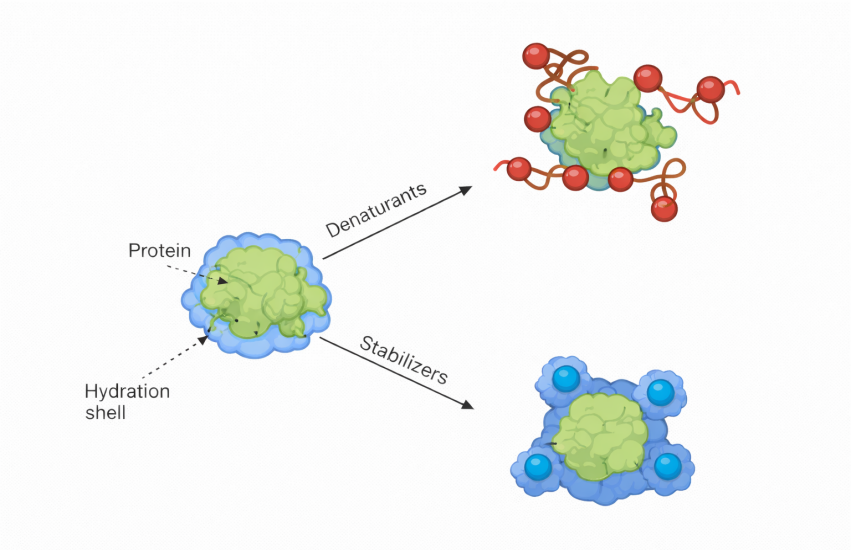

Figure 5: Mechanisms of osmolyte induced protein stabilization. A soluble protein in the cells is surrounded by its hydration sphere. With the addition of denaturants (destabilizing osmolytes) the hydration sphere becomes weaker, the protein is misfolded, and has increased Solvent Accessible Surface Area that the denaturants can interact with, to favor the misfolded state. In the case of stabilizers, the hydration sphere is reinforced and stabilizing osmolytes are excluded from the direct vicinity of the protein. With red are the destabilizing osmolytes such as urea, as they disrupt the hydration sphere. In contrast, the stabilizing osmolytes are marked with blue, as they reinforce the hydration sphere which is marked with darker blue.

1.6.4 Taurine as an osmolyte

Among known osmolytes, taurine represents a distinctive case as it is not only a compatible solute but also has several other functions such as modulating of ionic and redox homeostasis. Taurine, among other osmolytes, prevent aggregation, and assist in maintaining cell volume under stress conditions. However, in light of these aforementioned mechanisms, taurine has two opposing effects, and this is the case with most osmolytes. Ultimately, the extent of stabilization or destabilization is determined by the balance between the two opposing mechanisms and is influenced by which mechanism exerts greater influence and to what degree. Stabilizing osmolytes increase the enthalpy of the unfolded state, making it less favorable, while destabilizing osmolytes reduce the enthalpy difference, favoring unfolding.

In vitro, taurine has been shown to raise the denaturation temperature of lysozyme and ubiquitin in a concentration-dependent manner, indicating strong stabilizing potential. However, no comprehensive in vivo study has yet connected these effects to cellular or organismal phenotypes. On a molecular level evidence suggests that osmolytes with

functional groups with high polarity interact more favorably with the protein backbone, however also other factors affecting the overall performance of the osmolyte. Examples for this are Trimethylamine N-oxide (TMAO) (a strong stabilizer) and urea (a denaturant). Both have high polarity and similar surface area, highlighting the complexity of the system. Because protein missfolding and loss of proteostasis are hallmarks of aging, osmolyte accumulation may serve as a conserved biochemical defense that buffers age-related proteostatic decline and supports longevity.

1.7 Rationale

Genetic determinants of Accelerated Senescence

Understanding the mechanisms of cellular senescence is central to ageing biology, as senescence contributes to various age-associated diseases, including cancer, neurodegeneration, and metabolic disorders. In this study, we investigated the genetic determinants of accelerated senescence using *Saccharomyces cerevisiae* as a model. Specifically, we aimed to identify the mRNA expression signature of single-knockout, telomerase-positive mutants that exhibit rapid senescence upon telomerase removal. Because pathways such as telomere maintenance, DNA damage signaling, and telomere capping are conserved across species, this approach provides a valuable framework for identifying novel biomarkers of senescence and potential therapeutic targets and enhance our understanding of the interplay between genetic and environmental factors in aging.

To facilitate this, collaborators from Prof. Kathi Zarnack's group developed a machine-learning model that integrates transcriptomic profiles to predict and classify mutants with an accelerated senescence (AS) signature. Using this model, we identified new AS mutants and characterized their molecular features, providing new insights into the regulatory networks that predispose these cells to rapid senescence upon telomerase removal, improving our understanding of the factors that drive accelerated senescence.

Environmental modulators of proteostasis and lifespan

While genetic predisposition shapes the onset of senescence, environmental and metabolic factors strongly influence its progression and the capacity for cellular maintenance. Small molecules can profoundly modulate lifespan by acting on conserved stress-response and proteostasis pathways. Among these, taurine has emerged as a molecule of particular interest, with studies reporting beneficial effects across diverse systems, yet its underlying mechanisms remain poorly understood.

Here, we question yeast's insusceptibility to taurine in a telomerase negative background, investigate the mechanisms behind taurine's profound effects in longevity, shed light upon the underlying mechanisms and characterize its effects using *S. cerevisiae* as a model.

Yeast offers a tractable system to dissect these mechanisms due to its conserved stress-response networks and well-defined ageing phenotypes. Our experiments revealed that taurine exerts broadly beneficial effects, improving cellular fitness across multiple stress conditions. This prompted the hypothesis that taurine's pro-longevity actions may stem from entirely distinct molecular processes, such as enhanced proteostasis, rather than direct modulation of senescence-related pathways.

Our findings support this idea, showing that taurine acts as a compatible osmolyte with high protein-stabilizing capacity, potentially buffering the proteostatic decline commonly associated with ageing. By reinforcing protein folding and cellular homeostasis, taurine promotes stress resilience and may influence lifespan through mechanisms distinct from canonical senescence signaling. Here, our comprehensive approach to identify why taurine is such a potent supplement and which primary hallmarks of ageing taurine impacts is described. We have solid data confirming our hypothesis that taurine's broad effects are achieved due to its excellent protein stabilizing potential as an osmolyte, and its phenotype is a direct result of the cells boosted proteostasis.

Together, these investigations integrate genetic and environmental perspectives on ageing. The genetic analysis defines intrinsic determinants that accelerate senescence, while the environmental studies highlight the capacity of small molecules like taurine to counteract proteostatic stress. This dual approach provides a unified framework for understanding how intrinsic genomic factors and extrinsic modulators converge to regulate cellular ageing and longevity.

Materials and methods

2.1 Key resources table

Table 1: Reagents and kits

REAGENT - RESOURCE	SOURCE	IDENTIFIER
Chemicals		
5-Fluoroorotic Acid	Zymo Research	Cat#F9003
NEBufferTM 4	New England Biolabs	Cat#B7004S
Phenol	Merck	77608-500G
Sodium Acetate	Merck	S2889-1Kg
EDTA	Sigma Aldrich	03620
SDS	Applichem	A0675,1000
PCI	Applichem	A2279,0500
Ethanol	Fisher Scientific	10437341
SC-Leu	MP biomedicals	114410322
SC-Leu-Ura	MP biomedicals	114420922
SC-Ura	MP biomedicals	410-622
Lithium acetate	Sigma Aldrich	517992
NaOH	Sigma Aldrich	30620
Evagreen	Jena Bioscience	PCR-379
Precision Blue RT-PCR Dye	BioRad	172-5555
Polyethylene glycol 400	Merck	81240-1kg
Tris·HCL	Merck	T1503-5KG
Enzymes/Antibodies		
XhoI restriction enzyme	New England Biolabs	R0146L
Anti-Digoxigenin-AP, Fab fragments	ROCHE	11093274910
Critical commercial assays		
Superscript III kit	Invitrogen	10308632
RNAse-free DNAse kit	Qiagen	79254

RNeasy MinElute kit	Qiagen	74204
Q5 DNA Polymerase	New England Biolabs	M0491
Taq MasterMix	New England Biolabs	M0270L

Table 2: software used

Software used	**Edition**
Prism	9
Adobe Illustrator	2023
Microsoft Office	2016
Microsoft Copilot	M365 corporate edition
ChatGPT	-
Bio-Rad RFX Manager	3.1
Bio-Rad Image Lab	V5

Table 3: Oligonucleotides used

Oligonucleotides		
Identifier	Use	Sequence (5'-3')
oRD259	CRG1 qpcr forward	TTGTGGACTTTCCCGAAGCC
oRD260	CRG1 qpcr rev	CCCGTTGGTTGTCGTTCAGA
oRD261	YDR034W-B qpcr forward	TATGCCCCACAACAACAACCA
oRD262	YDR034W-B qpcr rev	TACAGCAACCACCGGATTCTC
oRD263	NCW2 qpcr forward	ACGTCAAGCGGAATCACCAA
oRD264	NCW2 qpcr rev	GTTGTGGCTGAGGACGGTAG
oRD265	KDX1 qpcr forward	ATGGGGCACTAAATGGCGTT
oRD266	KDX1 qpcr rev	CAGGCGTTGTTCGGACCTTA
oRD267	GSC2 qpcr forward	TGTGGAAGGCGACACAAAGA
oRD268	GSC2 qpcr rev	ATAACGAGCACCACCCACAG
oRD269	ARO10 qpcr forward	TGCCATGCAAGACCACTCAA
oRD270	ARO10 qpcr rev	CTGCACCGTCACCTTCAAAC

Table 4: Plasmids used

Plasmid	Function
pBL810	
pBL975	overexpression of FMP45
pBL976	overexpression of LDB7
pBL977	overexpression of ATG7
pBL978	overexpression of RNH1
pBL979	overexpression of GPB1
pBL980	overexpression of YPL247C
pBL981	overexpression of IDS2
pBL982	overexpression of ZDS2
pBL983	overexpression of PAN2
pBL984	overexpression of HNM1
pBL988	overexpression of RCR1
pBL989	overexpression of KDX1
pBL990	overexpression of BAT2
pBL991	overexpression of SOM1
pBL992	overexpression of PLN1
pBL993	overexpression of BXI1
pBL994	overexpression of SET2
pBL995	overexpression of CAT2
pBL996	overexpression of YDR034W
pBL997	overexpression of LSC2
pBL998	overexpression of ATG3
pBL999	overexpression of CDA1
pBL1000	overexpression of YGR045C
pBL1001	overexpression of MLS1
pBL1002	overexpression of SNM1
pBL1003	overexpression of TRS31
pBL1004	overexpression of UYP6
pBL1005	overexpression of SME1
pBL1006	overexpression of URB1
pBL1007	overexpression of DRE2

pBL1008	overexpression of YOL162W
pBL1009	overexpression of UBC8
pBL1010	overexpression of ROQ1
pBL1011	overexpression of BNA2
pBL1012	overexpression of FBP26
pBL1013	overexpression of SGA1
pBL1014	overexpression of SRX1
pBL1015	overexpression of PPZ2
pBL1016	overexpression of CRG1
pBL1017	overexpression of SIP5
pBL1018	overexpression of OPI10
pBL1019	overexpression of ARO9
pBL1020	overexpression of YHR138C
pBL1021	overexpression of YPS6
pBL1022	overexpression of SNA3
pBL1023	overexpression of PAI3
pBL1024	overexpression of YPL088W
pBL1025	overexpression of DAP1
pBL1026	overexpression of OYE3
pBL1027	overexpression of YPL199C
pBL1028	overexpression of THI6
pBL1029	overexpression of PAU8
pBL1030	overexpression of PEX11
pBL1031	overexpression of PRB1
pBL1032	overexpression of UGA2
pBL1033	overexpression of CCR4
pBL1034	overexpression of UGX2
pBL1035	overexpression of PAU11
pBL1036	overexpression of YBR220C
pBL1037	overexpression of GYP7
pBL1038	overexpression of PTP1
pBL1039	overexpression of FYV8
pBL1040	overexpression of YCL049C

pBL1041	overexpression of RTS3
pBL1042	overexpression of TOP3
pBL1043	overexpression of RNR1
pBL1044	overexpression of TOP3
pBL1045	overexpression of RNR1

2.2 Experimental model and subject details

Saccharomyces cerevisiae strains used in this study are derivatives of the BY4741 background (*MATa his3Δ1 leu2Δ0 met15Δ0 ura3Δ0*). Strains were grown under standard conditions in YPD (1% [w/v] yeast extract, 2% [w/v] peptone supplemented with 2% glucose) or SC derivatives (0.2% [w/v] Synthetic Complete without amino acids, 1% [w/v] yeast nitrogen base supplemented with 2% glucose) at 30°C.

2.3 Yeast Strains used in this study

Strain	**Genotype**	**Origin**
yNL120	MATa/MATα *his3Δ1/his3Δ1*; *leu2Δ0/leu2Δ0*; *ura3Δ0/ura3Δ0*; *MET15/met15Δ0*; *LYS2/lys2Δ0*; *TLC1/tlc1*::NAT; *PTC1/ptc1*::KAN	This study
yNL129	MATa/MATα *his3Δ1/his3Δ1*; *leu2Δ0/leu2Δ0*; *ura3Δ0/ura3Δ0*; *MET15/met15Δ0*; *LYS2/lys2Δ0*; *TLC1/tlc1*::NAT; *PHO85/pho85*::KAN	This study
yNL131	MATa/MATα *his3Δ1/his3Δ1*; *leu2Δ0/leu2Δ0*; *ura3Δ0/ura3Δ0*; *MET15/met15Δ0*; *LYS2/lys2Δ0*; *TLC1/tlc1*::NAT; *YVH1/yvh1*::KAN	This study
yNL134	MATa/MATα *his3Δ1/his3Δ1*; *leu2Δ0/leu2Δ0*; *ura3Δ0/ura3Δ0*; *MET15/met15Δ0*; *LYS2/lys2Δ0*; *TLC1/tlc1*::NAT; *KIN3/kin3*::KAN	This study
yNL137	MATa/MATα *his3Δ1/his3Δ1*; *leu2Δ0/leu2Δ0*; *ura3Δ0/ura3Δ0*; *MET15/met15Δ0*; *LYS2/lys2Δ0*; *TLC1/tlc1*::NAT; *PTC7/ptc7*::KAN	This study

yNL140	MATa/MATα *his3Δ1/his3Δ1*; *leu2Δ0/leu2Δ0*; *ura3Δ0/ura3Δ0*; *MET15/met15Δ0*; *LYS2/lys2Δ0*; *TLC1/tlc1*::NAT; *FMP48/fmp48*::KAN	This study
yNL143	MATa/MATα *his3Δ1/his3Δ1*; *leu2Δ0/leu2Δ0*; *ura3Δ0/ura3Δ0*; *MET15/met15Δ0*; *LYS2/lys2Δ0*; *TLC1/tlc1*::NAT; *ALK2/alk2*::KAN	This study
yNL146	MATa/MATα *his3Δ1/his3Δ1*; *leu2Δ0/leu2Δ0*; *ura3Δ0/ura3Δ0*; *MET15/met15Δ0*; *LYS2/lys2Δ0*; *TLC1/tlc1*::NAT; *GIN4/gin4*::KAN	This study
yEG144	MATa/MATα *his3Δ1/his3Δ1*; *met15Δ0/met15Δ0*; *leu2Δ0/leu2Δ0*; *ura3Δ0/ura3Δ0*; *tlc1*::NAT; *sit4*::KAN	This study
yEG145	MATa/MATα *his3Δ1/his3Δ1*; *met15Δ0/met15Δ0*; *leu2Δ0/leu2Δ0*; *ura3Δ0/ura3Δ0*; *tlc1*::NAT; *sit4*::KAN	This study
yEG146	MATa/MATα *his3Δ1/his3Δ1*; *met15Δ0/met15Δ0*; *leu2Δ0/leu2Δ0*; *ura3Δ0/ura3Δ0*; *tlc1*::NAT; *sit4*::KAN	This study
yEG147	MATa/MATα *his3Δ1/his3Δ1*; *met15Δ0/met15Δ0*; *leu2Δ0/leu2Δ0*; *ura3Δ0/ura3Δ0*; *tlc1*::NAT; *cla4*::KAN	This study
yEG148	MATa/MATα *his3Δ1/his3Δ1*; *met15Δ0/met15Δ0*; *leu2Δ0/leu2Δ0*; *ura3Δ0/ura3Δ0*; *tlc1*::NAT; *cla4*::KAN	This study
yEG149	MATa/MATα *his3Δ1/his3Δ1*; *met15Δ0/met15Δ0*; *leu2Δ0/leu2Δ0*; *ura3Δ0/ura3Δ0*; *tlc1*::NAT; *cla4*::KAN	This study
yEG150	MATa/MATα *his3Δ1/his3Δ1*; *met15Δ0/met15Δ0*; *leu2Δ0/leu2Δ0*; *ura3Δ0/ura3Δ0*; *tlc1*::NAT; *ypk1*::KAN	This study
yEG151	MATa/MATα *his3Δ1/his3Δ1*; *met15Δ0/met15Δ0*; *leu2Δ0/leu2Δ0*; *ura3Δ0/ura3Δ0*; *tlc1*::NAT; *ypk1*::KAN	This study
yEG152	MATa/MATα *his3Δ1/his3Δ1*; *met15Δ0/met15Δ0*; *leu2Δ0/leu2Δ0*; *ura3Δ0/ura3Δ0*; *tlc1*::NAT; *ypk1*::KAN	This study
yEG192	MATa/MATα *his3Δ1/his3Δ1*; *met15Δ0/met15Δ0*; *leu2Δ0/leu2Δ0*; *ura3Δ0/ura3Δ0*; *tlc1*::NAT; *ptp1*::KAN	This study

yEG193	MATa/MATα *his3Δ1/his3Δ1*; *met15Δ0/met15Δ0*; *leu2Δ0/leu2Δ0*; *ura3Δ0/ura3Δ0*; *tlc1*::NAT; *ptp1*::KAN	This study
yEG194	MATa/MATα *his3Δ1/his3Δ1*; *met15Δ0/met15Δ0*; *leu2Δ0/leu2Δ0*; *ura3Δ0/ura3Δ0*; *tlc1*::NAT; *ptp1*::KAN	This study
yEG195	MATa/MATα *his3Δ1/his3Δ1*; *met15Δ0/met15Δ0*; *leu2Δ0/leu2Δ0*; *ura3Δ0/ura3Δ0*; *tlc1*::NAT; *sak1*::KAN	This study
yEG196	MATa/MATα *his3Δ1/his3Δ1*; *met15Δ0/met15Δ0*; *leu2Δ0/leu2Δ0*; *ura3Δ0/ura3Δ0*; *tlc1*::NAT; *sak1*::KAN	This study
yEG197	MATa/MATα *his3Δ1/his3Δ1*; *met15Δ0/met15Δ0*; *leu2Δ0/leu2Δ0*; *ura3Δ0/ura3Δ0*; *tlc1*::NAT; *sak1*::KAN	This study
yEG198	MATa/MATα *his3Δ1/his3Δ1*; *met15Δ0/met15Δ0*; *leu2Δ0/leu2Δ0*; *ura3Δ0/ura3Δ0*; *tlc1*::NAT; *lcb4*::KAN	This study
yEG199	MATa/MATα *his3Δ1/his3Δ1*; *met15Δ0/met15Δ0*; *leu2Δ0/leu2Δ0*; *ura3Δ0/ura3Δ0*; *tlc1*::NAT; *lcb4*::KAN	This study
yEG200	MATa/MATα *his3Δ1/his3Δ1*; *met15Δ0/met15Δ0*; *leu2Δ0/leu2Δ0*; *ura3Δ0/ura3Δ0*; *tlc1*::NAT; *lcb4*::KAN	This study
yEG201	MATa/MATα *his3Δ1/his3Δ1*; *met15Δ0/met15Δ0*; *leu2Δ0/leu2Δ0*; *ura3Δ0/ura3Δ0*; *tlc1*::NAT; *sdp1*::KAN	This study
yEG202	MATa/MATα *his3Δ1/his3Δ1*; *met15Δ0/met15Δ0*; *leu2Δ0/leu2Δ0*; *ura3Δ0/ura3Δ0*; *tlc1*::NAT; *sdp1*::KAN	This study
yEG203	MATa/MATα *his3Δ1/his3Δ1*; *met15Δ0/met15Δ0*; *leu2Δ0/leu2Δ0*; *ura3Δ0/ura3Δ0*; *tlc1*::NAT; *sdp1*::KAN	This study
yBL229	MATα *his3Δ1*; *leu2Δ0*; *ura3Δ0*; *lys2Δ0*; *rad52*::KAN	Lab stock
ySLG70	MATa *his3Δ1*; *leu2Δ0*; *ura3Δ0*; *met15Δ0*; *rad9*::KAN; *cdc13-1* KAN	Lab stock
yHP669	MATa *his3Δ1*; *leu2Δ0*; *ura3Δ0*; *met15Δ0*; *cdc13*::*cdc13-1* HIS; *upf1*::KAN	Lab stock
yVP79	MATa *his3Δ1*; *leu2Δ0*; *ura3Δ0*; *met15Δ0*; *cdc13-1*::KAN; *exo1*::NAT	Lab stock

yJK418	MATa *his3Δ1*; *leu2Δ0*; *met15Δ0*; *ura3Δ0*; *cdc13-1* (HIS); *san1*::KAN	Lab stock
ySLG522	MATa *his3Δ1*; *leu2Δ0*; *ura3Δ0*; *met15Δ0*; *mrc1*::KAN; *cdc13-1*::HIS3	Lab stock
yJK472	MATa *his3Δ1*; *leu2Δ0*; *met15Δ0*; *ura3Δ0*; *cdc13*::*cdc13-1* (NAT); *mec1*::HIS; *sml1*::KAN	Lab stock
yJK869	MATa *his3Δ1*; *leu2Δ0*; *met15Δ0*; *ura3Δ0*; *cdc13*::*cdc13-1* (NAT); *rad53*::HIS; *sml1*::KAN	Lab stock
yHP703	MATa *his3Δ1*; *leu2Δ0*; *ura3Δ0*; *met15Δ0*; *cdc13*::*cdc13-1*::HIS; *tel1*::KAN	Lab stock
yKB137	MATa *his3Δ1*; *leu2Δ0*; *met15Δ0*; *ura3Δ0*; *cdc13*::*cdc13-1* (HIS); *rad53*::*rad53-11* (URA)	Lab stock
yLM56	MATa *his3Δ1*; *leu2Δ0*; *ura3Δ0*; *met15Δ0*; *cdc13*::*cdc13-1* HIS; *pif1*::KAN	Lab stock
yJK575	MATa *his3Δ1*; *leu2Δ0*; *met15Δ0*; *ura3Δ0*; *cdc13*::*cdc13-1* (HIS); *sae2*::KAN	Lab stock
yJK329	MATa *his3Δ1*; *leu2Δ0*; *met15Δ0*; *ura3Δ0*; *CDC20*::*cdc20-1* (KAN)	Lab stock
yBL375	MATa *his3Δ1*; *leu2Δ0*; *ura3Δ0*; *cdc4-1* KAN	Lab stock
ySH81	MATa *his3Δ1*; *leu2Δ0*; *ura3Δ0*; *met15Δ0*; *sen1-1*::KAN	Lab stock
yBL7	MATa *his3Δ1*; *leu2Δ0*; *ura3Δ0*; *met15Δ0*	Lab stock
yJK34	MATa *his3Δ1*; *leu2Δ0*; *met15Δ0*; *ura3Δ0*; *STN1*::*stn1-13*KAN	Lab stock
ySH238	MATa *his3Δ1*; *leu2Δ0*; *ura3Δ0*; *met15Δ0*; *dam1-11*::KAN	Lab stock
ySH211	MATa *his3Δ1*; *leu2Δ0*; *ura3Δ0*; *met15Δ0*; *rsp5-3*::KAN	Lab stock
ySH235	MATa *his3Δ1*; *leu2Δ0*; *ura3Δ0*; *met15Δ0*; *afg2-18*::KAN	Lab stock
ySH236	MATa *his3Δ1*; *leu2Δ0*; *ura3Δ0*; *met15Δ0*; *rio2-1*::KAN	Lab stock
ySH216	MATa *his3Δ1*; *leu2Δ0*; *ura3Δ0*; *met15Δ0*; *rfc2-1*::KAN	Lab stock
ySH243	MATa *his3Δ1*; *leu2Δ0*; *ura3Δ0*; *met15Δ0*; *cus1-3*::KAN	Lab stock
yRD329	MATa *tlc1*::NAT; +pBL810; +pRCR1; *met*+; *lys*+	This study
yRD330	MATa *tlc1*::NAT; +pBL810; +pRCR1; *met*+; *lys*+	This study

yRD331	MATa *tlc1*::NAT; +pBL810; +pKDX1; *met+*; *lys+*	This study
yRD332	MATa *tlc1*::NAT; +pBL810; +pKDX1; *met+*; *lys+*	This study
yRD333	MATa *tlc1*::NAT; +pBL810; +pBAT2; *met+*; *lys+*	This study
yRD334	MATa *tlc1*::NAT; +pBL810; +pBAT2; *met+*; *lys+*	This study
yRD335	MATa *tlc1*::NAT; +pBL810; +pSOM1; *met+*; *lys+*	This study
yRD336	MATa *tlc1*::NAT; +pBL810; +pSOM1; *met+*; *lys+*	This study
yRD337	MATa *tlc1*::NAT; +pBL810; +pPLN1; *met+*; *lys+*	This study
yRD338	MATa *tlc1*::NAT; +pBL810; +pPLN1; *met+*; *lys+*	This study
yRD339	MATa *tlc1*::NAT; +pBL810; +pBXI1; *met+*; *lys+*	This study
yRD340	MATa *tlc1*::NAT; +pBL810; +pBXI1; *met+*; *lys+*	This study
yRD341	MATa *tlc1*::NAT; +pBL810; +pSET2; *met+*; *lys+*	This study
yRD342	MATa *tlc1*::NAT; +pBL810; +pSET2; *met+*; *lys+*	This study
yRD343	MATa *tlc1*::NAT; +pBL810; +pCAT2; *met+*; *lys+*	This study
yRD344	MATa *tlc1*::NAT; +pBL810; +pCAT2; *met+*; *lys+*	This study
yRD345	MATa *tlc1*::NAT; +pBL810; +pYDR034W-B; *met+*; *lys+*	This study
yRD346	MATa *tlc1*::NAT; +pBL810; +pYDR034W-B; *met+*; *lys+*	This study
yRD347	MATa *tlc1*::NAT; +pBL810; +pLSC2; *met+*; *lys+*	This study
yRD348	MATa *tlc1*::NAT; +pBL810; +pLSC2; *met+*; *lys+*	This study
yRD349	MATa *tlc1*::NAT; +pBL810; +pATG3; *met+*; *lys+*	This study
yRD350	MATa *tlc1*::NAT; +pBL810; +pATG3; *met+*; *lys+*	This study
yRD351	MATa *tlc1*::NAT; +pBL810; +pCDA1; *met+*; *lys+*	This study
yRD352	MATa *tlc1*::NAT; +pBL810; +pCDA1; *met+*; *lys+*	This study
yRD353	MATa *tlc1*::NAT; +pBL810; +pMLS1; *met+*; *lys+*	This study
yRD354	MATa *tlc1*::NAT; +pBL810; +pMLS1; *met+*; *lys+*	This study
yRD355	MATa *tlc1*::NAT; +pBL810; +pSNM1; *met+*; *lys+*	This study
yRD356	MATa *tlc1*::NAT; +pBL810; +pSNM1; *met+*; *lys+*	This study
yRD357	MATa *tlc1*::NAT; +pBL810; +pTRS31; *met+*; *lys+*	This study
yRD358	MATa *tlc1*::NAT; +pBL810; +pTRS31; *met+*; *lys+*	This study
yRD359	MATa *tlc1*::NAT; +pBL810; +pUTP6; *met+*; *lys+*	This study
yRD360	MATa *tlc1*::NAT; +pBL810; +pUTP6; *met+*; *lys+*	This study

yRD361	MATa *tlc1*::NAT; +pBL810; +pSME1; *met+*; *lys+*	This study
yRD362	MATa *tlc1*::NAT; +pBL810; +pSME1; *met+*; *lys+*	This study
yRD363	MATa *tlc1*::NAT; +pBL810; +pURB1; *met+*; *lys+*	This study
yRD364	MATa *tlc1*::NAT; +pBL810; +pURB1; *met+*; *lys+*	This study
yRD365	MATa *tlc1*::NAT; +pBL810; +pDRE2; *met+*; *lys+*	This study
yRD366	MATa *tlc1*::NAT; +pBL810; +pDRE2; *met+*; *lys+*	This study
yRD367	MATa *tlc1*::NAT; +pBL810; +pYOL162W; *met+*; *lys+*	This study
yRD368	MATa *tlc1*::NAT; +pBL810; +pYOL162W; *met+*; *lys+*	This study
yRD369	MATa *tlc1*::NAT; +pBL810; +pUBC8; *met+*; *lys+*	This study
yRD370	MATa *tlc1*::NAT; +pBL810; +pUBC8; *met+*; *lys+*	This study
yRD371	MATa *tlc1*::NAT; +pBL810; +pROQ1; *met+*; *lys+*	This study
yRD372	MATa *tlc1*::NAT; +pBL810; +pROQ1; *met+*; *lys+*	This study
yRD373	MATa *tlc1*::NAT; +pBL810; +pBNA2; *met+*; *lys+*	This study
yRD374	MATa *tlc1*::NAT; +pBL810; +pBNA2; *met+*; *lys+*	This study
yRD375	MATa *tlc1*::NAT; +pBL810; +pFBP26; *met+*; *lys+*	This study
yRD376	MATa *tlc1*::NAT; +pBL810; +pFBP26; *met+*; *lys+*	This study
yRD377	MATa *tlc1*::NAT; +pBL810; +pSGA1; *met+*; *lys+*	This study
yRD378	MATa *tlc1*::NAT; +pBL810; +pSGA1; *met+*; *lys+*	This study
yRD379	MATa *tlc1*::NAT; +pBL810; +pSRX1; *met+*; *lys+*	This study
yRD380	MATa *tlc1*::NAT; +pBL810; +pSRX1; *met+*; *lys+*	This study
yRD381	MATa *tlc1*::NAT; +pBL810; +pPPZ2; *met+*; *lys+*	This study
yRD382	MATa *tlc1*::NAT; +pBL810; +pPPZ2; *met+*; *lys+*	This study
yRD383	MATa *tlc1*::NAT; +pBL810; +pCRG1; *met+*; *lys+*	This study
yRD384	MATa *tlc1*::NAT; +pBL810; +pCRG1; *met+*; *lys+*	This study
yRD385	MATa *tlc1*::NAT; +pBL810; +pSIP5; *met+*; *lys+*	This study
yRD386	MATa *tlc1*::NAT; +pBL810; +pSIP5; *met+*; *lys+*	This study
yRD387	MATa *tlc1*::NAT; +pBL810; +pOPI10; *met+*; *lys+*	This study
yRD388	MATa *tlc1*::NAT; +pBL810; +pOPI10; *met+*; *lys+*	This study
yRD389	MATa *tlc1*::NAT; +pBL810; +pARO9; *met+*; *lys+*	This study
yRD390	MATa *tlc1*::NAT; +pBL810; +pARO9; *met+*; *lys+*	This study

yRD391	MATa *tlc1*::NAT; +pBL810; +pYHR138C; *met*+; *lys*+	This study
yRD392	MATa *tlc1*::NAT; +pBL810; +pYHR138C; *met*+; *lys*+	This study
yRD393	MATa *tlc1*::NAT; +pBL810; +pYPS6; *met*+; *lys*+	This study
yRD394	MATa *tlc1*::NAT; +pBL810; +pYPS6; *met*+; *lys*+	This study
yRD395	MATa *tlc1*::NAT; +pBL810; +pSNA3; *met*+; *lys*+	This study
yRD396	MATa *tlc1*::NAT; +pBL810; +pSNA3; *met*+; *lys*+	This study
yRD397	MATa *tlc1*::NAT; +pBL810; +pPAI3; *met*+; *lys*+	This study
yRD398	MATa *tlc1*::NAT; +pBL810; +pPAI3; *met*+; *lys*+	This study
yRD399	MATa *tlc1*::NAT; +pBL810; +pYPL088W; *met*+; *lys*+	This study
yRD400	MATa *tlc1*::NAT; +pBL810; +pDAP1; *met*+; *lys*+	This study
yRD401	MATa *tlc1*::NAT; +pBL810; +pDAP1; *met*+; *lys*+	This study
yRD402	MATa *tlc1*::NAT; +pBL810; +pOYE3; *met*+; *lys*+	This study
yRD403	MATa *tlc1*::NAT; +pBL810; +pOYE3; *met*+; *lys*+	This study
yRD404	MATa *tlc1*::NAT; +pBL810; +pYPL199C; *met*+; *lys*+	This study
yRD405	MATa *tlc1*::NAT; +pBL810; +pTHI6; *met*+; *lys*+	This study
yRD406	MATa *tlc1*::NAT; +pBL810; +pTHI6; *met*+; *lys*+	This study
yRD407	MATa *tlc1*::NAT; +pBL810; +pPAU8; *met*+; *lys*+	This study
yRD408	MATa *tlc1*::NAT; +pBL810; +pPAU8; *met*+; *lys*+	This study
yRD409	MATa *tlc1*::NAT; +pBL810; +pPEX11; *met*+; *lys*+	This study
yRD410	MATa *tlc1*::NAT; +pBL810; +pPEX11; *met*+; *lys*+	This study
yRD411	MATa *tlc1*::NAT; +pBL810; +pPRB1; *met*+; *lys*+	This study
yRD412	MATa *tlc1*::NAT; +pBL810; +pPRB1; *met*+; *lys*+	This study
yRD413	MATa *tlc1*::NAT; +pBL810; +pUGA2; *met*+; *lys*+	This study
yRD414	MATa *tlc1*::NAT; +pBL810; +pUGA2; *met*+; *lys*+	This study
yRD415	MATa *tlc1*::NAT; +pBL810; +pCCR4; *met*+; *lys*+	This study
yRD416	MATa *tlc1*::NAT; +pBL810; +pCCR4; *met*+; *lys*+	This study
yRD417	MATa *tlc1*::NAT; +pBL810; +pUGX2; *met*+; *lys*+	This study
yRD418	MATa *tlc1*::NAT; +pBL810; +pUGX2; *met*+; *lys*+	This study
yRD419	MATa *tlc1*::NAT; +pBL810; +pPAU11; *met*+; *lys*+	This study
yRD420	MATa *tlc1*::NAT; +pBL810; +pPAU11; *met*+; *lys*+	This study

yRD421	MATa *tlc1*::NAT; +pBL810; +pYBR220C; *met+*; *lys+*	This study
yRD422	MATa *tlc1*::NAT; +pBL810; +pYBR220C; *met+*; *lys+*	This study
yRD423	MATa *tlc1*::NAT; +pBL810; +pGYP7; *met+*; *lys+*	This study
yRD424	MATa *tlc1*::NAT; +pBL810; +pGYP7; *met+*; *lys+*	This study
yRD425	MATa *tlc1*::NAT; +pBL810; +pPTP1; *met+*; *lys+*	This study
yRD426	MATa *tlc1*::NAT; +pBL810; +pPTP1; *met+*; *lys+*	This study
yRD427	MATa *tlc1*::NAT; +pBL810; +pFYV8; *met+*; *lys+*	This study
yRD428	MATa *tlc1*::NAT; +pBL810; +pFYV8; *met+*; *lys+*	This study
yRD429	MATa *tlc1*::NAT; +pBL810; +pYCL049C; *met+*; *lys+*	This study
yRD430	MATa *tlc1*::NAT; +pBL810; +pYCL049C; *met+*; *lys+*	This study
yRD431	MATa *tlc1*::NAT; +pBL810; +pRTS3; *met+*; *lys+*	This study
yRD432	MATa *tlc1*::NAT; +pBL810; +pRTS3; *met+*; *lys+*	This study
yRD435	MATa *tlc1*::NAT; +pBL810; +pYGR045C; *met+*; *lys+*	This study
yRD436	MATa *tlc1*::NAT; +pBL810; +pYGR045C; *met+*; *lys+*	This study
yRD217	MATa/MATα *UBC8/ubc8*::KAN; *TLC1/tlc1*::NAT	This study
yRD219	MATa/MATα *ATG3/atg3*::KAN; *TLC1/tlc1*::NAT	This study
yRD221	MATa/MATα *PRB1/prb1*::KAN; *TLC1/tlc1*::NAT	This study
yRD223	MATa/MATα *YBR220C/ybr220c*::KAN; *TLC1/tlc1*::NAT	This study
yRD225	MATa/MATα *YCL049C/ycl049c*::KAN; *TLC1/tlc1*::NAT	This study
yRD227	MATa/MATα *SRX1/srx1*::KAN; *TLC1/tlc1*::NAT	This study
yRD229	MATa/MATα *RCR1/rcr1*::KAN; *TLC1/tlc1*::NAT	This study
yRD231	MATa/MATα *YPS6/yps6*::KAN; *TLC1/tlc1*::NAT	This study
yRD233	MATa/MATα *PLB1/plb1*::KAN; *TLC1/tlc1*::NAT	This study
yRD235	MATa/MATα *BXI1/bxi1*::KAN; *TLC1/tlc1*::NAT	This study
yRD237	MATa/MATα *KDX1/kdx1*::KAN; *TLC1/tlc1*::NAT	This study
yRD241	MATa/MATα *WSS1/wss1*::KAN; *TLC1/tlc1*::NAT	This study
yRD242	MATa/MATα *CPC26/cpc26*::KAN; *TLC1/tlc1*::NAT	This study
yRD243	MATa/MATα *DOA4/doa4*::KAN; *TLC1/tlc1*::NAT	This study
yRD244	MATa/MATα *CIN8/cin8*::KAN; *TLC1/tlc1*::NAT	This study
yRD245	MATa/MATα *BIM1/bim1*::KAN; *TLC1/tlc1*::NAT	This study

yRD246	MATa/MATα *SWI4/swi4*::KAN; *TLC1/tlc1*::NAT	This study
yRD247	MATa/MATα *RPN10/rpn10*::KAN; *TLC1/tlc1*::NAT	This study
yRD249	MATa/MATα *SWI6/swi6*::KAN; *TLC1/tlc1*::NAT	This study
yRD250	MATa/MATα *SPT21/spt21*::KAN; *TLC1/tlc1*::NAT	This study
yRD251	MATa/MATα *CDH1/cdh1*::KAN; *TLC1/tlc1*::NAT	This study
yRD252	MATa/MATα *ESC2/esc2*::KAN; *TLC1/tlc1*::NAT	This study
yRD253	MATa/MATα *DOC1/doc1*::KAN; *TLC1/tlc1*::NAT	This study
yRD254	MATa/MATα *RNR4/rnr4*::KAN; *TLC1/tlc1*::NAT	This study
yRD255	MATa/MATα *UGA2/uga2*::KAN; *TLC1/tlc1*::NAT	This study
yRD259	MATa/MATα *BNA2/bna2*::KAN; *TLC1/tlc1*::NAT	This study
yRD264	MATa/MATα *PAU15/pau15*::KAN; *TLC1/tlc1*::NAT	This study
yRD266	MATa/MATα *PAU22/pau22*::KAN; *TLC1/tlc1*::NAT	This study
yRD468	MATa/MATα *ARO9/aro9*::KAN; *TLC1/tlc1*::NAT	This study
yRD469	MATa/MATα *ARO10/aro10*::KAN; *TLC1/tlc1*::NAT	This study
yRD312	MATa/MATα *DUN1/dun1*::KAN; *TLC1/tlc1*::NAT	This study
yRD315	MATa/MATα *CKA2/cka2*::KAN; *TLC1/tlc1*::NAT	This study
yRD318	MATa/MATα *FAB1/fab1*::KAN; *TLC1/tlc1*::NAT	This study
yRD321	MATa/MATα *YAK1/yak1*::KAN; *TLC1/tlc1*::NAT	This study
yRD323	MATa/MATα *TPK2/tpk2*::KAN; *TLC1/tlc1*::NAT	This study
yRD326	MATa/MATα *KIN2/kin2*::KAN; *TLC1/tlc1*::NAT	This study
yRD439	MATa/MATα *YCK1/yck1*::KAN; *TLC1/tlc1*::NAT	This study
yRD591	MATα +pGALs-TDP43-GFP	This study
yRD592	MATa +pGALs-TDP43-GFP	This study
yRD600	MATa/MATα *ELM1/elm1*::KAN; *TLC1/tlc1*::NAT	This study

Table 5: Yeast strains used

2.4 Transformation

5mL of appropriate medium were inoculated with yeast, and incubated overnight at 30°C. The following day, it was diluted in 25mL of YPD to an OD_{600} of 0.1 and grown to OD_{600} 0.4 – 0.8 before being centrifuged at 3000g 5min at RT. The supernatant was removed; the cells were washed with 5mL of LiAc-mix and re-suspended in 250µL of LiAc-mix (100µL LiAc-mix / 10mL culture). 100µL of cells were used per transformation by adding 0,5µL (0,2 – 0.5µg) of plasmid, 10µL of carrier DNA (SSDNA) and 700µL of PEG-mix. The samples were incubated on a rotating wheel in RT for 30 minutes, followed by a heatshock at 42°C for 15 minutes. Cells were centrifuged at 3000g at RT for 1 minute, the supernatant was replaced with 300µL of appropriate medium and incubated for 30minutes at 30°C. The cells were then sowed on the appropriate plate (SC-Leu or SC-Leu-Ura) and grown at 30°C for 2 days.

Buffers used:

PEG-Mix consists of 40% w/v Polyethylene glycol 400 (80g) and LiAc-Mix to a final volume of 200mL

LiAc-Mix consists of 10% v/v Lithium acetate 1N solution, 10% v/v 10X TE and 80% v/v water

10X TE consists of 0.1M Tris·HCL and 10mM EDTA.

2.5 Overexpression of genes using the MoBY 2.0 library

In order to overexpress the genes comprising the AS signature, we utilized 2-micron MoBY plasmids that feature the gene of interest under its endogenous promoter. To selectively knock out telomerase activity, the endogenous *TLC1* gene was deleted and the cells were complemented by a plasmid expressing telomerase under its own promoter. For selection of telomerase negative cells that lost the plasmid, cells were incubated on 5-FOA plates.

Spotting assays were performed on cells lacking endogenous telomerase activity (*tlc1*), with the gene of interest expressed from a 2-micron MoBY plasmid under its endogenous promoter to ensure at least twofold overexpression. Cells were grown on YPD agar plates and shown above are serial dilutions with a dilution factor 1:10. Cells were incubated for

48h per passage at 30 °C. For the senescence spottings, *tlc1* haploid cells covered with pBL810 (TLC1 gene under its own promoter) and transformed with pYFG (2μ-YFG-LEU2) acquired from MoBY 2.0 collection to overexpress the protein of interest, were streaked out on SC-Leu-Ura plates. Colonies were re-suspended to 0.5 OD_{600} and spotted in ten-fold dilutions onto the appropriate agar plates (SC-Leu-Ura for telomerase positive control and SC-Leu+5'FOA, to kick out the TLC1 plasmid for the senescing single mutants. The plates were incubated at 30°C for 2 days, and imaged with the ChemiDocTM Touch Imaging System (Bio-Rad). Subsequently, the second spot from each replicate was re-suspended in water, and passed to SC-Leu-Ura for telomerase positive control and SC-Leu for the senescing single mutants. Plates shown here are SC-Leu spotted after the selection for cells that do not have telomerase activity.

2.6 Colony PCR

A small amount of yeast was picked with the 10μL pipette tip and incubated in 10μL 0.02N sodium hydroxy solution, at 100°C. Cell debris was pelleted via centrifugation, 2μL of the supernatant were transferred to a new tube with 10μL of PCR-mix (Taq) for PCR-reaction, 6μL water, and 1μL of each primer solution of 10μM (forward and reverse, from the KO collection primer suggestions). The cycling profile is indicated below, and for the deletion confirmation PCRs, the same annealing temperature was used.

Steps	Temperature	Time
1	95°C	3 minutes
2	95°C	10 seconds
3	55°C	30 seconds
4	68°C	1 minute
5	Go to step 2, 34X	
6	68°C	5 minutes
7	4°C	∞

Table 6: Colony PCR conditions

2.7 Senescence curves

Liquid senescence assays were performed as described in Balk et al., 2013. In brief, diploid cells heterozygous for tlc1 and *yfg* (your favorite gene) were incubated in sporulation medium and dissected to acquire the haploid mutants for the curves. 2 days following dissection, a portion of the colonies was patched on YPD plates and incubated overnight at 30°C. These plates were then replicated onto selection plates to assess the genotypes of the spores. The selected cells were re-suspended from the dissection plates in water and subsequently diluted in 5 mL YPD to an OD_{600} of 0.01 and grown overnight at 30°C. Each day, the OD_{600} was measured and cultures were diluted to OD_{600} 0.01 again. Population doublings were calculated each day as the $\log_2 (OD_{600}/0.01)$, where the OD_{600} is the cell density measured after 24h. Graphs were plotted using Prism9.

2.8 Spotting assay

Appropriate plates for the spottings were produced in advance, to ensure freshness. Overnight cultures of the cells to be spotted, were diluted to a final OD_{600} of 0.5 and spotted in ten-fold dilutions onto the appropriate agar plates and temperatures using the 48 well plate replica plater. Plates with cells were subsequently left open to dry in the hood to avoid moisture during incubation. Images of the plates were taken after 48h and 72h using the ChemiDoc (Colorimetric mode, 0.3 s imaging time and largest possible imaging frame). The images were cropped and had their color balance adjusted in Adobe Illustrator, to facilitate readout.

For the senescence spottings of the MoBY overexpression mutants, the second spot from each replicate was re-suspended in water, and passed to SC-Leu-Ura for telomerase positive control and SC-Leu for the senescing single mutants. Plates shown here are SC-Leu spotted after the selection for cells that do not have telomerase activity.

2.9 Up-Down assay

The up-down assay was originally used a screening method used to identify genetic factors that affect telomere integrity and cell cycle regulation in budding yeast. In the “up” phase, cells are exposed to non-permissive temperatures resulting in telomere deprotection and trigger of the DNA damage checkpoint. In the subsequent “down” phase, cells are shifted back to permissive temperatures, telomeres get protected again and checkpoint proficient cells can resume growing, whereas checkpoint deficient cells cannot, due to having accumulated critical amounts of DNA damage[8888]. The plates used are YPD unless differently indicated.

2.10 DNA damage tolerance

In order to address the tolerance of different strains in DNA damage condition, chemical DNA damaging agents were used. Although all of the following chemicals lead to DNA damage, the actual type of damage varies. MMS is an alkylating agent that primarily methylates DNA bases, especially guanine and adenine. This leads to the formation of lesions like 7-methylguanine and 3-methyladenine. It causes a wide array of downward lesions such as base mispairing, replication blocks, single-strand breaks and even impairs nuclear membrane function and alteration of its lipid content[89,9089,90]. Zeocin is a radiomimetic agent that induces DNA double-strand breaks (DSBs), by intercalating into the DNA[9191]. Hydroxyurea (HU) inhibits ribonucleotide reductase, leading to depletion of deoxyribonucleotide triphosphates (dNTPs). This stalls DNA replication forks, induces replication stress and cell cycle arrest in the S phase[9292]. All of these agents were added to the plates (YPD unless differently indicated) in the displayed concentrations, and the tolerance of each strain corresponds to the growth of the colonies during a spotting assay.

2.11 Telomere PCR

Cells from an overnight culture (0.2 ODunits) were washed with water and resuspended in 20µL 0.02N NaOH and incubated at 100^{o}C for 10 minutes. Samples were spun down in a tabletop centrifuge and 2µL of the supernatant were transferred to a new PCR tube containing 3µL of water. The new tubes were incubated at 96^{o}C for 10 minutes and 5µL of tailing mix were immediately added (speed is crucial), and subsequently the next step

was initiated on the PCR machine. After the tailing step, the PCR mastermix is added to each tube, before the next step.

Tailing mix (5µL/sample)	
Reagent	Volume (µL)
water	3.7
10X NEB4 buffer	1
dCTP (10mM)	0.1
NEB Terminal Transferase (20U/µL)	0.2
Reaction mix (30µL/sample)	
water	21
10X PCR buffer (50% glycerol)	4
dNTPs (2mM)	4
Y' oBL361, 6R oBL360 or 1L oBL358 (100 µM)	0.3
G18 oBL359 (100 µM)	0.3
Q5 Hot-Start DNA Polymerase (2U/µL NEB)	0.5

C-tailing cycler profile		
Step	Temperature (°C)	Duration
1	37	30min
2	65	10min
3	96	5min
4	65	Until addition of next mastermix
5	95	3min
6	95	30sec
7	63	15sec
8	68	20sec
9	68	5min
10	Go to step 6 (X45)	Until electrophoresis

Table 7: PCR reaction mixes and conditions.

2.12 Southern Blot of Genomic DNA with DIG-Labeled Probes

Genomic DNA extraction

Genomic DNA was isolated from 30–50 mL of exponentially growing cells using the Teeny Protocol. The resulting pellet was resuspended in TE buffer, and DNA concentration was

estimated by measuring the absorbance at 260 nm (NanoDrop). Although the NanoDrop reading can be unreliable for low-concentration samples, values between 500–100 ng/µL were considered trustworthy. To avoid inaccuracies between samples, gel quantification was then performed by loading 2µL of undigested DNA on an agarose gel and quantifying the band intensity in silico. Alternatively, a Qubit fluorometric assay can be performed, yielding 600 ng of DNA for the subsequent restriction digestion.

Restriction digestion

A 25 mL final volume of digestion buffer (2.5 µL Cutsmart Buffer) was prepared and the DNA sample was added to reach 600 ng total. XhoI (1 mL of enzyme) was added, and the reaction was incubated at 37 °C for 5 h to ensure complete linearisation of the genomic DNA.

Agarose gel electrophoresis

A 0.8 % agarose gel was cast in 350 mL of 1× TBE containing 17.5 µL CyberSafe. The fully digested DNA was mixed with 6× blue loading dye and loaded entirely into the gel, together with 2 µL of DIG labelled ladder. Gels were run overnight at 60 V (after a 10-min “high-speed” pre-run at 100 V). A UV image of the gel was taken to confirm complete digestion.

Denaturation and neutralisation of the gel

The gel was transferred to 1L of a denaturing solution for 45 min, with frequent manual shaking. Following this, the gel was placed in 1L of a neutralising solution for an identical period.

Capillary transfer onto nylon membrane

Transfer was performed onto a positively charged nylon membrane using a capillary system. Prior to transfer, 1.2 L of 10× SSC was prepared used to pre-soak the membrane and filter papers. The transfer assembly comprised an inverted electrophoresis tray placed in a bigger tray which is filled with the SSC buffer and covered with a Whatman filter paper. The gel was placed on top of the wet filter paper, inverted so that the top is now on the bottom. The wetted membrane was carefully added on top of the gel ensuring

no bubles are ever present. Two 3 mm Whatman paper pads of the same size were dipped in the SSC buffer and placed on top of the membrane, followed by two stacks of kitchen towels weighted by an object of around 800g. The assembly was left overnight for the transfer to take place.

Hybridisation with DIG-labelled probes

After transfer, the membrane was rinsed briefly in 2× SSC or water (inverted, so that the DNA side faced upward) and allowed to dry on Whatman paper at room temperature. The membrane was then cross-linked in a Stratalinker (Auto-Cross-link, first a dummy run without the membrane, then a cross-linking run with the membrane). Pre-hybridisation was carried out in 20 mL of hybridisation solution in a hybridisation incubator at 47.5 °C for at least 1 h; this solution can be reused for multiple blots. A DIG-labelled probe was denatured at 95 °C for 5 min, immediately placed on ice, and then added to the pre-hybridisation solution, ensuring that the probe was fully diluted before contacting the membrane (this can be achieved by tilting the hybridization tube, adding the probe to the solution surface and swiftly mixing). Hybridisation proceeded overnight at 47.5 °C.

Washing and blocking

The membrane was first thawed from 10× blocking solution. It was then washed twice for 5 min each in 2× SSC + 0.1 % SDS at 47.5 °C, followed by two 20-min washes in 0.5× SSC + 0.1 % SDS. A brief rinse in 1× DIG wash buffer was performed, and a 1× blocking solution (10× stock diluted in maleic acid buffer, pH 7.5) was prepared and applied to block the membrane for 30 min at room temperature. An α-DIG Fab antibody was centrifuged (2000 rpm, 5 min, 5 °C), 1 µL of the supernatant collected, and diluted 1:5000 in the blocking solution; the membrane was incubated with this antibody solution for 30 min at room temperature (the antibody is not reused).

Detection

Following the antibody incubation, the membrane was washed four times for 15 min each in 1× DIG wash buffer at room temperature. It was then incubated with DIG detection

buffer for 5 min at room temperature. CDP-Star reagent (ready-to-use, stored in a cold room) was pipetted directly onto the membrane (1–1.5 mL per blot), and the reagent was spread evenly by allowing a plastic sheet to slide over the membrane. The membrane was incubated for 10 min in the dark, after which the CDP-Star solution was drained. The membrane was transferred to a new plastic sheet, left in the dark for 10 min, and subsequently exposed to either film or a CCD-based imaging system (Chemidoc). Chemiluminescence images were acquired in accumulation mode, typically one image per one minute for 10 minutes total.

Denaturing Solution	
Reagent	Total volume 1L
NaOH	16g
NaCl	35,1g
dd H_2O	to 1L

Neutralizing solution (pH7.4	
Reagent	Total volume 1L
Trizma base	121,4 g
NaCl	87,75 g
dd H_2O	to 1L

20X SSC (pH=7.0)	
Reagent	Total volume 1L
Sodium citrate	88,2 g
NaCl	175,3 g
dd H_2O	ad 1L

Hybridization Solution	
Reagent	Total volume 20mL
Formamide	10mL
20x SSC	5mL
50x Denhardt`s sol.	2mL
0,5M EDTA	0.2mL
1M PIPES pH 6.4	0.2mL
yeast RNA	8 mg in 0.8mL ddH2O
10% SDS (add last)	2mL

5x DIG-wash buffer pH 7.5	
Reagent	Total volume 1L
Maleic acid	58g
NaCl	43.8g
Tween-20	15mL

Maleic acid buffer pH 7.5	
Reagent	Total volume 1L
Maleic acid	11.67g
NaCl	8.76g

DIG-detection buffer pH 9.5	
Reagent	Total volume 1L
Tris, HCl	15.8g
NaCl	5.8g

Table 8: Southern blot buffers

2.13 RNA extraction

Yeast overnight cultures were prepared and their optical density at 600 nm (OD_{600}) was measured. The cultures were then diluted to a final volume of 20 mL and an OD_{600} of 0.2

in YPD medium. The diluted cultures were incubated at 30°C until the OD_{600} reached 0.6-1. After reaching the desired OD_{600}, the cells were harvested by centrifugation at 13,000 x g for 5 minutes at 4°C. The supernatant was discarded, and the cell pellet was transferred to a 1.5 mL tube. The cells were then re-suspended in 400 µL AE buffer. To lyse the cells, 40 µL of 10% w/v SDS and 500 µL of equilibrated phenol were added to the tube, and the solution was thoroughly mixed. The tube was incubated at 65°C for 5 minutes, followed by 5 minutes on ice. Next, the samples were centrifuged at 18,000 x g for 3 minutes at 4°C, and the aqueous phase was carefully transferred to a new 1.5 mL tube. To further purify the RNA, 500 µL of PCI (phenol: chloroform: isoamyl alcohol) was added to the tube and incubated at room temperature for 5 minutes. The samples were centrifuged again at 18,000 x g for 3 minutes at 4°C, and the aqueous phase was transferred to a new 1.5 mL tube. Then, 40 µL of a 3N sodium acetate solution with a pH of 5.3 was added to the aqueous phase and thoroughly mixed. Nucleic acids were precipitated by adding 1 mL of pre-cooled (-20°C) ethanol and incubating the tube on ice for 20 minutes. Following centrifugation at 18,000 g for 3 minutes at 4°C, the resulting pellet was washed with 80% v/v ethanol and left to air dry at room temperature for 5 minutes. The pellet was subsequently incubated with 87 µL of RNase-free water, 3 µL of DNase 3U/µL, and 10 µL of DNase RDD buffer from the RNAse-free DNase Kit at 37°C for 30 minutes. Finally, the RNA concentration was measured using a Nanodrop spectrophotometer, and 50 µg of RNA was purified using the RNeasy MinElute Kit with an elution volume of 38 µL H2O. 25mL of phenol were added in a 50 ml Tube and placed in warm water to melt. The phenol was then washed with an equal volume of AE buffer 3 times, the aqueous phase was removed and the pH was confirmed to be 5.3. AE buffer was an aqueous solution of Sodium acetate to a final concentration of 50 mN, 10 mN EDTA and pH 5.3. Extracted RNA was stored at -80 °C.

2.14 cDNA synthesis

For the cDNA synthesis, the reverse transcriptase Superscript III kit from Invitrogen was used. 1µg of RNA, 1µL NTPs (Invitrogen, 10 mM each) and 2µL random hexamers primers (Invitrogen, 0.2 m/µl) were mixed with 13µL $H_2O$and incubated at 65°C for 5min

and left on ice for 2 additional minutes. 7 µL of RT master-mix were added, the samples were incubated as indicated on the following table and 30µL of water were added.

Table 9: cDNA synthesis conditions

Cycling profile			RT Master-mix	
Steps	Temperature	Time	Reagent	Volume
1	25°C	5 minutes	5X first strand buffer	4µL
2	50°C	1 hour	0.1M DTT	1µL
3	75°C	15 minutes	RNAse out	1µL
			Superscript 3	1µL

2.15 qPCR

For the qPCR (quantitative reverse transcription PCR), the cDNA from 2.8 was used, after being diluted to a final volume of 50 µl. 1 µg RNA was also diluted to 50µl and used as a negative control. The PCR was carried out in 384 well plates using the CFX Real-Time PCR cycler with 384 well add-in from BioRad. The reaction consistency and cycling program are shown on

Reagent	Volume
Water	0,9µL
Primer 1 100 µM stock	0.05 µL
Primer 2 100 µM stock	0.05 µL
Evagreen	5 µL
blue dye	0.05 µL
In each sample, 4µL of cDNA were added after the distribution of the mastermix	

Table 10 and had a total volume of 10 µl per well. The PCR plate was sealed using Microseal® 'B' PCR Plate Sealing Film and the spun down shortly. For the qPCR routine, the initial denaturation takes part at 95°C for 10 minutes, subsequently followed by 40

cycles of 15 s at 95°C and 1 minute at 60°C. The melting curves were measured from 65.0°C to 96.5°C in 0.5°C increments.

The qPCR results were analyzed using the Bio-Rad RFX Manager software. The cq determination method was set to ‘regression’ and the data was exported. The final analysis was carried out in Excel. The mean of the technical replicates was calculated and values for the housekeeping gene were subtracted.

Reagent	Volume
Water	0,9µL
Primer 1 100 µM stock	0.05 µL
Primer 2 100 µM stock	0.05 µL
Evagreen	5 µL
blue dye	0.05 µL
In each sample, 4µL of cDNA were added after the distribution of the mastermix	

Table 10: qPCR reagents

2.16 Measurement of TDP43 intensity in cells, with Fiji.

Yeast cultures carrying the GAL induced TDP43-GFP overexpression construct were grown in synthetic medium supplemented with raffinose, to saturation, then diluted to an OD_{600} of 0.1 in SC medium containing 2 % galactose and cultured at 30 °C for 6 h to induce over-expression of TDP43-GFP. Induction was halted by adding 2 % glucose, while simultaneously introducing taurine (to a final concentration of 0.5M). Fluorescence images were acquired with an Echo Revolve microscope at 0.5, 1.5, and 4.5 h after glucose addition, using identical exposure settings for bright-field and GFP channels. In Fiji, a custom macro processed the bright-field images to segment cells (enhance contrast, convert to mask, watershed, and analyze particles) and another macro measured GFP mean intensity and integrated density for the ROIs defined by the cell masks. Raw intensity results were compiled into CSV files and imported into GraphPad Prism, where mean fluorescence values were plotted as bar graphs with standard error bars for each time point, enabling comparison between the taurine-treated and untreated groups.

2.17 Genome wide screenings / analysis

All yeast strains used were taken from the commercially available libraries and were cultured in YPD plates and at 30 ºC, unless differentially indicated.

The screening of the TS library was conducted on YPD plates supplemented with G418, in 1536-colony plate format. This allowed for four technical replicates placed next to each other in a 4-colony square. To correct for regional bias along the plate, control strains were grown in between experimental samples, so that there is always a local, normal-growing strain (*bar1*) to compare to. After the plate layout was constructed and the colonies grew (24h), all plates were repined on control and taurine supplemented plates, before being placed at different temperatures (23°C, 27°C, 30°C, 32°C, 34°C and 37°C). Following an incubation time of 24h and 48h, plates were imaged and analyzed by Eduardo Gameiro using custom scripts in R.

To segment the photographs and determine colony sizes, the published gitter package was utilized. For the plate manipulation a pinning robot was used (Rotor, Singer Instruments) and for the imaging a colony imager (Phenobooth, Singer Instruments). Leveraging on the presence of local controls along the plate, measurements were normalized to the local control quadrants. The four sides of the plates were also control strains (to avoid differential colony growth due to higher nutrient availability on the rim), and were subsequently excluded from the analysis. Following this, the size median of the control strains was calculated per plate, and was used to normalize the experimental strains to avoid plate variability. Finally, to compensate for plate topology effects, all measurements were further normalized to the median of the local control strain, and the mean value and standard deviation for each measurement was noted.

To compare the growth of strains at each temperature, the normalized colony sizes of + and – Taurine samples were compared with a two-sided t-test and p-values were adjusted for multiple testing using the Benjamini-Hochberg method. A strain was characterized as rescued if size(*Taurine*$^-$)/size(*Taurine*$^+$) < 0.8 and p-value < 0.05. In some cases, the colonies were very small for reliable results to be gained, hence the aforementioned analysis only took place if: size(*Taurine*$^-$) >= 0.125 size and (*Taurine*$^+$) >= 0.25. By the nature of the screening, TS strains were measured in several temperatures. To identify

the ideal rescue temperature for each mutant, the temperature where the rescue in growth was calculated as the lowest was chosen. Finally, in an attempt to quantify the temperature sensitivity of each individual strains, the following formula was used: TSensitivity=size(*Taurine*$^-$ at a T)/size(*Taurine*$^-$ at 23°C). A strain is considered TS only if the number from the previous formula is < 0.8 for at least two consecutive temperatures.

Results

3.1 Machine learning identifies the signature of AS, and predicts novel AS mutants

It has been reported in the literature that 200 single deletion mutants have an accelerated entry into replicative senescence in the absence of telomerase. Here, we investigate the mechanisms underlying this AS (Accelerated Senescence) phenotype by comparing the mRNA expression profiles of reported AS mutants (in telomerase proficient cells) to normal senescing ones, to come up with the AS signature. Subsequently, we use this signature to identify novel AS mutants and proceed with a basic phenotypic characterization.

3.1.1 Accelerated senescence is independent of initial telomere length

If the AS mutants reported in the original publication entered senescence earlier due to pre-existing short telomeres, which leads them to stop dividing earlier than their WT counterparts. Therefore telomere length measured before telomerase ablation should be shorter in AS strains than in controls. The deletion of single KO mutants was confirmed, and performed telomere PCR on 168 AS mutants (all in telomerase-positive backgrounds). Telomere length was measured in the form of the 1L telomere (bp).

The telomere length measurement shows that these mutants have variable telomere lengths ranging from 310 bp to 470 bp (Appendix figure 1). As summarized on Figure 6, the majority of mutants had normal-sized telomeres. Some mutants had telomeres shorter than average, but there was no overall enrichment for short telomere mutants, while others had even longer than average lengths. These results suggests that inherently shorter telomeres are not the reason AS mutants senesce faster, and there might be some other trait, common among the AS mutants, that characterizes them.

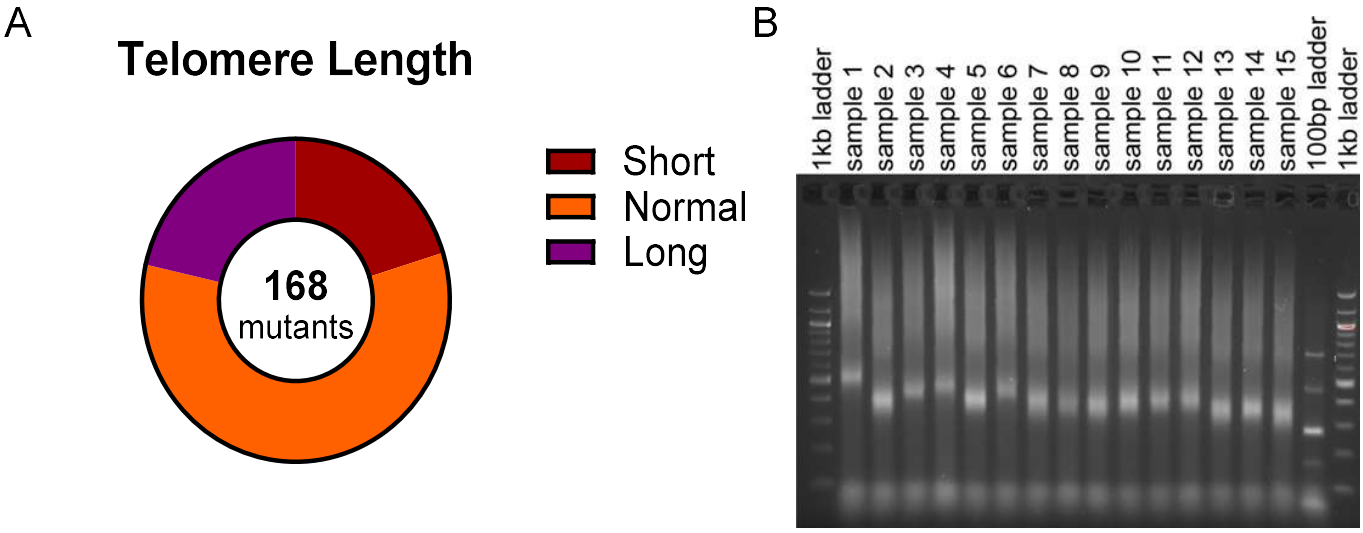

Figure 6: Telomere length measurements of AS prone mutants. A. Telomere length measurement of single KO mutants reveals no correlation with AS phenotype. Deletions mutants that exhibit AS when in a telomerase deficient background (as described by Chang et al 2011 were cultured and had their telomere length measured using telomere PCR, to determine whether this AS phenotype could arise due to cells having shorter telomeres by default. Short are telomere length measurements below 380bp, normal 380-440bp and long are above 440bp. B. representative gel showing 1L telomere bands amplified after telomere PCR. The complete list of individual mutants can be found on A1.

3.1.2 Identification and evaluation of the AS signature

Since the initial telomere length prior to telomerase deletion is not the reason the KO mutants senesce faster, we searched for commonalities among the AS mutants. Go term analysis did not show any enrichment of pathways or processes, hence we decided to look into the mRNA expression profiles of the AS mutants, in an attempt to find common mRNA expression patterns. To this extend, we utilized publicly available mRNA expression datasets of KO mutants in telomerase proficient cells, and compared the profiles of the mutants that will senesce fast if telomerase would be knocked out. To achieve this, our collaborators developed a Random Forest algorithm which was used in combination with several feature selection models, to distil an mRNA expression signature of the AS strains, in telomerase positive conditions. Subsequently, these signature components were individually investigated for being sufficient to lead to the AS phenotype manifestation.

3.1.2.1 Training of a ML model to identify the AS signature

To find commonalities among the AS mutants, we developed a Random Forest algorithm. Its purpose is to identify mRNA expression patterns in AS mutants in the presence of telomerase (non-senescing) that are not present among random, normally senescing strains. This was achieved by training a RF (Random Forest) algorithm on publicly available mRNA databases, and getting the senescence rate data from Chang et al. 2011.

Dataset assembly. We collated publicly available RNA-seq profiles from yeast strains carrying single-gene knockouts that, upon telomerase ablation, exhibit accelerated senescence (AS) according to Chang et al. 2011. The dataset contains 98 AS mutants and 98 non-AS controls, all profiled in telomerase-positive conditions. The overlap of the published datasets we were based on and used to identify the AS signature is depicted on Figure 7.

Machine-learning pipeline. Collaborators Matthias Peter under the guidance of Prof. Kathi Zarnack developed a machine learning (ML) algorithm, aiming to identify transcripts whose expression patterns differ between AS and non-AS strains. Furthermore, additional quality checks such as fivefold cross validation, they obtained an average precision > 0.83 for the control sets. Additionally by using the optimized control set with 98 AS strain and 98 control strains, they also achieved an area under the precision-recall curve (AUPRC) of 0.89. Following the model establishment, three complementary feature-selection methods, VSURF, Boruta, and TreeSHAP were applied to the RF (Random Forest) outputs, yielding a consensus set of 61 candidate genes that constitute the AS signature.

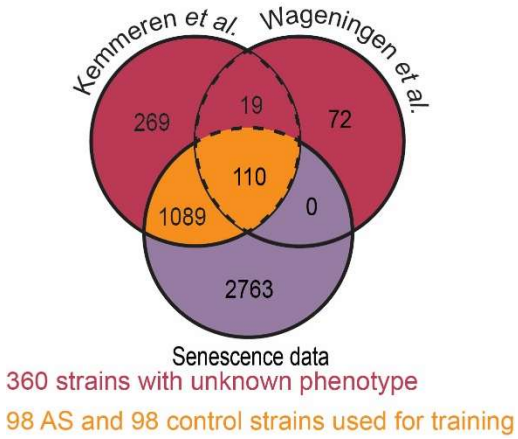

Figure 7: Venn diagram of datasets used in signature discovery. (A) AS mutants with both senescence data and expression profiles (orange); (B) mutants with only expression data (bordeaux); (C) mutants with senescence data only (purple). The intersection (orange) was used to train the RF; the other two subsets were reserved for validation.

3.1.2.2 Bna2 as a potential determinant of AS

Bna2 emerged as a promising candidate in the AS signature due to its role in tryptophan metabolism towards NAD+, but also due to the presence of two more VSURF features in the same pathway, Aro9 and Aro10. NAD+ has gotten a lot of attention from the scientific community due to its role in organismal ageing, especially after the popularity of sirt2 activation among lifespan enthusiasts. Collectively, it seemed reasonable that inhibiting with NAD+ biogenesis might be a reason the AS mutants would senesce faster. In order to determine whether this is the case, but also assess the potential role of Bna2 in telomere biology, a series of pilot experiments was conducted as shown on Figure 8.

To test whether AS mutants affect telomere protection, we crossed each AS deletion with the temperature-sensitive cdc13-1 allele (TS -allele that destabilizes telomeres at temperatures higher than 25°C). Growth at 23 °C (permissive), 27 °C (semi-permissive) and 30 °C (restrictive) was compared. However, Bna2 deletion did not seem to lead to any telomere length changes, and although *bna2* mutants seem to have improved growth

in *cdc13-1* background in most biological replicates, it became apparent that the Bna2 was an feature selection error and did not actually take part in the AS signature.

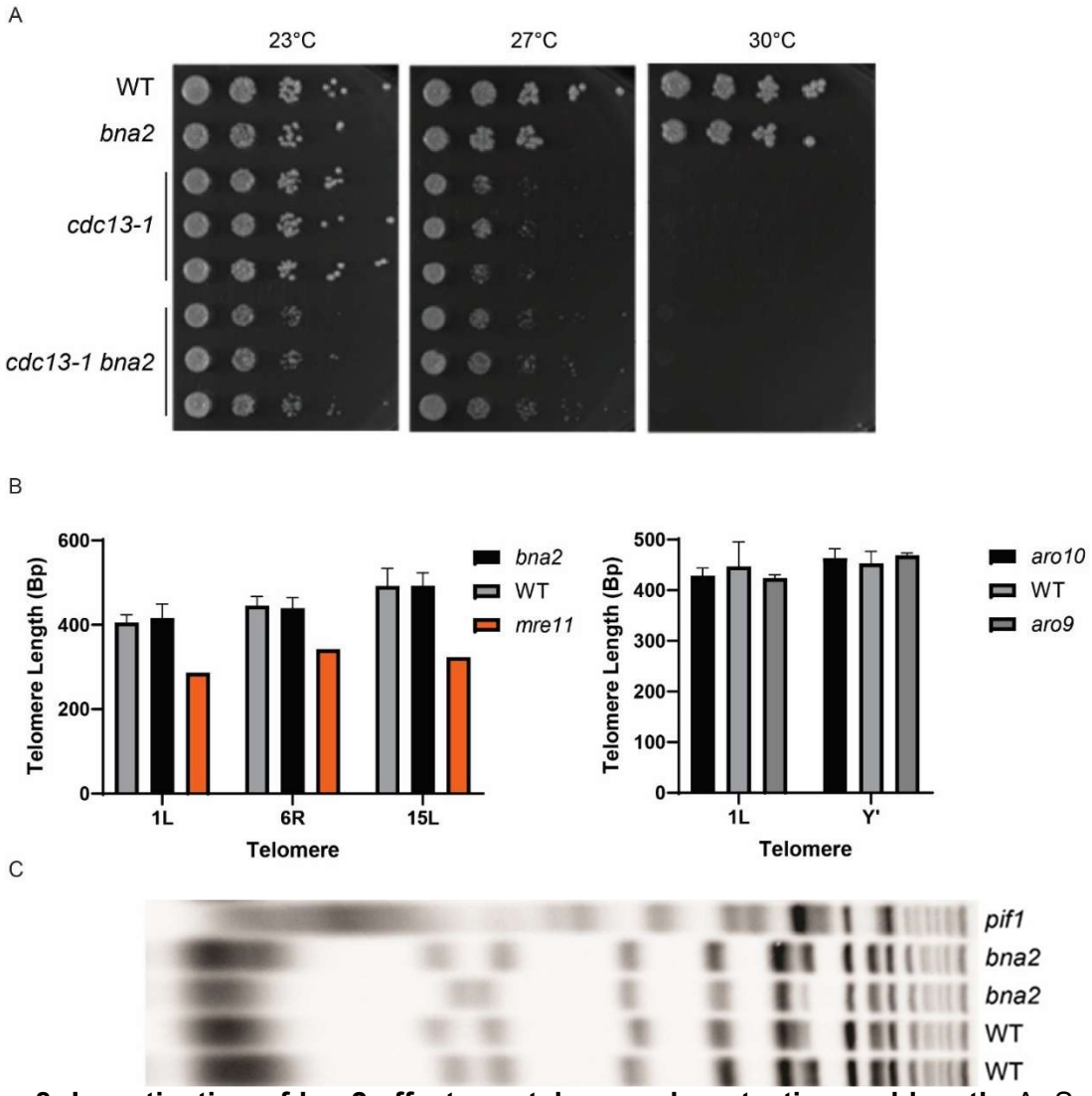

Figure 8: Investigation of bna2 effects on telomere deprotection and length. A. Spottings assay of wild type, cdc13-1, bna2 mutants and cdc13-1 bna2 mutant strains at 23 °C, 25°C and 30 °C. B. Telomere PCR results (biological replicates at least 3). C. Southern blot stained for telomeres.

3.1.2.3 Overexpression of signature genes is not sufficient to induce the AS phenotype

To evaluate whether increasing the dosage of the AS signature genes could trigger accelerated senescence, we overexpressed each of the 42 signature transcripts from a corresponding 2μ plasmid under its native promoter, to ensure at least a twofold overexpression, in a *tlc1* background. Spotting assays on YPD + 5-FOA (to purge telomerase covering plasmid) revealed no accelerated growth defect relative to the empty-vector control (Figure 9).

Phenotypic analysis of senescence rates from Figure 9 revealed that all tested mutants displayed senescence kinetics comparable to the vector control, with no consistently accelerated senescence observed across biological replicates.

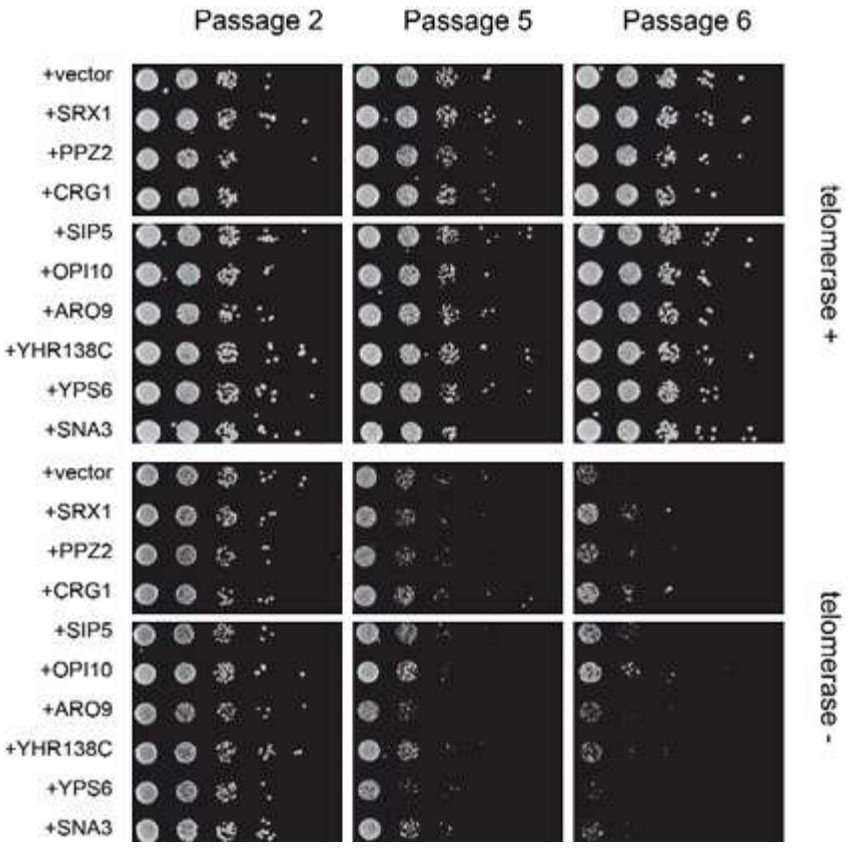

Figure 9: Overexpression of AS signature genes in telomerase negative background. Spotting assay images of different passages, showing the senescence progression among different overexpression mutants. The plates were incubated at 30°C for 2 days, and imaged with the ChemiDocTM Touch Imaging System (Bio-Rad). Full list of mutants can be seen on Appendix figure 3.

3.1.2.4 Deletion of VSURF-Selected Genes Does Not Confer AS

VSURF feature selection algorithm identified 21 transcripts that were consistently up-regulated in AS mutants. Having previously shown that the overexpression of individual AS signature genes does not suffice to yield the AS phenotype, we decided to investigate whether the deletion of AS signature genes leads to any measurable difference in the senescence rate of the corresponding mutants. To minimize variability due to background mutations, diploid cells heterozygous for these genes of interest and *TLC1/tlc1*, which were then tetrad-dissected to generate double deletion mutants that start from the same telomere length. These diploid cells were dissected and samples for all genotypes of each curve were isolated from a single strain (instead of using a different *tlc1* strain, different wt and different single KO mutant). These haploid mutants were subsequently tested in a liquid senescence curve assay, where cultures are diluted every 24 hours to a fixed OD_{600} number.

As shown on Figure 10, *tlc1* strains exhibit senescence between 40 and 60 population doublings, while all 21 mutants displayed senescence kinetics indistinguishable from the *tlc1* control. This finding aligns with the algorithm's prediction that the overexpression of these genes is associated with the AS phenotype.

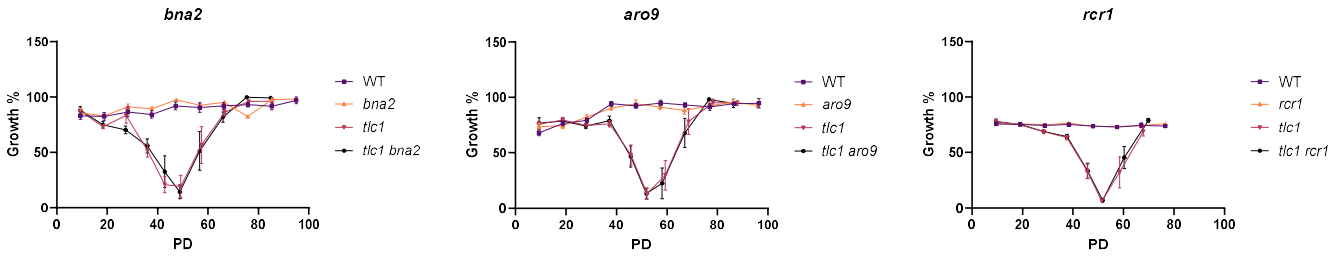

Figure 10: Deletion of VSURF selected genes does not lead to AS. There is no significant difference in the senescence rate of any mutants tested, confirming that the KO of these genes is not associated with AS. For the growth calculation, cell culture density was measured daily with the maximum measurement set to 100%. Data are shown as mean ± SEM; n≥5 biological replicates per genotype. Complete list can be found on A2.

3.1.3 The AS signature as a predictor of novel AS mutants

After demonstrating that no single component of the AS signature can independently account for the phenotype, we explored whether the entire signature is required for AS to manifest. To address this, we interrogated the remaining KO mutants in the mRNA dataset for additional mutants that exhibit the AS signature yet are not reported to induce AS in the Chang et al. study. Identified mutants were subsequently introduced into a telomerase-deficient background and subjected to experimental validation similarly to the previous ones. This approach uncovered several novel AS mutants, thereby confirming the predictive power of our model. Beyond the training dataset and the initial set of predictions, we also leveraged a secondary single-KO mRNA expression dataset. Analysis of this dataset revealed additional mutants harboring the AS signature that are likewise absent from the list of known AS-causing genes following telomerase deletion. Predictions from both datasets were then cross-examined and subjected into experimental validation, where additional novel AS mutants were reported.

These findings collectively reinforce the notion that the full AS signature is necessary for disease manifestation and demonstrate the utility of our model in uncovering previously unrecognized AS-associated genes.

3.1.3.1 From the mRNA expression data to the confirmation of novel AS mutants

Collectively, none of the individual AS signature genes was sufficient to alter the senescence rate of the corresponding mutant. However, the signature comprises multiple gene alterations that characterize the single KO mutant with AS when telomerase removed. Hence, we hypothesized that the collective presence of the signature might be required for cells to exhibit accelerated senescence. Instead of constructing multi-mutants incorporating all signature components, we turned to mRNA expression databases to identify single KO mutants displaying the AS signature but not previously reported as AS by Chang et al. 2011. On Figure 11, the workflow of our approach is summarized, and it is later reported that although individual signature components are not sufficient to lead to an accelerated entry to replicative senescence, the AS signature has subsequently been used to identify novel AS strains.

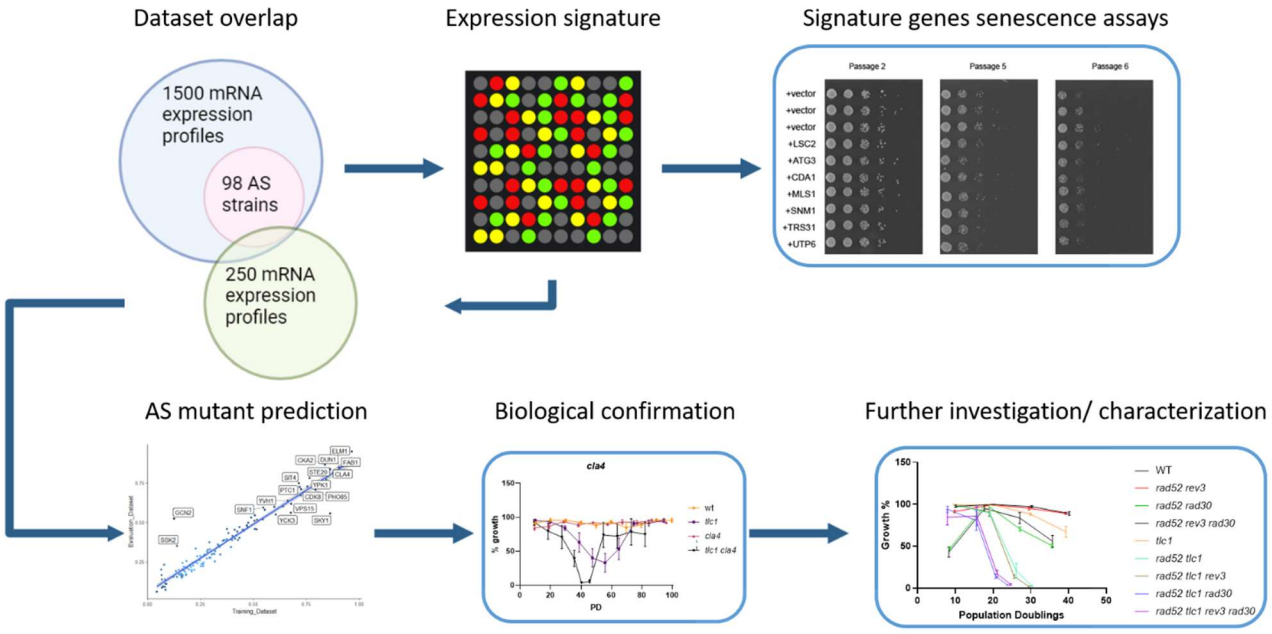

Figure 11: Schematic depicting the procedure identifying the AS signature to validating novel AS mutants. Workflow-chart followed, from the algorithm training to the confirmation of the novel AS mutants. The model was applied to identify and compare mRNA.

3.1.3.2 Confirming the AS phenotype in predicted strains not previously classified as AS

By re-examining mRNA expression profiles of KO mutants previously identified as normal senescing by Chang et al.2011, we found five that lacked characterization as AS but displayed our predicted AS signature. To verify whether these strains exhibit the AS signature on a transcript level, qPCR experiments on a subset of strains were performed. Selected transcripts of the signature were tested. The strains picked to confirm the signature (*cla4, swi6, esc2)* served as proof of concept and were selected at random, similarly to the AS signature components tested. The mRNA expression data shows an overexpression of the signature components in mutants primed to be AS. In Figure 12A, it is shown that the single KO mutants indeed have an increased expression rate of the AS signature components tested, when compared to wt cells.

Having confirmed that the predicted AS strains actually possess the randomly selected signature components, their senescence rate was measured in the lab using senescence curves. Some of these mutants, such as *bim1* or *esc2* in combination with *tlc1,* were confirmed to exhibit an accelerated entry into senescence, as shown on Figure 12, validating the algorithm's predictions.

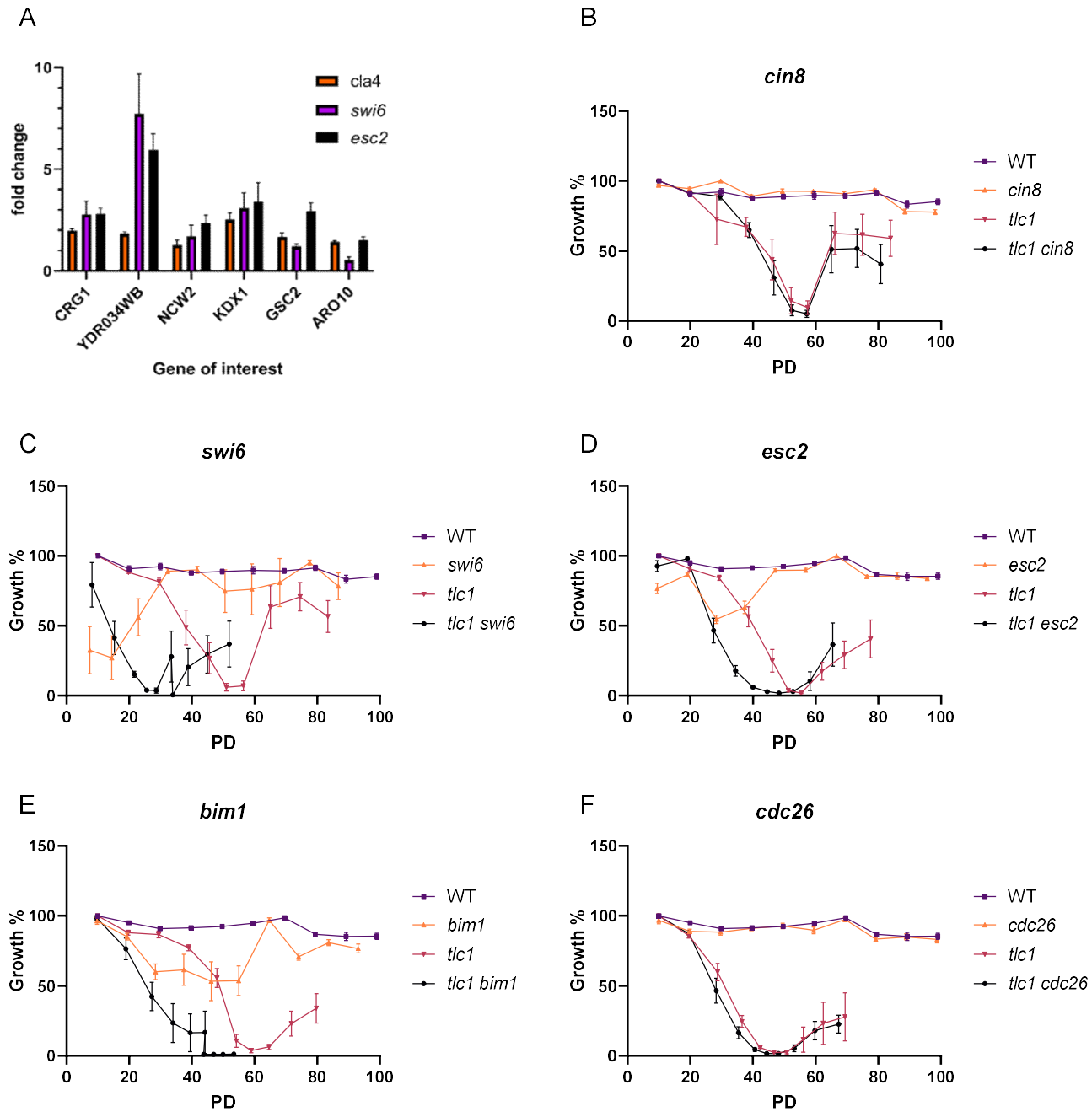

Figure 12:A. Plot summarizing qPCR results from the signature confirmation. Signature components (X-axis) are upregulated among the AS mutants (the values are ΔΔct, with normalization to the WT controls). Data are shown as mean ± SEM; n≥3 biological replicates per sample. B. Senescence curves of strains possessing the AS signature, albeit previously reported to not be AS. As shown above, 3 out of 5 show an accelerated entry into senescence in spite of not being reported to do so.

3.1.3.3 Aggregate Probability Curve facilitates the prediction of novel AS strains

Upon confirming that the AS signature is a reliable predictor of the AS phenotype, we looked for mRNA profiles of single KO mutants in the training dataset and an additional similar dataset and identify mutants that possess the newly characterized AS signature but have not been reported by Chang et al. 2011 to be AS. We discovered that several mutants not initially reported as AS, possessed the AS signature, which led us to question whether these mutants senesce in an accelerated manner or not. These candidates were ranked based on probability scores derived from the respective mRNA datasets, and the results were plotted for easy visualization on Figure 13, validating predictions with both mRNA expression datasets. This visualization allows us to identify mutants with the higher probability to be AS, along with the mutants that are predicted to senesce in a normal manner.

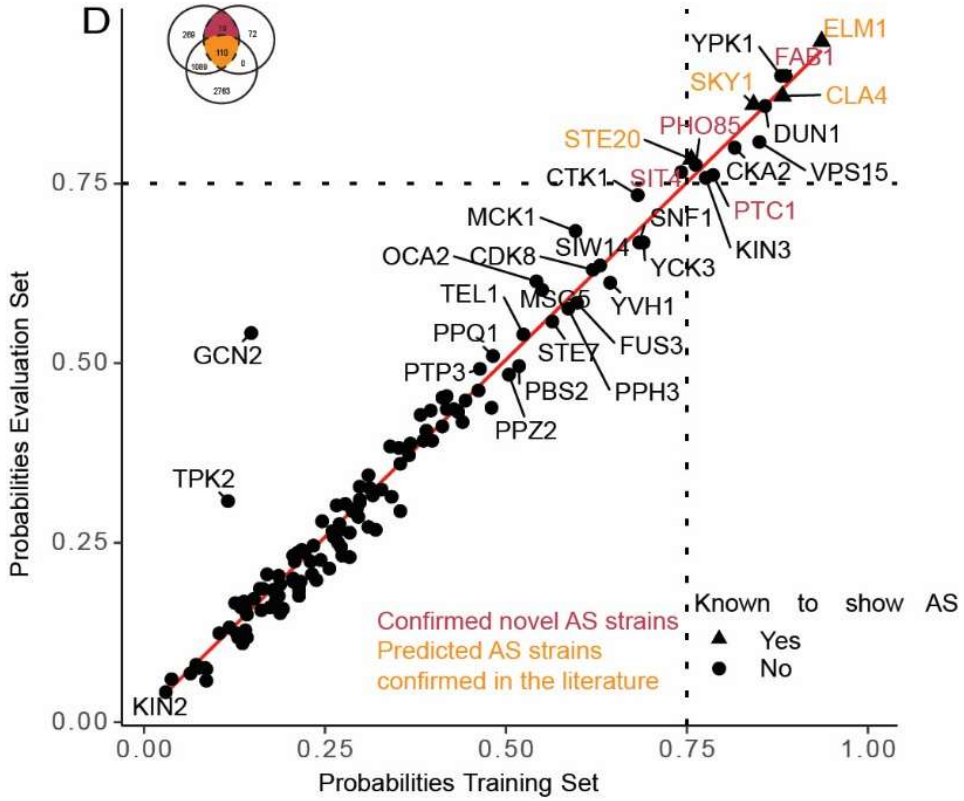

Figure 13: Aggregate Probability Curve. Algorithm predictions were plotted on a curve, where the X-axis represents the probability of each strain to be rad52-like based on the training set, and the Y-axis shows the corresponding probability based on the evaluation dataset (which included additional mRNA expression profiles). Strains colored orange are part of the training dataset but were not reported as AS. Mutants colored bordeaux are strains for which we had no data on their senescence rate status, as they were not included in the training dataset. Figure was generated by Matthias Peter for his MSc thesis and adapted for clarity.

3.1.3.4 Confirmation of the AS phenotype in predicted AS strains

Having validated the algorithm's ability to predict AS strains, we proceeded to predict more AS strains that were not labeled to be AS in the Chang et al. 2011 original publication. Upon experimentally testing them using senescence curves (

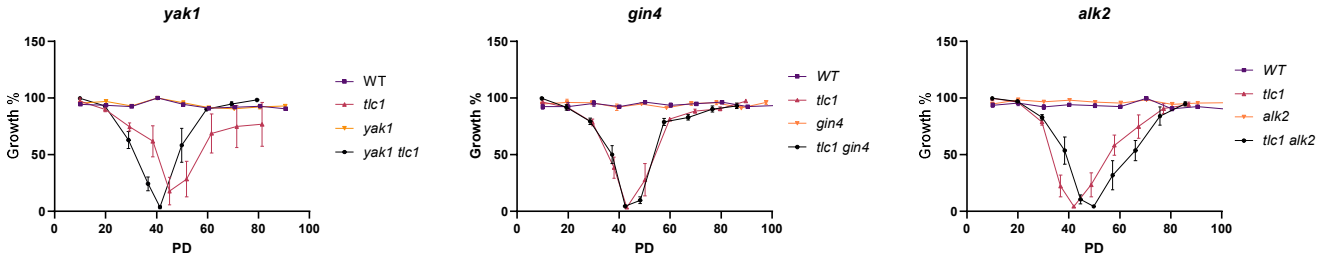

Figure 14A), we concluded that around half of the strains predicted to be AS were confirmed, while only one of the predicted control strains exhibited a *rad52*-like phenotype. Subsequently, we leveraged additional microarray datasets to identify single KO mutants that exhibit the AS signature. We then categorized these mutants based on their degree of similarity to the AS signature and selected 12 strains with high probability (the most likely to be AS) and 12 strains with low probability (the least likely to be AS) for further testing (Figure 12). Our analysis revealed that more than half of the mutants with the AS signature were experimentally confirmed to be AS, while only one mutant not predicted to be AS was a false negative (

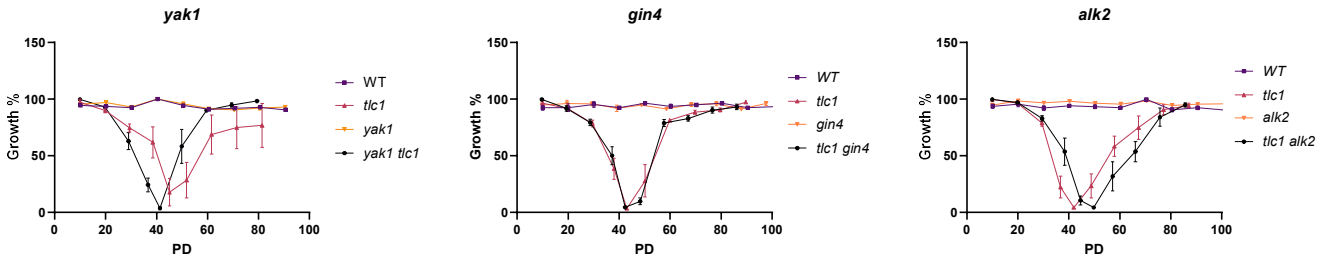

Figure 14B). It is noteworthy that in the original publication, the AS strains were termed “rad52-like cells” as they had a senescence phenotype similar to *rad52* cells. Since our method is based on that study, the AS strains we report here are technically *rad52*-like which usually is accompanied by an accelerated entry into senescence but not necessarily, as in the case of *elm1* which although it does not senesce faster, it has

impaired survivor formation, which is in-line with the *rad52* phenotype. Whereas many times they are also senescing in an accelerated manner, AS is only one aspect of the *rad52* phenotype, and there are other strains likely do have a *rad52*-like phenotype but not senesce in an accelerated manner.

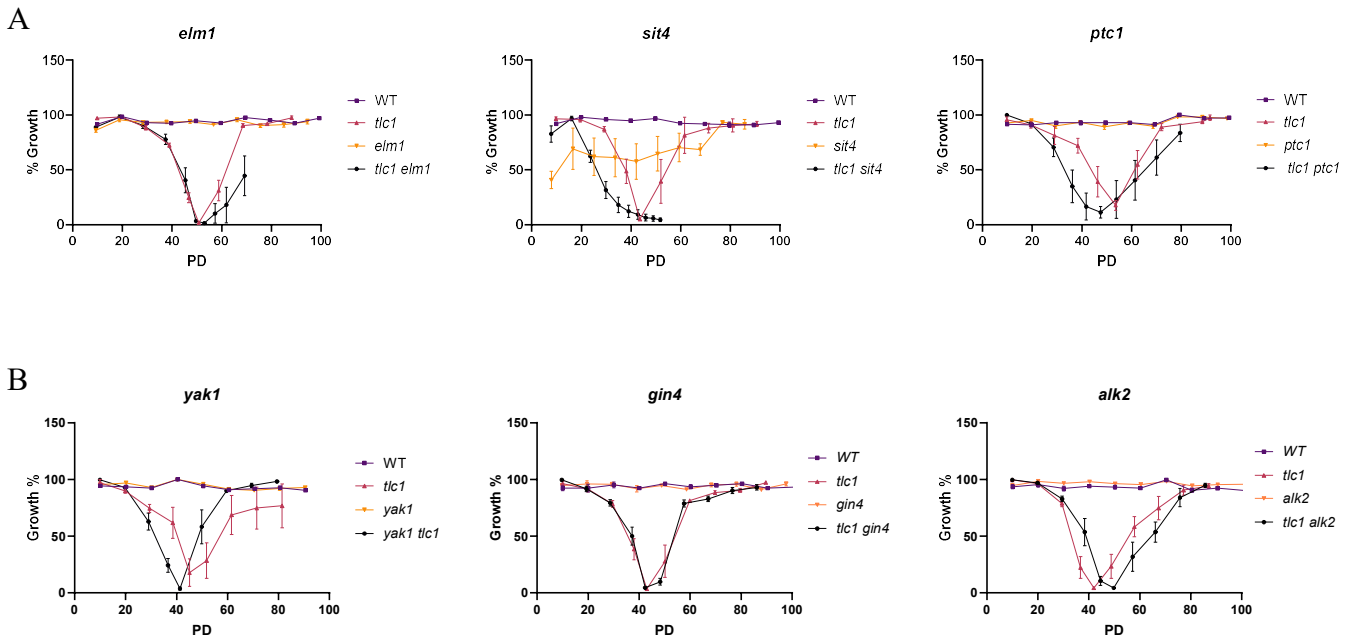

Figure 14: Senescence curve validation of model predictions. A. senescence curves of strains predicted to be AS. Full list of mutants tested can be seen at A4. B. Senescence curves of strains not having the AS signature and thus predicted to senesce normally. Data are shown as mean ± SEM; n≥5 biological replicates per genotype. Full list of mutants tested can be seen at A5.

3.1.4 Mechanistic insights on novel AS mutants

Using our model, we characterized the mRNA signature of accelerated senescence (AS) and leveraged it to predict and discover novel AS mutants. Yet, the underlying reason why these mutants enter replicative senescence so rapidly remains poorly understood. To uncover shared mechanistic features among AS mutants, we performed a series of targeted experiments: telomere shortening-rate assays, MMS exposure, and additivity

tests involving *rad52* or the temperature-sensitive *cdc13-1* allele. Although critically short telomeres trigger senescence, the rate at which telomeres shorten, rather than their initial length alone, determines which cell reaches the threshold first. In the next section, it is show that not all AS mutants exhibit accelerated telomere erosion, indicating that multiple, telomere-independent pathways can drive AS. A plausible explanation to why they are senescing fast then is that the cells are primed to be AS, due to them being already over encumbered with DNA damage or other dysfunctions, and the added burden of telomeric attrition pushes them to senesce faster than non-primed counterparts. To probe this further, we repeated the senescence-rate measurements in a *rad52* background, which is defective in homologous recombination and senesces rapidly, to detect any additive effects. Additionally, we exposed cells to DNA damage (methyl-methanesulfonate, MMS) and to telomere deprotection conditions in the *cdc13-1* background, thereby interrogating the contribution of DNA-damage responses and telomere protection to the AS phenotype.

3.1.4.1 Telomere shortening rate

To determine whether the telomere-shortening rate is faster in AS mutants, telomere PCRs, on three time-points along the progression of a senescence curve were performed. As shown in Figure 15, in the telomerase-proficient KOs the 1L telomere length remained essentially constant, whereas the telomerase-deficient KO and control strains exhibited the expected linear decline, to different extents. Such decline is evident in the case of *esc2*, where a telomere shortening can be observed, albeit without any observable difference in the slope of the telomere-length versus population-doubling, which represents the rate of shortening. Interestingly, in some cases such as with *cla4*, there is no observable decline in telomere length for the measurement time window, whereas there is a rapid decline in growth, for the same population doublings, as shown on the corresponding senescence curve.

Collectively, there seems to be no trend among the mutants tested, with the shortening rate being very similar between the AS mutant and the plain *tlc1* cells. This indicates a mechanism of action different from the one of telomeric attrition, raising the question

whether it is not the telomere length per-se that dictates the entry into AS, rather than the telomere state.

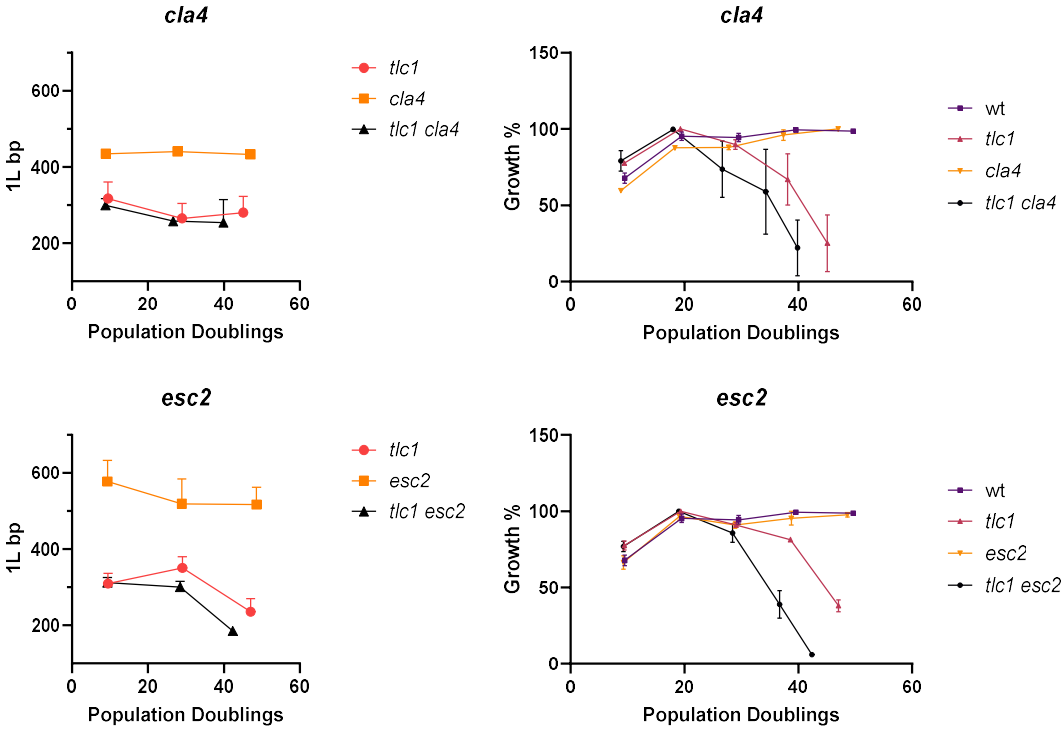

Figure 15: Telomere shortening measurements along the course of senescence.
On the left, 1L telomere length (bp) plotted against population doublings (PD), along with the corresponding senescence curve of novel AS mutants on the right. Data are shown as mean ± SEM; n≥5 biological replicates per genotype. The complete list of mutants can be seen on A9.

3.1.4.2 The AS phenotype is additive with rad52

Thus far, we have developed an algorithm able to extrapolate an mRNA signature of AS, based on the mRNA expression profiles of single KO mutants that do not senesce. This suggests that these mutants are predisposed to senesce in an accelerated manner once telomerase stops being active.

To test whether AS mutants act through a mechanism distinct from homologous recombination, we examined senescence in a *rad52* background. In a wild-type strain, *tlc1* causes senescence at ~30 PD. Deletion of RAD52 alone accelerates the onset of growth deterioration to ~20 PD. When we combined *rad52* with each of the novel AS mutants, in some cases senescence rate did not change, and in some other cases it accelerated further to ~10 PD as shown on Figure 16. This additive effect indicates that AS mechanisms are not shared among all mutants tested, and in some cases it operates in a pathway separate from RAD52-mediated DNA repair.

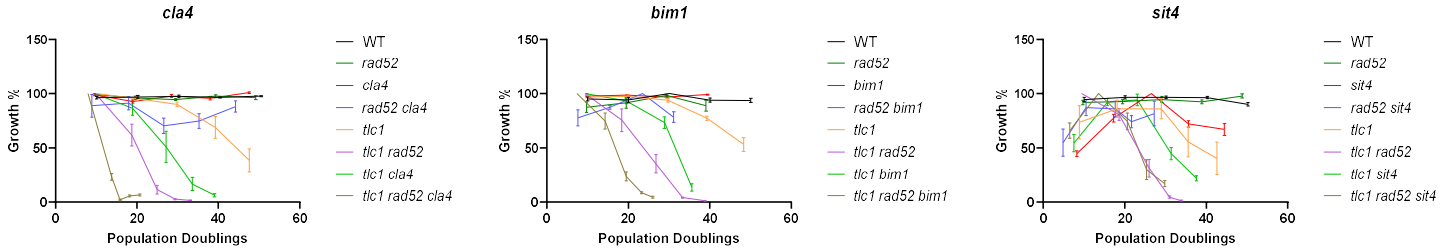

Figure 16: Senescence curves with AS mutants in a *rad52* background. Senescence curves performed in the absence of RAD52. Data are shown as mean ± SEM; n≥5 biological replicates per genotype. Full list of mutants tested can be seen on A6.

3.1.4.3 Single KO mutants are not susceptible to MMS, but might be additive to rad52

We assessed the DNA-damage response of AS mutants by spot-testing growth on YPD plates containing 0–0.004% (v/v) methyl-methanesulfonate (MMS), to determine whether the accelerated senescence in these cells is due to their impaired ability to handle DNA damage. All single-gene deletions showed growth comparable to wild type, indicating no MMS hypersensitivity. In contrast, the *rad52* strain was markedly sensitive. Combining *rad52* with *cla4*, *esc2*, or *bim1* further reduced viability compared with *rad52* alone (Figure

17). This suggests that the AS mutants do not compromise homologous recombination per se, because their single deletions are MMS-tolerant.

In the MMS sensitivity tests, some *rad52* single and double mutants showed variable sensitivity among the biological replicates. This attenuation is most likely due to strain-specific background mutations that reduce MMS sensitivity. Importantly, the single *esc2* and *bim1* mutants themselves were not MMS-hypersensitive, indicating that these genes do not impair homologous recombination (HR). Consequently, the additive effect observed in the *rad52* background is unlikely to result from a reduction in HR activity but may reflect an unrelated mechanism or stem from the lack of sensitivity combined with high variability among biological replicates.

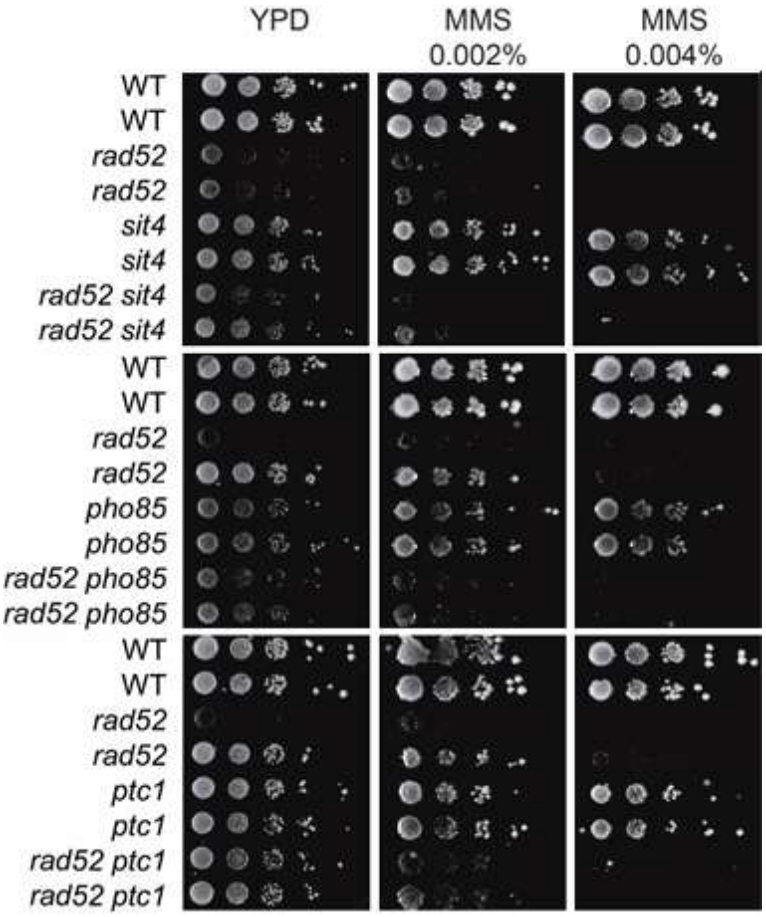

Figure 17: MMS sensitivity spottings. Spottings done on YPD plates supplemented with different MMS concentrations. Plates were incubated at 30 °C for 48h. Differences in MMS sensitivity for the rad52Δ × esc2Δ and rad52Δ × bim1Δ strains may be caused by background mutations. Full list of mutants tested can be seen at A7.

3.1.4.4 Single KO AS mutants are not sensitive to telomere deprotection via cdc13-1

To test whether AS mutants affect telomere protection, each AS deletion was crossed with the temperature-sensitive *cdc13-1* allele. In all cases except *pho85*, the double mutants displayed the same growth defect as *cdc13-1* alone, as shown on

Figure **18**. *pho85* yielded a slight phenotypic rescue at 25 °C, consistent among biological replicates. Although the extent of telomere deprotection varied between experiments, suggesting that background suppressors may emerge, the overall trend is that none of the AS gene deletions markedly alter the survival of the *cdc13-1* mutant. Thus, our data support the conclusion that the AS pathway does not influence telomere protection, reinforcing the notion that AS functions independently of telomere maintenance.

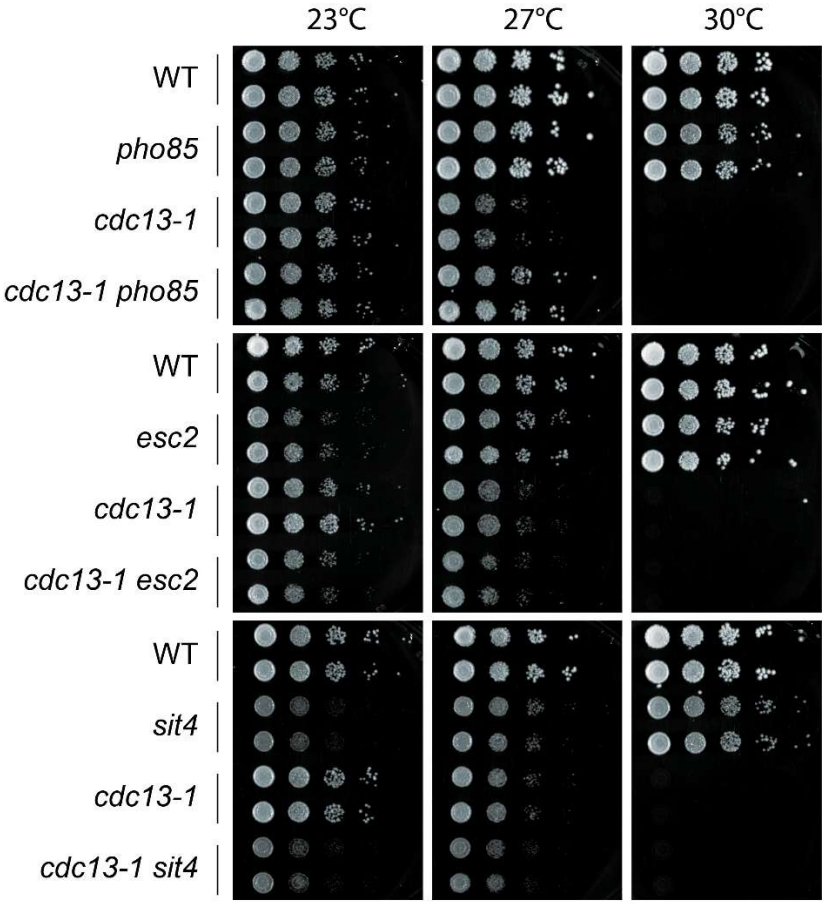

Figure 18: Spottings under telomere deprotection conditions. Spottings assay of wild type, *cdc13-1*, single KO AS mutants and *cdc13-1* × AS mutant strains at 23 °C, 25°C and 27 °C . Strains were grown on YPD, images were acquired after 48h. Full list of mutants tested can be seen on A8.

3.1.4.5 The AS of the predicted mutants is independent of Rad52

In our analyses of senescence, MMS sensitivity, and telomere deprotection, the majority of AS mutants behaved in a manner that does not depend on RAD52. When combined with a *rad52* background, most AS deletions exhibited an additive effect on senescence rate (Table 11), except for *sit4*, which showed an epistatic (non-additive) interaction. None of the AS single KO mutants displayed inherent MMS hypersensitivity in the concentrations tested. In the *rad52* background, only *cla4* and *bim1* appeared to reduce the cells' resistance to MMS, while *esc2* had a very slight effect. Upon exposure to telomere-deprotection (the *cdc13-1* allele), the survival of the AS mutants was largely indistinguishable from that of cdc13-1 alone; the only noticeable deviation was a slight rescue in the *pho85* strain. Taken together, the data indicate that the accelerated-senescence phenotype operates independently of RAD52-mediated homologous recombination and telomere-deprotection mechanisms.

Gene deletion	Senescence rate with *rad52*	MMS sensitivity	Additivity with *rad52* in MMS	*Cdc13-1* phenotype
PTC1	Additive	No	No	
PHO85	Additive	No	No	Slight rescue
FAB1	Additive	No	No	No
CLA4	Additive	No	Yes	No
SIT4	Epistatic	No	No	No
ESC2	Additive	No	Slightly	No
BIM1	Additive	No	Additive	No

Table 11: Summary of the results from Figures14, 15 and 16. Additive: senescence rate is more severe than either single mutant alone. Epistatic: combined mutant shows the same phenotype as the rad52 single mutant. No: no measurable change in MMS sensitivity or cdc13-1 phenotype. Slightly affected: a subtle, but reproducible reduction in MMS resistance. Slight rescue: cdc13-1 growth is marginally better in the double mutant

3.2 Investigation of the mechanisms underlying taurine's effects on lifespan using yeast as a model

3.2.1 Effects of Taurine on Yeast Viability and Lifespan

Although taurine has been shown to not lead to any difference in the budding yeast lifespan, we wanted to investigate the effects of taurine on the replicative lifespan of yeast, in telomerase deficient cells. In addition, we report that taurine supplementation was able to raise the maximum temperature in which WT yeast cells can grow, indicating that although *S. cerevisiae* does not have annotations for taurine import nor biogenesis, it can be benefited by taurine like other organisms, and can potentially serve as a model to study how taurine impacts cells.

3.2.1.1 Taurine supplementation does not increase the replicative lifespan of yeast

While taurine has been shown to prolong lifespan in a variety of organisms—from C. elegans to mammals, it was initially reported to not alter the lifespan of budding yeast. In contrast to these organisms which are generally telomerase negative, *S. cerevisiae* is a telomerase positive organism. Additionally, budding yeast has a cell wall which makes the uptake of molecules more difficult. A representative example is the case of Hydroxyurea, which's concentration is required to be orders of magnitude higher than the concentrations used in mammalian cells, which is additive to the fact that the concentrations used by Singh et al. 2023 were much lower than the normal taurine concentrations in several mammalian tissues. Taking these into consideration, we hypothesized that, like these other organisms, taurine might have a beneficial effect on lifespan in telomerase-deficient yeast, in higher concentrations. However, even at higher concentrations, we found no evidence to support this hypothesis, as taurine supplementation did not increase the replicative lifespan of yeast cells, as shown on *Figure 19*.

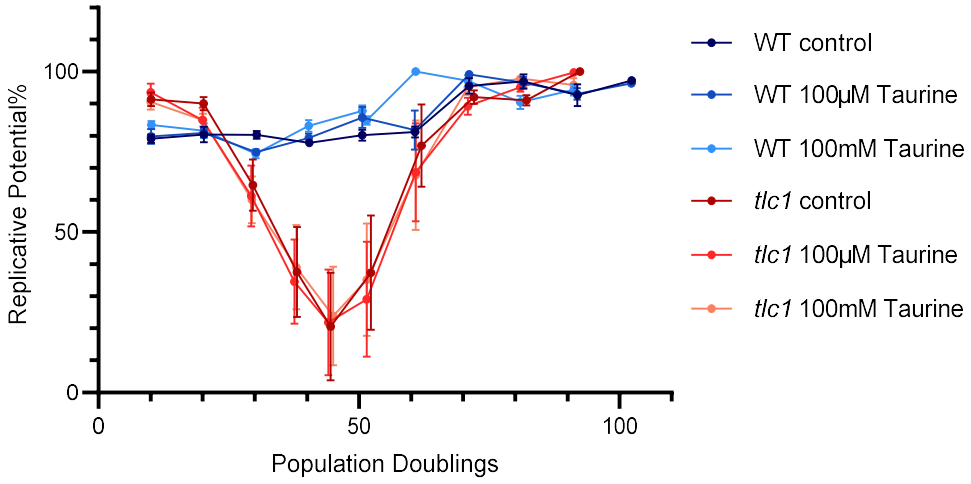

Figure 19: Senescence curve in medium supplemented with taurine. Senescence curve performed by Franziska Roithner in the framework of her Bachelor thesis with me. Data are shown as mean ± SEM; n≥5 biological replicates per genotype.

3.2.1.2 Taurine improves growth of WT at high temperatures

Taurine is an osmolyte, similar to the ones used by several extremophiles to survive denaturing environments, such as high temperatures. To investigate whether it can also alleviate temperature sensitivity in WT (wild type) cells, a spotting assay on YPD plates containing 0 or 500 mM taurine was conducted, to test its effect on WT cells at temperatures not compatible with WT growth. As shown in Figure 20, this stands true as WT cells are able to survive when supplemented with taurine, in contrast to the plain YPD plates. These results support a general protective role for taurine under acute heat stress.

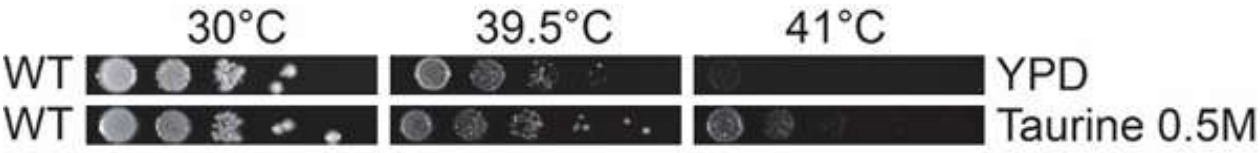

Figure 20: spotting assay of WT cells in high temperatures, with and without taurine supplementation. Wt yeast was spotted on YPD plates and incubated in different high temperatures, with and without taurine supplementation. Images were acquired after 48h.

3.2.2 Taurine's effects on DNA damage and telomere uncapping

To explore the cellular benefits of taurine and uncover any additional roles it may play, cell viability under a range of DNA-damage and stress conditions was evaluated. Specifically, *rad52* background cells were selected and exposed to various DNA-damaging agents, and subjected them to telomere-deprotection stress using the temperature-sensitive cdc13-1 allele. Remarkably, taurine produced a pronounced rescue phenotype in the cdc13-1 cells, prompting the question: does taurine act through a telomere-specific *pathway*, or is this effect part of a broader, underlying *mechanism*?

3.2.2.1 Taurine improves viability of wt and rad52 cells in the presence of Zeocin and HU

Although taurine has been tied with improvements in mitochondria function and prevention of DNA damage due to oxidative stress, we wanted to investigate whether taurine can also alleviate chemically induced DNA damage. To this extent, I conducted a series of spottings with taurine combined with different DNA damaging agents. As shown below, taurine causes a slight improvement in cell viability in the Zeocin and HU samples, but not with MMS, as shown on

Figure 21A. Interestingly, in the case of MMS, lower taurine concentration (250mM) decreases cell's viability, however it is partially restored with higher taurine concentrations (500mM) as demonstrated on

Figure 21b. These qualitative results suggest that taurine might have a mild but consistent improvement of cellular growth in WT cells treated with Zeocin and HU, but not in the case of MMS.

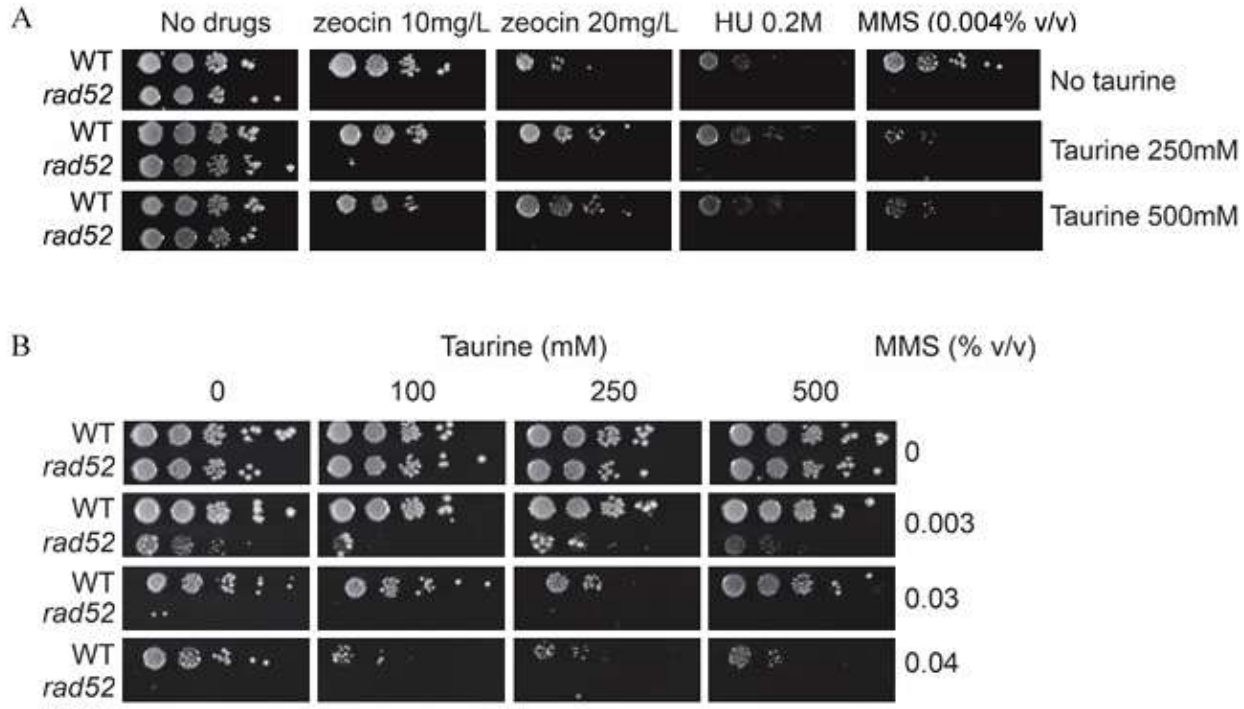

Figure 21: Spottings with combination of taurine and different DNA damaging agents. A: Spottings of WT and *rad52* cells on different DNA damaging drugs in the presence or absence of taurine. B: Spottings of taurine and MMS in various concentrations. Cells were cultured on YPD supplemented with the different drugs and taurine, and plates were incubated at 30 °C. Images were acquired 48h after spotting.

3.2.2.2 Taurine rescues telomere deprotection caused by cdc13-1

Telomere attrition is one of the primary hallmarks of ageing, and is specific to the telomeric loci instead of genome-wide DNA damage caused by chemical agents. While taurine did not increase the replicative lifespan of cells with shortening telomeres, taurine treatment could mildly improve viability of some cells treated with DNA damaging agents. Subsequently, it was of interest to investigate whether this effect would still be seen when telomeres are specifically damaged through deprotection. Interestingly, taurine has a strong rescue phenotype in cells carrying the *cdc13-1* TS allele (Figure 22), which could imply specific activity in telomeres in response to damage.

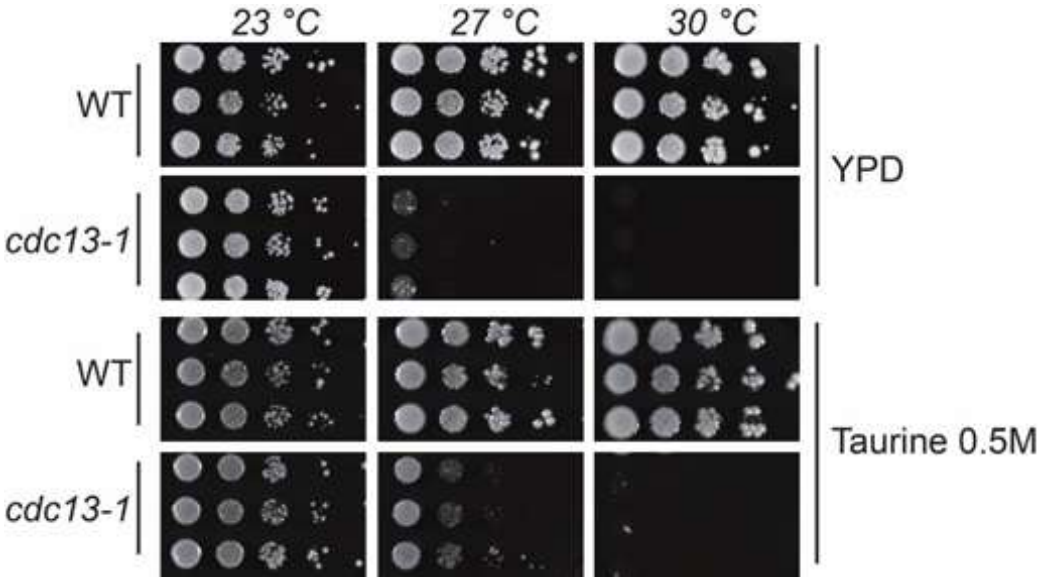

Figure 22: Spotting assays with *cdc13-1* TS (Temperature Sensitive) strains under taurine supplementation. Cells with the *cdc13*-1 mutation were cultured on YPD supplemented with taurine, and plates were incubated at variable temperatures. Images were acquired 48h after spotting.

3.2.3 Investigation of biological mechanisms underlying taurine's effects on cells suffering telomere uncapping

In order to dissect the mechanism by which taurine rescues the TS *cdc13-1* phenotype, we first examined whether its effect is epistatic with known genetic suppressors of telomere deprotection. spotting assays on a panel of such double mutants revealed that taurine markedly improves viability of several but fails to rescue *stn1-13* despite both proteins belonging to the CST complex, suggesting a cdc13-specific, rather than a general telomere-capping, mechanism. To probe the role of the DNA-damage checkpoint, an "up-down" temperature cycling assay was performed. Although taurine enhanced growth at 30 °C, it did not restore cdc13-1 rad9 viability during the oscillatory regimen, indicating that checkpoint bypass prevention is not the driver of the rescue. Parallel experiments with rapamycin and the non-proteinogenic amino acid D-alanine, which are known to impede checkpoint adaptation and structurally resemble taurine accordingly, showed that taurine and D-alanine have more similarities than taurine and rapamycin, pointing to a distinct pathway. Extending the analysis to more mutants that suppress *cdc13-1*, we found that taurine, rapamycin, and D-alanine all conferred growth benefits, however in a broader screen of TS mutants taurine's rescue was both more robust and more ubiquitous than rapamycin's, which failed to rescue most, confirming that taurine does not share its mechanism with rapamycin.

A comparative antioxidant panel confirmed that while these molecules can rescue *cdc13-1*, they are ineffective against the other temperature-sensitive mutants rescued by taurine, implying that taurine's action extends beyond generic antioxidant capacity to a more global effect. Taken together, these data converge on a model in which taurine engages a telomere-independent mechanism, beyond traditional *cdc13-1* suppressors or rapamycin.

3.2.3.1 Taurine rescue is additive to most pathways known to rescue cdc13-1

The *cdc13-1* rescue phenomenon has been thoroughly studied and characterized. If the mechanism underlying taurine's effects is biological, then taurine will be epistatic with any of the genes reported in the literature to also rescue *cdc13-1*. To rule out possible taurine roles in telomere deprotection, we had to investigate the effect of taurine on *cdc13-1* mutants carrying an additional deletion in a distinct pathway known to rescue the *cdc13-1* phenotype. Rad9 is a key player in the DNA damage checkpoint, and in its absence, *cdc13-1* cells bypass the checkpoint and continue dividing until they accumulate massive DNA damage. Upf1 is part of the nonsense-mediated mRNA decay (NMD) pathway, and indirectly affects telomere maintenance by regulating the stability of mRNAs involved in telomere capping. Exo1 is a nuclease responsible for generating single-stranded DNA (ssDNA) at uncapped telomeres. Finally, San1 is an ubiquitin ligase involved in protein quality control, San1 may play a role in degrading misfolded or damaged proteins that accumulate in the nucleus, and by deleting it the amount of *cdc13-1p* in the nucleus is higher indicating a rescuing effect. Finally, Stn1 is also part of the CST complex and essential for telomere capping and replication.

As evident on Figure 23, taurine can improve some mutants' viability such as *upf1 and exo1,* but this is not apparent in the case of *rad9* or *san1*. Interestingly, although taurine rescues *cdc13-1*, and both cdc13 and stn1 are parts of the CST complex, it is not rescuing *stn1-13*, indicating that there is something specific with the cdc13-1 that stn1-13 doesn't have.

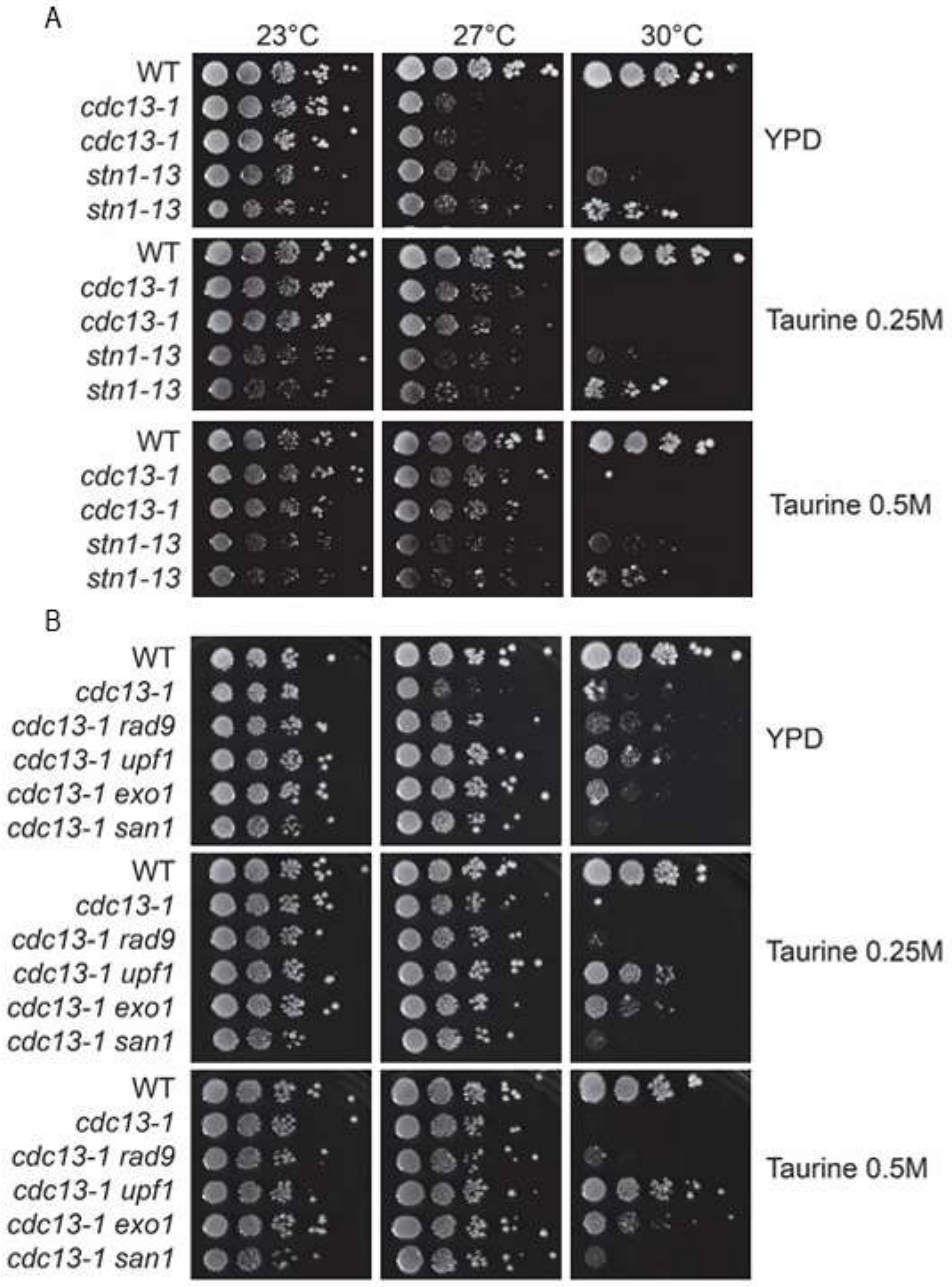

Figure 23: Spotting assays of mutants of different backgrounds in the presence of taurine. A. Spotting assay on variable taurine concentrations show a dose dependent increase in the rescue degree in some of the mutants tested. B. Spotting assay of double mutants known to suppress the *cdc13*-1 temperature sensitivity, in combination with taurine. Plates were incubated at designated temperatures and images were acquired 48h post spotting. Figure 24: Spottings of two telomere maintenance mutants in the presence or absence of taurine, in various temperatures and concentrations. Cells were culture at the designated temperatures in YPD supplemented with different taurine concentrations. Images were acquired after 48h.

3.2.3.2 Rapamycin and D-alanine share taurine's effects and are not epistatic with rad9

In order to further understand whether taurine improves growth of *cdc13-1 rad9* cells, and to see how it affects them we proceeded with an up-down assay. Here, temperatures oscillate between permissive and non-permissive temperatures and *cdc13-1 rad9* cells fail to grow normally. This is expected, as they do not have a functional checkpoint, they proceed to divide with massive amounts of DNA damage leading to cell death. In contrast, *cdc13-1* cells arrest at high temperatures and continue growing at permissive temperatures, ultimately outgrowing the *cdc13-1 rad9* cells. In the case of *exo1 cdc13-1*, cells grow even faster because they don't have long DNA overhangs and can exit arrest faster than *cdc13-1* cells. On

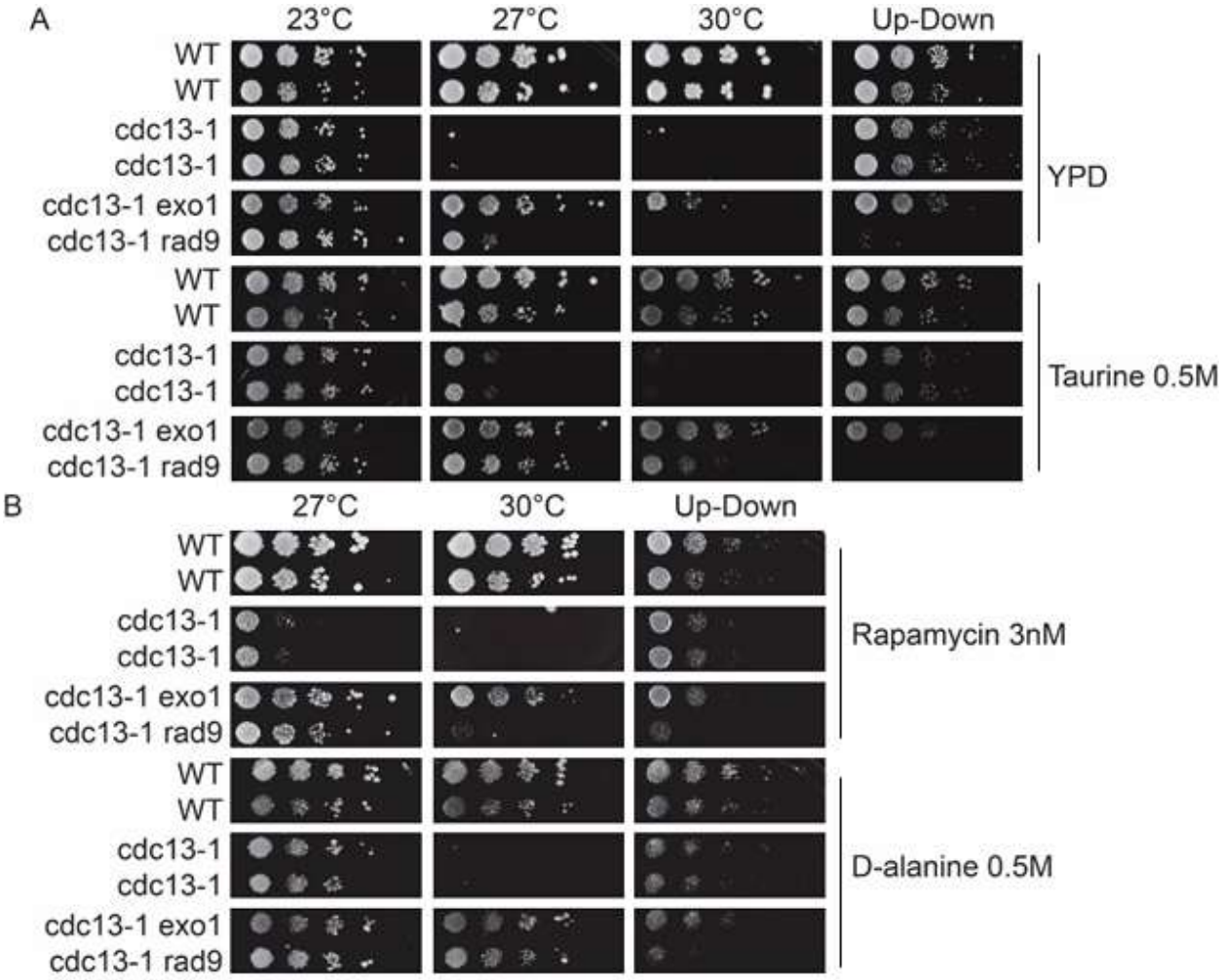

Figure **25** panel A, it is evident that taurine improves the growth of *cdc13-1 rad9* and *cdc13-1 exo1* at 30 °C but does not lead to increased growth of the *cdc13-1 rad9* cells in the Up-down assay, indicating a separate mechanism of function. On panel B, we utilized

two different molecules, to spot potential similarities between rapamycin, which is known to prevent checkpoint adaptation[7], and D-alanine which is a non- proteinogenic aminoacid while being structurally similar to taurine. It is evident that both rapamycin and D-alanine led to a *cdc13-1* rescue. Additionally, rapamycin marginally improves the *cdc13-1 rad9* viability in the Up-down assay, although since this is a qualitative method no robust conclusions can be drown from such a small difference. Additionally, at 30 °C both taurine and D-alanine show a moderate improvement in growth of both *cdc13-1 rad9* and *cdc13-1 exo1* double mutants, whereas rapamycin only improves *cdc13-1 exo1* to a much milder extend.

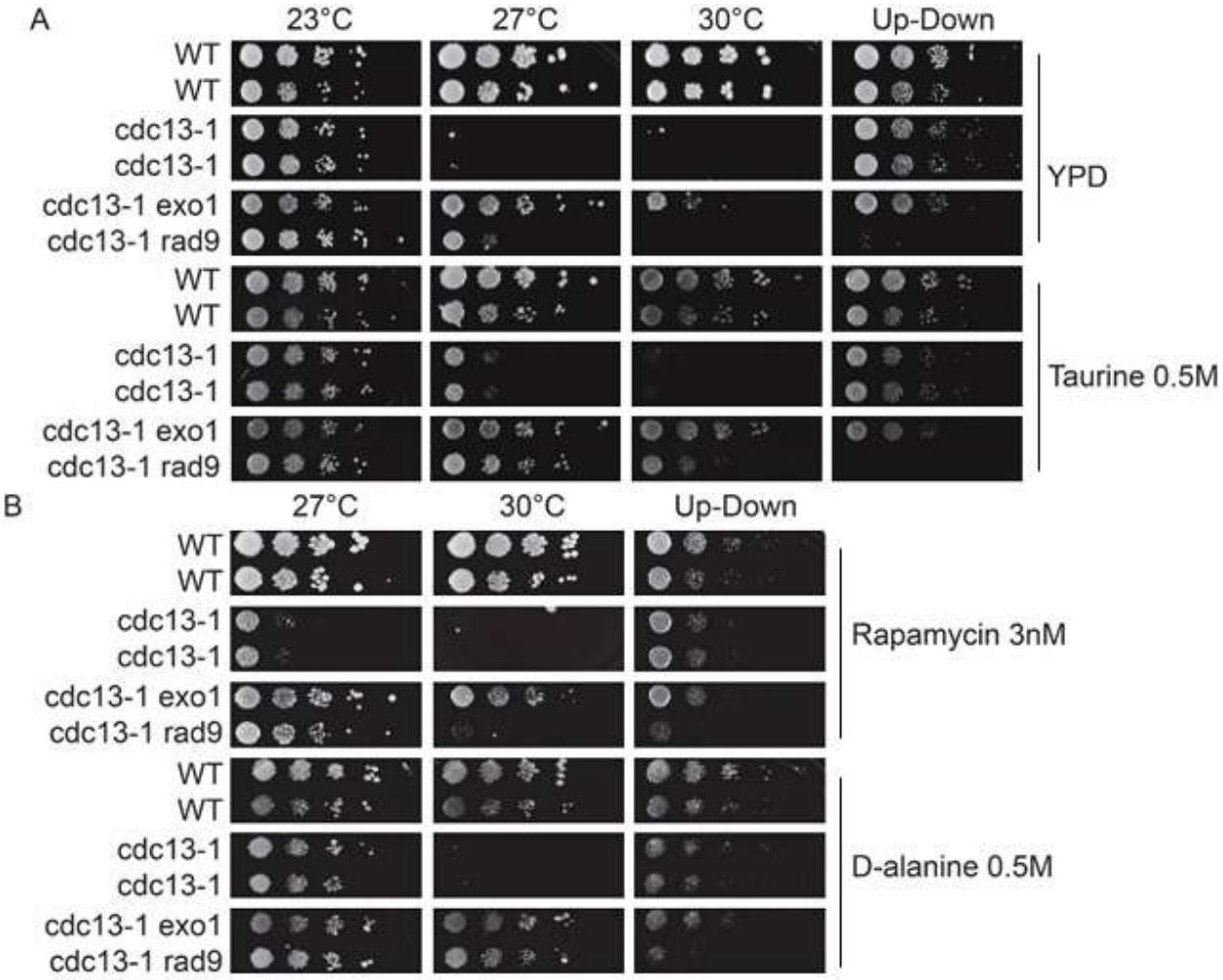

Figure 25: Spotting investigation of taurine's *cdc13-1* rescue mechanism A. spotting assay using the up-down method to differentiate the phenotype of *cdc13-1, cdc13-1 exo1* and *cdc13-1 rad9*. B. continuation of panel A, with the addition of rapamycin and D-alanine. C. spotting assay with *san1* including higher temperatures to identify potential additivity of taurine. Plates were incubated at designated temperatures and images were acquired 48h post spotting. All genotypes per condition come from the same plates and were cropped in sets of two so that the genotypes are rearranged for clarity.

3.2.3.3 Comparison between Taurine, D-alanine and rapamycin in terms of cdc13-1 rescue capabilities

Taurine, rapamycin and D-alanine all rescue the *cdc13-1* temperature-sensitive phenotype, therefore they may act through a common pathway. We therefore wanted to investigate whether these molecules are additive or epistatic with resection mutants that already exhibit a rescue effect of the *cdc13-1* TS sensitivity. Specifically, Exo1 is important for the creation of ssDNA in the telomeres, a process called resection. Pif1 is

normally positioned at the telomeres and works with Exo1 to coordinate the checkpoint activation upon telomere uncapping. Sae2 also contributes to resection of uncapped telomeres and is involved in the processing of dsDNA breaks and prevention of accumulation of ssDNA at the telomeres. Figure 26 shows that taurine, rapamycin and D-alanine resulted to growth benefits for all mutants. This could be an indication of common mechanisms, however as all of the mutants are in *cdc13-1* which all molecules can rescue, further experiments are required to confirm or deny this hypothesis.

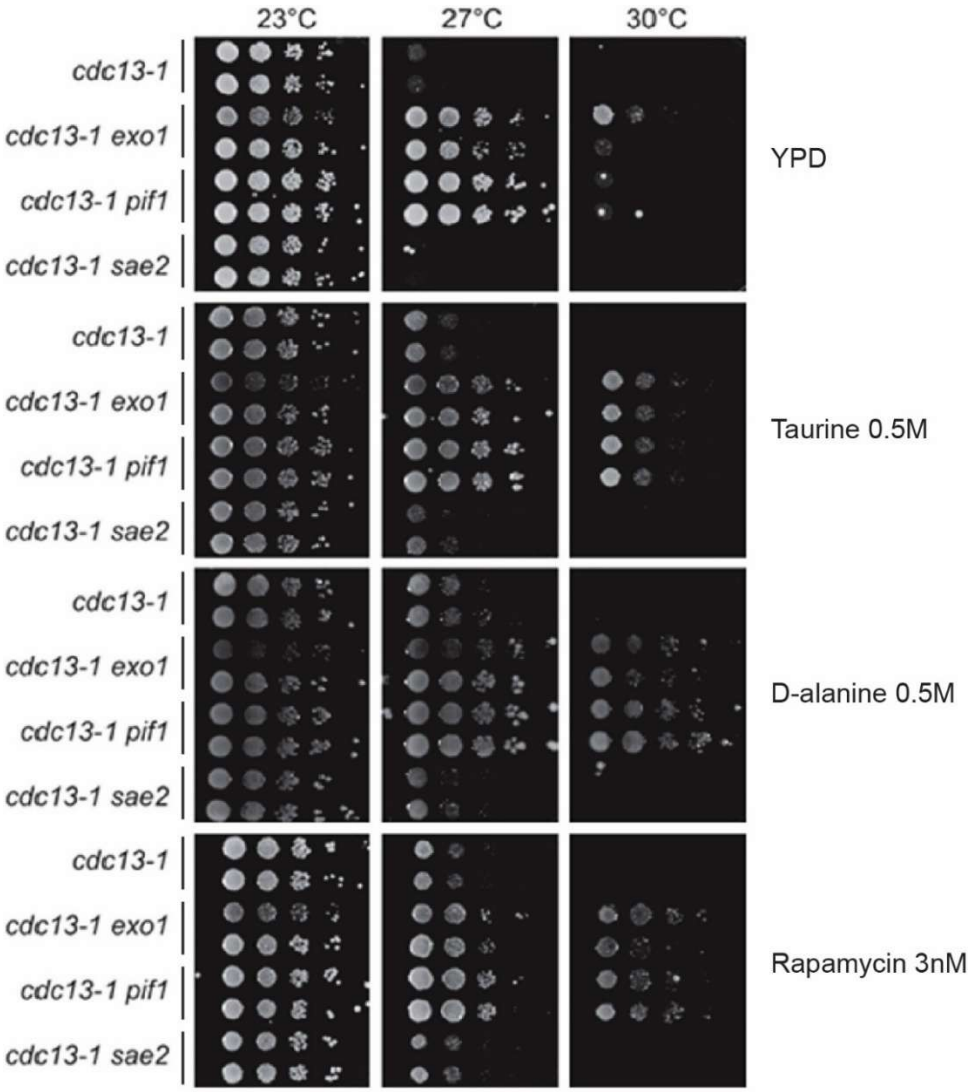

Figure 26: Spotting assay to compare taurine, D-alanine and rapamycin's effects on resection mutants known to rescue *cdc13-1*. Resection mutants known to improve viability of *cdc13-1* cells in non-permissive temperatures were spotted on YPD plates and supplemented with rapamycin, taurine, and another non-proteinogenic, structurally similar aminoacid, D-alanine. Plates were incubated at designated temperatures and images were acquired 48h post spotting.

3.2.3.4 Taurine improves viability of checkpoint and replication mutants in cdc13-1 background at semi-permissive temperatures, in a pattern different to rapamycin

Taurine improves the viability of many mutants tested so far, regardless of their function. To rule out the possibility of taurine employing pathways similar to rapamycin's, or any of the characterized *cdc13-1* rescuers, mutants with additional mutations that alter the *cdc13-1* phenotype were spotted, to investigate whether taurine is additive to them or not. In the absence of *RAD53* and *MEC1*, cells need the concomitant deletion of *SML1 to remain viable*. In the DNA damage checkpoint cascade, Mec1 is acting upstream of Rad9 and Mrc1, which are acting upstream of Rad53. In the absence of these DNA damage checkpoint genes, *cdc13-1* cells will continue dividing past the checkpoint thus appearing like a rescue. As shown in the spottings Figure 27 spottings, taurine improves the viability of most mutants, in contrast to rapamycin, such as in the *cdc13-1 rad53-11* mutant.

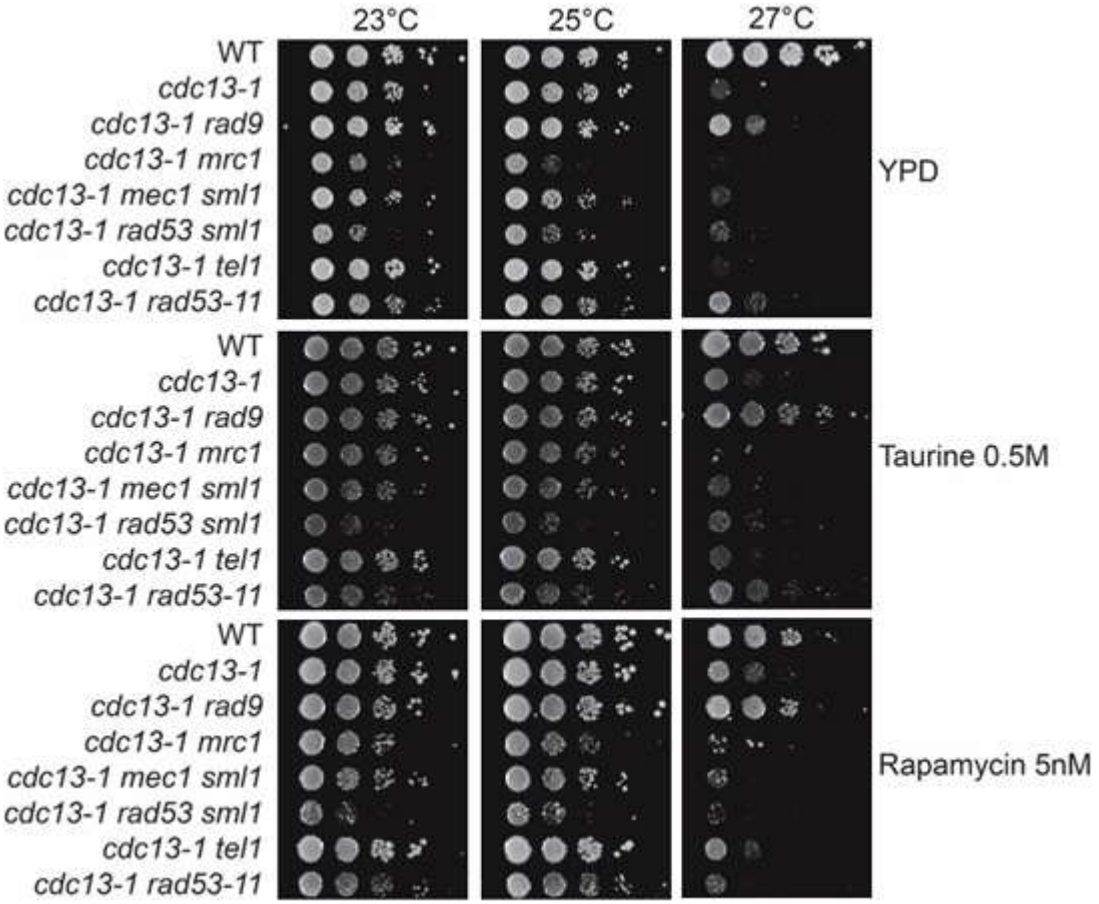

Figure 27: Spotting assay with several mutants in *cdc13-1* background with taurine or rapamycin supplementation. Checkpoint and replication mutants that alter the *cdc13-1* phenotype were spotted on YPD plates with the addition of taurine or rapamycin. Images were acquired 48h post spotting.

3.2.3.5 Taurine rescues TS mutants involved in cell cycle regulation, in contrast to rapamycin

To finally determine whether taurine's rescue activity is specific to telomere uncapping mutants or has a broader impact on cell cycle regulation, we conducted a spotting experiment with four different cell cycle regulators. Cdc20 activates the anaphase promoting complex (APC), which is essential for proper chromosome separation during mitosis and ensures the transition from metaphase to anaphase. Cdc15 is involved in MEN (Mitotic Exit Network), and promotes the exit from mitosis by activating downstream proteins such as Dbf2. Cdc4 is a component of the SCF (Skp1-Cullin-F-box) ubiquitin ligase complex, and targets phosphorylated proteins for degradation and it is crucial for G1/S transition. Finally, Sen1 has multiple roles ranging from disrupting R-loops at telomeres, transcription termination, meiotic function and DNA replication. As shown on

Figure 28, while rapamycin improved viability in cdc15-1 cells, taurine's effect was much more pronounced and observed across all TS mutants tested. This suggests that taurine has a different mechanism of action than rapamycin, which did not rescue the majority of the mutants tested.

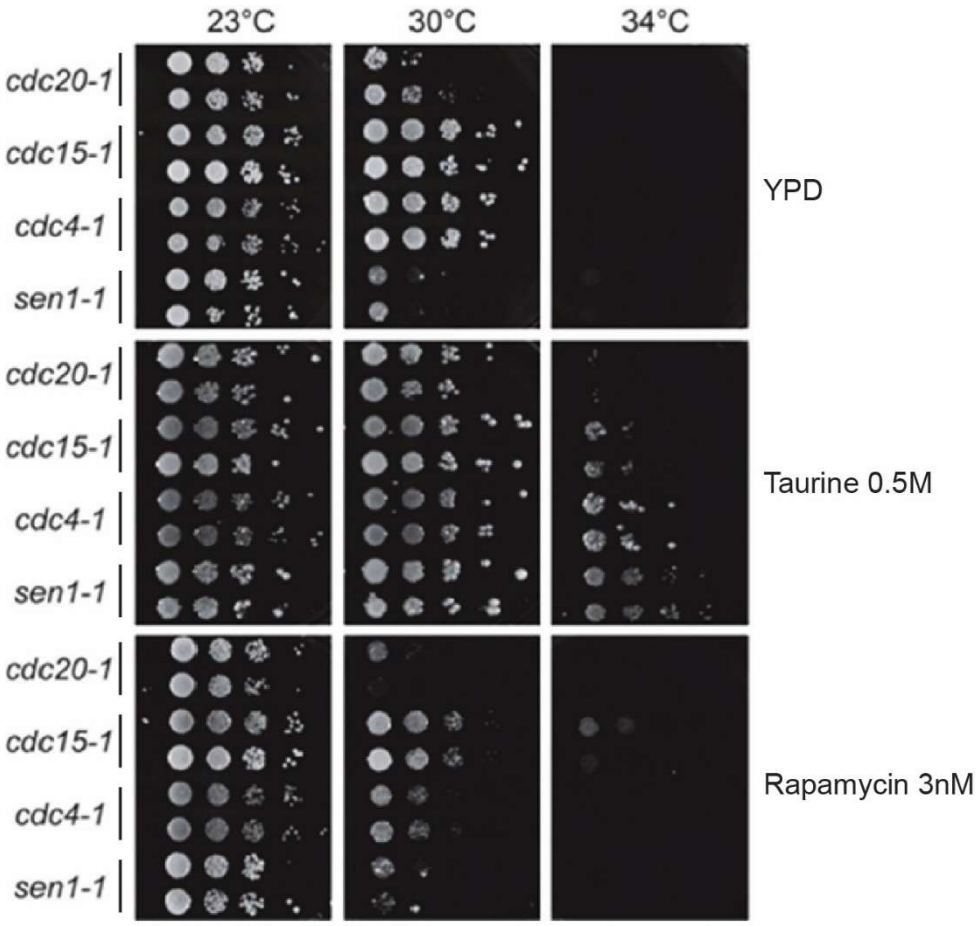

Figure 28: Spotting assay of different TS alleles of cell cycle regulators, supplemented with taurine and rapamycin. Spotting of TS mutants involved in timely cell cycle progression, plates on YPD supplemented with taurine and rapamycin. Plates were incubated at designated temperatures and images were acquired 48h post spotting.

3.2.3.6 Taurine rescues several TS mutants, in contrast to rapamycin

To further demonstrate the difference between taurine and rapamycin, a series of spottings were conducted, with mutants that exhibit rescue to variable degrees upon taurine supplementation (Figure 29). The following mutants were selected based on the extent of the rescue they exhibit upon treatment with taurine. *dam1-1, sen1-1, rsp5-3* are rescued very effectively, while *rsp5-3* is not viable upon rapamycin supplementation regardless of taurine. *Agf2-18, rio2-1* are marginally improved with taurine and *rfc2-1, cus1-3* are not impacted at all. As shown below, none of those are rescued by rapamycin, and in case of combination of taurine with rapamycin, taurine's effects are also limited.

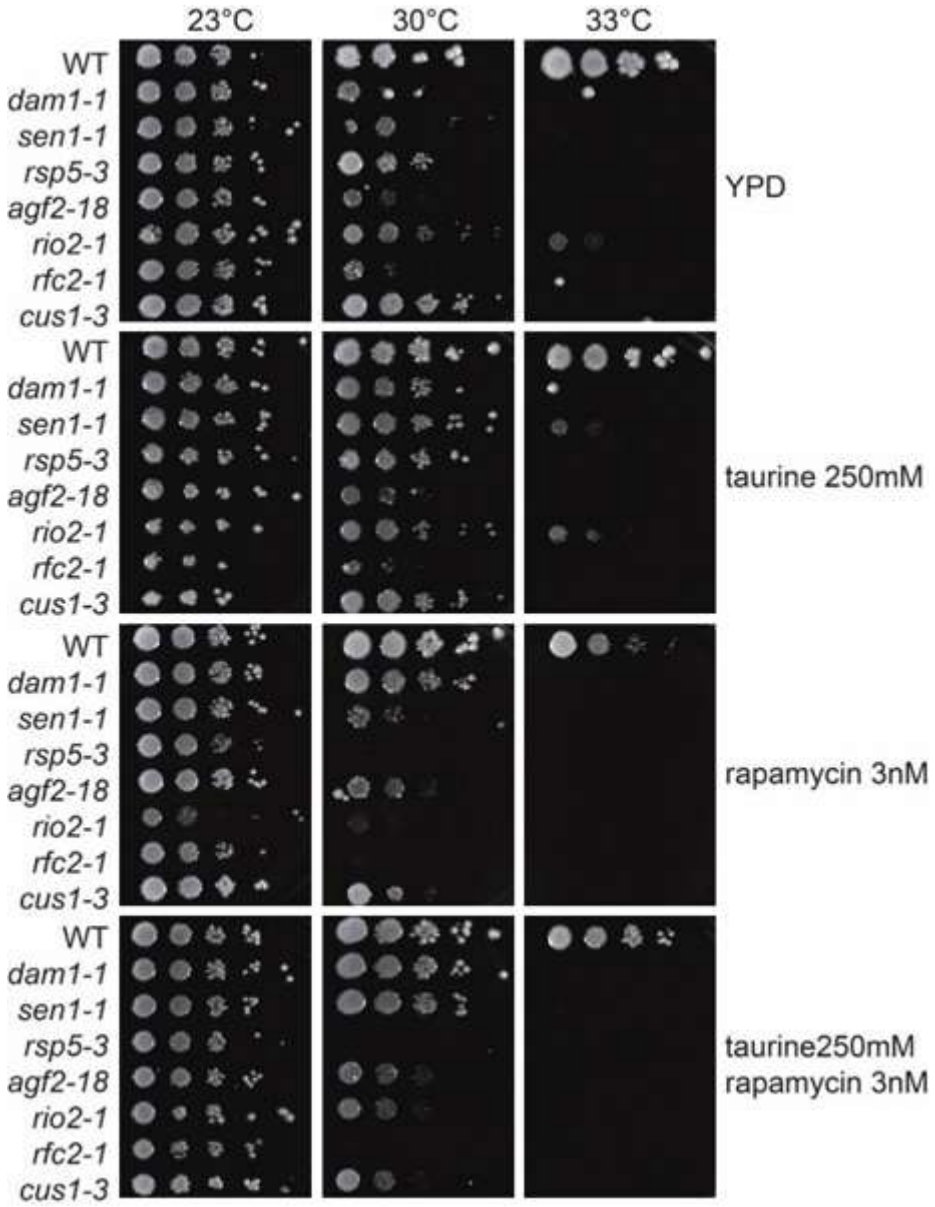

Figure 29: Spottings of different TS mutants with variable magnitude of rescue by taurine. Cells were cultured on supplemented YPD according to the label, and incubated in the designated temperatures. Images were acquired after 48h.

3.2.3.7 Taurine's effects are not due to direct antioxidant capabilities

It has been reported that antioxidants such as N-acetyl cysteine (NAC) and Ascorbic acid are able to improve the growth of *cdc13-1* in semi-permissive temperatures.

Taurine has been reported to have mild antioxidant capabilities besides its role in safeguarding proper mitochondria function. In order to examine whether taurine's profound effects are due to its natural antioxidant function, the following spottings were conducted, featuring different established antioxidants namely N-acetyl-cysteine and ascorbic acid, to investigate their effects on various TS mutants. The mutants we chose to test all encode proteins that control progression through specific stages of the cycle by modulating cyclin-dependent kinase (CDK) activity. The reason these were also included is that although antioxidants have been shown to rescue the *cdc13-1* TS phenotype, no reports of them rescuing the rest of these mutants could be found in the literature. In addition, we wanted to examine whether taurine can improve the viability of other, mechanistically unrelated TS mutants.

As shown on Figure 30, although these antioxidants indeed rescue *cdc13-1* to some extent, as already reported in the literature, taurine's effect is much more profound. Most importantly, the tested antioxidants fail to rescue the other tested mutants which taurine is able to rescue, indicating a separate mode of function for taurine's rescue apart from its antioxidant capabilities, and confirm that this mechanism is more global than just on telomeres.

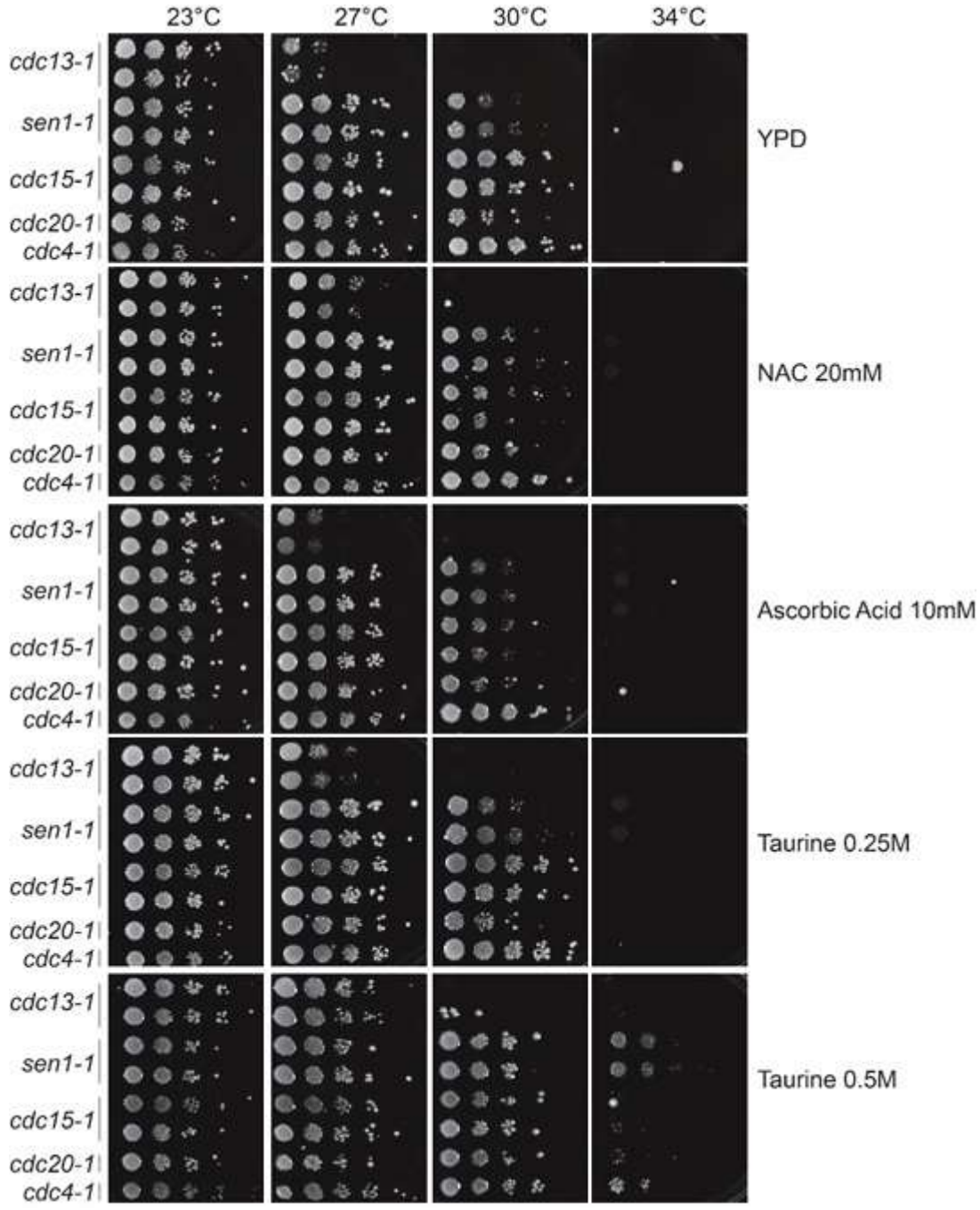

Figure 30: Spotting assay taurine with different antioxidants in reported functional concentrations. Cells were cultured on supplemented YPD according to the label, and incubated in the designated temperatures. Images were acquired after 48h.

3.2.4 Rescue of temperature-sensitive mutants by taurine

Taurine's protective effect on TS mutants has no obvious link to a single signaling pathway; instead, it appears to act broadly, likely as an osmolyte. To test this, we compared taurine with a panel of structurally diverse osmolytes, including the denaturant urea, and the non-osmolyte NaCl, to probe whether its benefit derives from general osmolyte chemistry, specific protein interactions with the osmolytes or sheer osmotic pressure. In vitro studies show that taurine's sulfonate group can both disrupt and reinforce the hydration shell, with the amino moiety enhancing water network stability; I therefore synthesized N,N,N-trimethyltaurine (TMT) to assess the role of the amino moiety. Spotting assays revealed that all tested osmolytes, especially taurine and betaine, rescue a subset of TS mutants to varying degrees, whereas urea abolished growth, confirming that denaturation leads to the opposite effects of taurine. TMT, although not expected to be an effective stabilizer, also conferred protection, albeit less potently, underscoring the importance of the amino group. Adjusting media pH to match that of taurine-supplemented cultures lead to no rescue, indicating that the effect is not due to medium acidification. When combined, taurine and betaine produced an intermediate rescue, suggesting epistasis and that they operate in the same generic osmolyte pathway. Finally, co-incubation with urea demonstrated that all osmolytes, with taurine the most effective, can counteract urea's destabilizing influence, further supporting a mechanism based on protein stabilization. Taken together, these data point to taurine functioning as a general osmolyte that fortifies protein conformation, thereby rescuing a broad spectrum of TS mutants through a mechanism distinct from individual biological pathways.

3.2.4.1 Rescue effects of different osmolytes and the synthesis of N,N,N-trimethyltaurine (TMT)

Taurine's mode of action appears to be quite broad and without being connected to a specific pathway. Given that taurine is not reported to easily bind to proteins, and its effective concentrations are much higher than the ones usually used for small molecules, I hypothesized that it might act as an osmolyte.

To evaluate the idea of taurine exhibiting its effects *via* functioning as an osmolyte, I tested taurine alongside other common osmolytes. Structurally similar compounds like glycin and D-alanine, as well as structurally distinct molecules such as proline and sorbitol were purposefully included to investigate the structure to activity relationship. Additionally, I tested well-characterized protein stabilizers like trimethylglycine (betaine), while urea was used as a destabilizer, Non-osmolyte NaCl was also included as an osmotic reference because it generates a hyperosmotic pressure without engaging in other osmolyte specific mechanisms of action(although it cannot from hydrogen bonds, it may modify the hydration sphere of proteins to some extent). NaCl is a fully dissociable ionic salt, producing two charged particles ($Na^+ + Cl^-$) per formula unit, whereas covalent, non-ionic compounds contribute only one particle per molecule, and only partially form ions. According to van't Hoff's law ($\Pi = iCRT$), the osmotic pressure of an ionic solution is roughly twice that of an equimolar non-ionic solution. Consequently, a 0.25 M NaCl solution delivers the same osmotic load as a 0.5 M non-ionic osmolyte, while remaining chemically inert. By comparing cellular responses to NaCl with those to the test molecules, we can attribute observed effects specifically to osmolyte-dependent mechanisms rather than to generic osmotic stress. In addition, due to NaCl being an ionic compound, Taurine's interaction with proteins and their hydration sphere has been studied in vitro, and it has been revealed that it has double, contradicting roles. The sulfonate group, although in theory able to form hydrogen bonds with the protein backbone, instead interacts with the water molecules around it and weakens the hydrogen bond network, taurine's amino moiety enhances the hydration sphere. TMT does not have the latter due to the protected amino group, however we know that it is not only the hydration sphere important for the osmolyte's stabilizing activity. To determine how important the amino moiety truly is for the phenotype we observed, I also included TMT.

TMT however, was not commercially available, therefore it needed to be synthesized. The synthesis of N,N,N-trimethyltaurine was performed according to Barnhurst et al. 1961 , and was split in two batches. For the pilot experiment, 0.02mol (5g) of the substituted ammonium bromide and 0.022 mol (2.68g) of Na_2SO_3 were used, which yielded in 2.7g of TMT. Since Mr_{TMT} (molecular mass)=167.23 ($C_5H_{13}NO_3S$), the yield after the

recrystallization was 80.7%, in line with the reported one which was 81%. For the main experiment, 0.08mol (20g) of substituted ammonium bromide and 0.88mol (10,72g) of Na_2SO_3 were used, and yielded in 12.6g of TMT after recrystallization. This translates to a yield of 94.1%, which although not very far off the reported 81%, is too high. However, there was no perceivable difference in the consistency of the product.

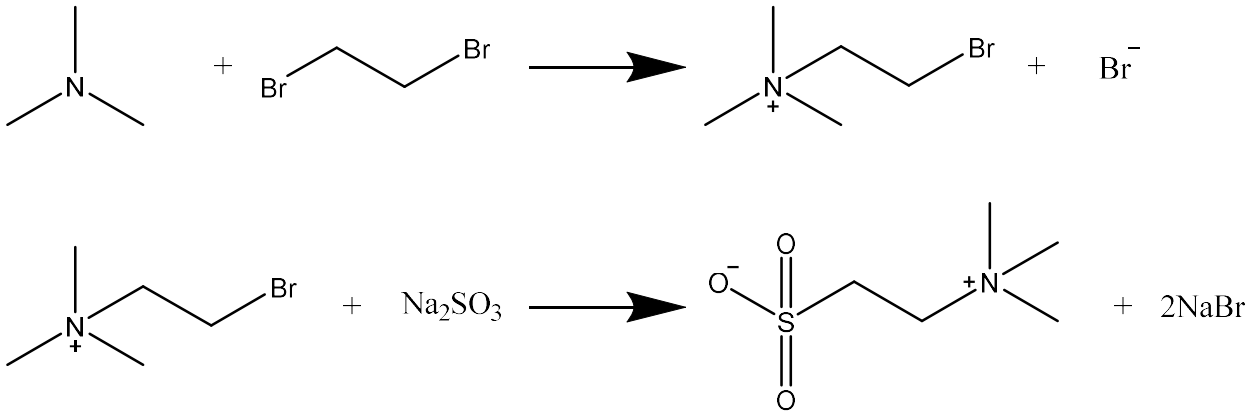

As seen on Figure 31, osmolytes share taurine's rescue effects on TS proteins, to different extends, with taurine and betaine being the most potent stabilizers. Interestingly, TMT has also stabilizing capabilities in contrast to our expectations, but is not as potent as taurine, whereas urea diminished the growth of all the TS alleles, which is in line with our expectations as urea is a well-known denaturant. Interestingly, the only TS alleles rescued by taurine are also rescued by the rest of the osmolytes, raising the question as to what discriminates this group of proteins from the group of proteins that is not rescued by osmolytes.

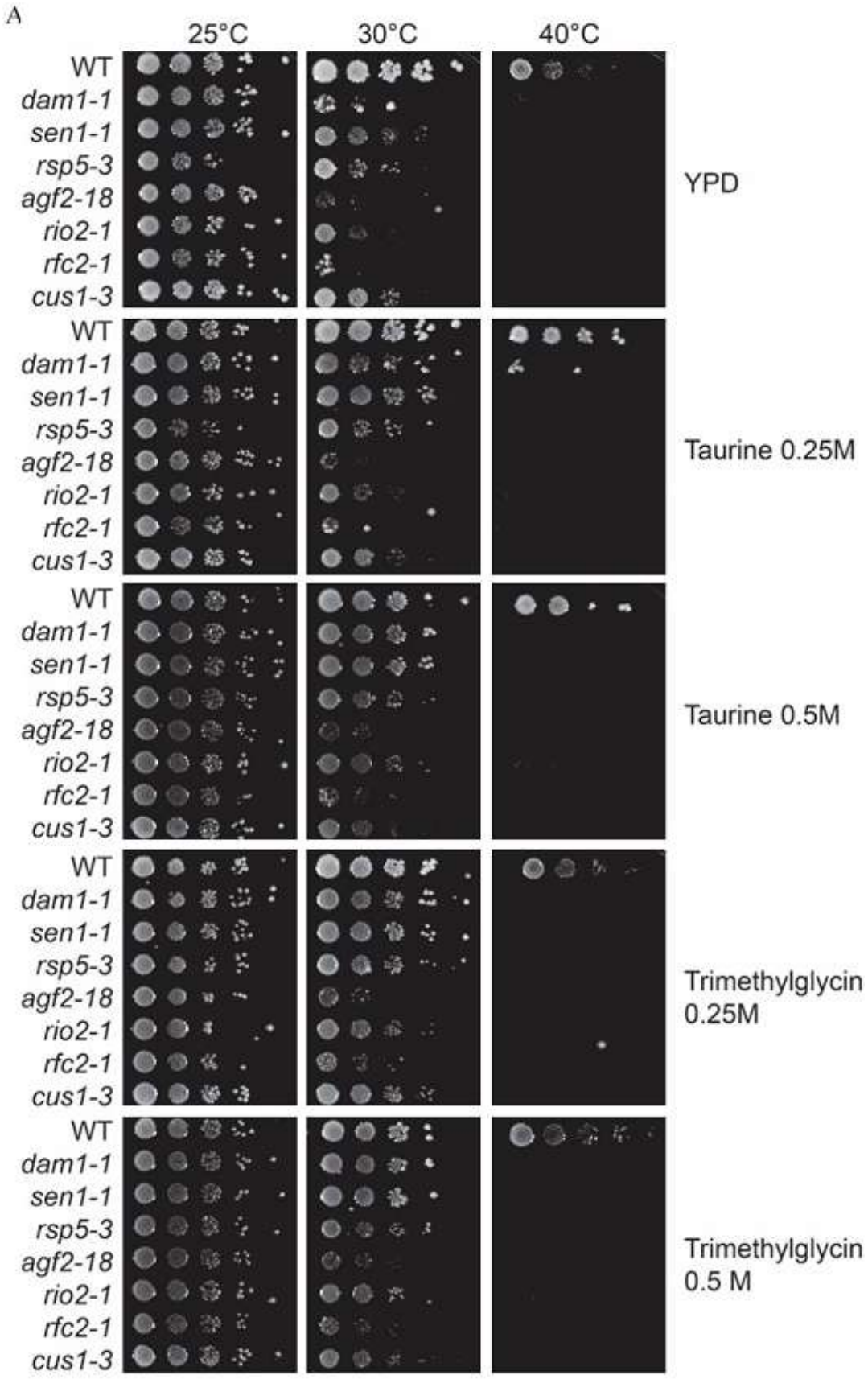
A
25°C
30°C
40°C
WT
dam1-1
sen1-1
rsp5-3
agf2-18
rio2-1
rfc2-1
cus1-3
YPD
Taurine 0.25M
Taurine 0.5M
Trimethylglycin 0.25M
Trimethylglycin 0.5 M

B

Osmolyte	Concentration (mM)	Structure	Rescue of TS at 30	Growth of WT at 40
Glycin	250	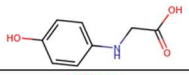	Marginal	Deteriorated
	500		Substantial	Equal to YPD
NaCl	250		Marginal	Equal to YPD
	500		Substantial	Equal to YPD
Sorbitol	250	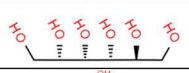	Marginal	Maximal
	500		Substantial	Equal to YPD
Myoinositol	250	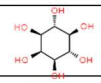	Marginal	Substantial
	500		Marginal	Equal to YPD
D-alanine	250		Substantial	Maximal
	500		Maximal	Maximal
Proline	250	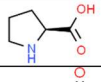	Substantial	Diminished
	500		Substantial	Diminished
Taurine	250	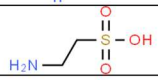	Substantial	Maximal
	500		Maximal	Substantial
Betaine (trimethylglycine)	250	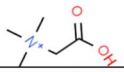	Maximal	Substantial
	500		Substantial	Maximal
Urea	250	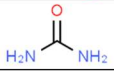	Diminished	Diminished
	500		Diminished	Diminished
Urea + Taurine	250		Substantial	Diminished
TMT (trimethyltaurine)	250	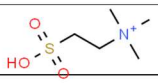	Substantial	Diminished
	500		Maximal	Diminished

Figure 31: Impact of different osmolytes on TS mutants. A. Spotting of different TS mutants shown to get different degrees of rescue by taurine, on YPD plates supplemented with a diverse chemical compound selection. Plates were incubated at designated temperatures to investigate both the rescue of TS mutants but also WT cells at high temperatures, and images were acquired 48h post spotting. B. table summarizing the rescue effects of various osmolytes with distinct chemical structures on cell spotting. This highlights taurine's role as a key osmolyte responsible for the rescue effect observed in this study. The rest of the osmolytes can be seen on appendix figure A10.

3.2.4.2 Role of pH in the rescue of TS mutants

High taurine concentrations slightly acidify the aqueous media. Protein conformation is highly sensitive to intracellular pH as a decline from the physiological pH can lead to protein missfolding or aggregation, which becomes more apparent the further away the pH is from the protein's isoelectric point. However, cells maintains tight intracellular pH homeostasis, allowing viability across moderate extracellular pH fluctuations. To exclude the possibility that the phenotypes observed upon taurine supplementation were driven by extracellular acidification, the culture medium was adjusted to match the pH of taurine-supplemented conditions.

No significant differences were detected between pH-matched controls and untreated cells, indicating that the effects of taurine are not driven by bulk medium acidification. This is consistent with previous studies showing that moderate pH changes within the physiological range (pH 5.5–7.5) exert minimal influence on protein stability or yeast growth, whereas larger deviations disrupt ion homeostasis and proteostasis. Thus, the cellular and proteostatic benefits observed upon taurine supplementation likely stem from its role as a compatible osmolyte rather than from pH-mediated effects.

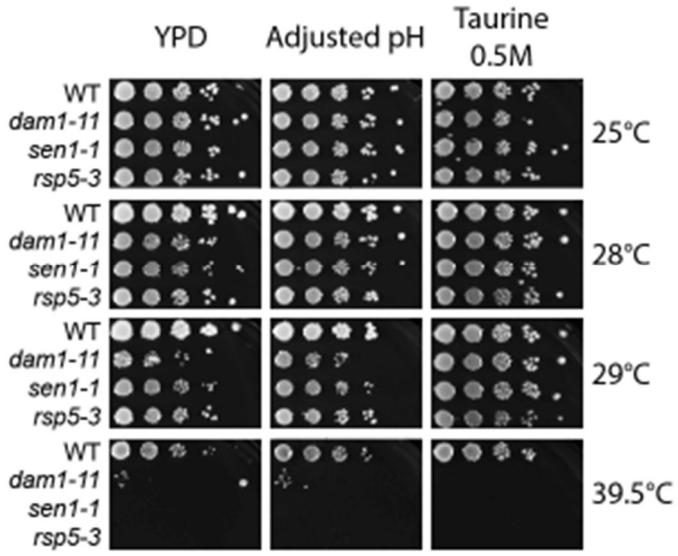

Figure 32: Spotting assay comparing taurine to acidified YPD matching taurine-supplemented YPD pH. Cells were cultures on YPD plates supplemented with taurine, or H_2SO_4. Plates were incubated at designated temperatures to investigate both the rescue of TS mutants but also wt cells at high temperatures, and images were acquired 48h post spotting.

3.2.4.3 Taurine is epistatic *with trimethylglycine*

If taurine acts as a general osmolyte, it should function in the same mechanistic pathway as the well-characterized protein stabilizer trimethylglycine (betaine) . Consequently, the combined use of the two compounds should not produce a synergistic rescue beyond the stronger of the two, but rather an intermediate effect. To evaluate this hypothesis, TS strains (were plated on YPD supplemented with taurine, betaine and their combination. Both taurine and betaine individually rescued all TS mutants to a substantial extent; betaine yielded a moderately higher rescue at 500 mM. The mixture of the two compounds produced a rescue that lay between the two single treatments, as colony sizes were intermediate and not significantly larger than either single treatment (Figure 33).

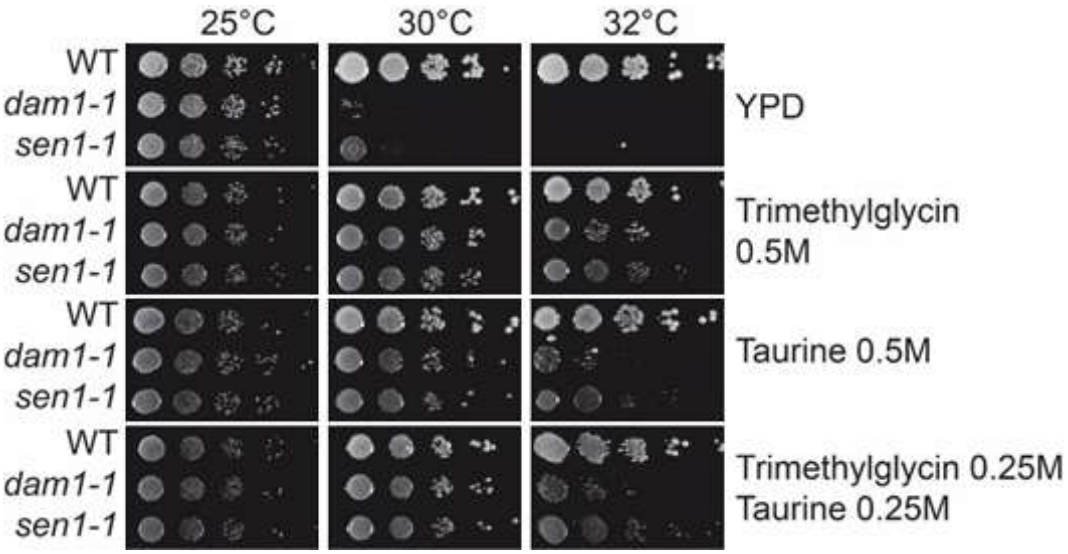

Figure 33: Spotting assay with mixture of taurine and trimethylglycine. Cells were cultures on YPD plates supplemented with taurine, trimethylglycine or both. Plates were incubated at designated temperatures to investigate both the rescue of TS mutants but also wt cells at high temperatures, and images were acquired 48h post spotting. The rest of the osmolytes can be seen on A12.

3.2.4.4 Taurine and other osmolytes counteract the diminishing effects of urea

If taurine functions as a generic osmolyte, it should counteract the destabilizing action of the protein denaturant urea on TS mutants, while other osmolytes should exhibit a similar protective effect. Urea alone abolished growth of every TS mutant and severely impaired WT growth at 39.5 °C. In the presence of any osmolyte, growth was markedly improved, with the most potent rescuer being taurine. The combination of urea + osmolyte restored cell growth for all mutants, whereas trehalose failed to rescue WT cells at the highest temperature. Notably, the combination of taurine and urea at 29°C resulted in better growth of *sen1-1* in YPD at 28°C, but worse for *rsp3-5.*

The ability of all tested osmolytes to mitigate urea's denaturing effect strongly supports the conclusion that taurine's protective action is governed by generic osmolyte chemistry rather than a specific protein interaction, although different proteins respond to osmolytes in different extends. This differential performance among proteins and osmolytes likely reflects variations in their ability to stabilize the protein hydration shell and counteract the water-structure-disrupting action of urea.

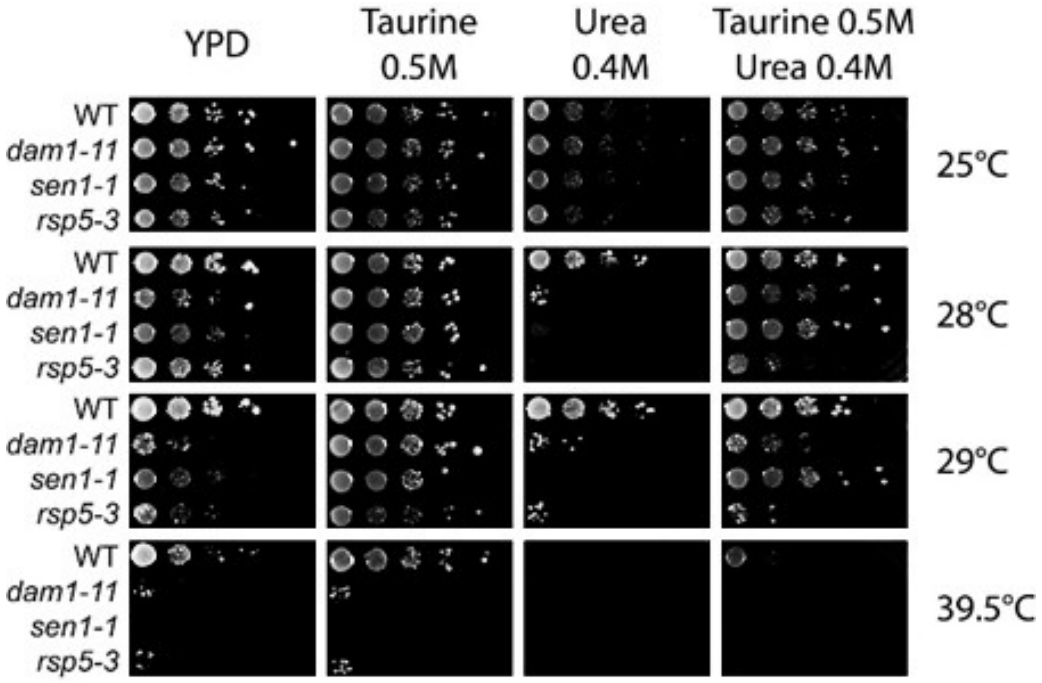

Figure 34: Spottings of well-rescued TS strains, with the addition of destabilizing urea. Cells were cultures on YPD plates supplemented with taurine and other osmolytes, protein destabilizing urea and a combination of both. Plates were incubated at the indicated temperatures to investigate both the rescue of TS mutants but also wt cells at high temperatures. Images were acquired 48h post spotting. The rest of the osmolytes can be seen on figure A11.

3.2.4.5 Taurine rescues TS actin allele regardless the condition of protein degradation machinery

Misfolded TS proteins are normally removed by the cytosolic E3 ubiquitin ligase Ubr1 and the nuclear E3 ligase San1. In the absence of these proteins, it has been reported that the misfolded proteins will not be degraded. Here we hypothesize that this accumulation of misfolded proteins will also lead to an increased number of folded proteins due to the misfolded and folded form being in equilibrium. If this is correct, the viability of the cells will be increased in the absence of the ubiquitin ligases and provide an observable rescue of the TS mutants, In order to investigate whether taurine can further improve the viability of the TS mutants, we utilized *act1-136* as a model, due to its high increase in Western blots upon taurine supplementation, which means that it is well-stabilized since the misfolded form would be degraded (unpublished work of Fabio Bento). As shown below however, both ubiquitin ligases were not able to improve the viability of the TS mutants, regardless of the increase in actin reported, but taurine supplementation visibly improved the growth of all mutants, regardless of the state of protein degradation machinery.

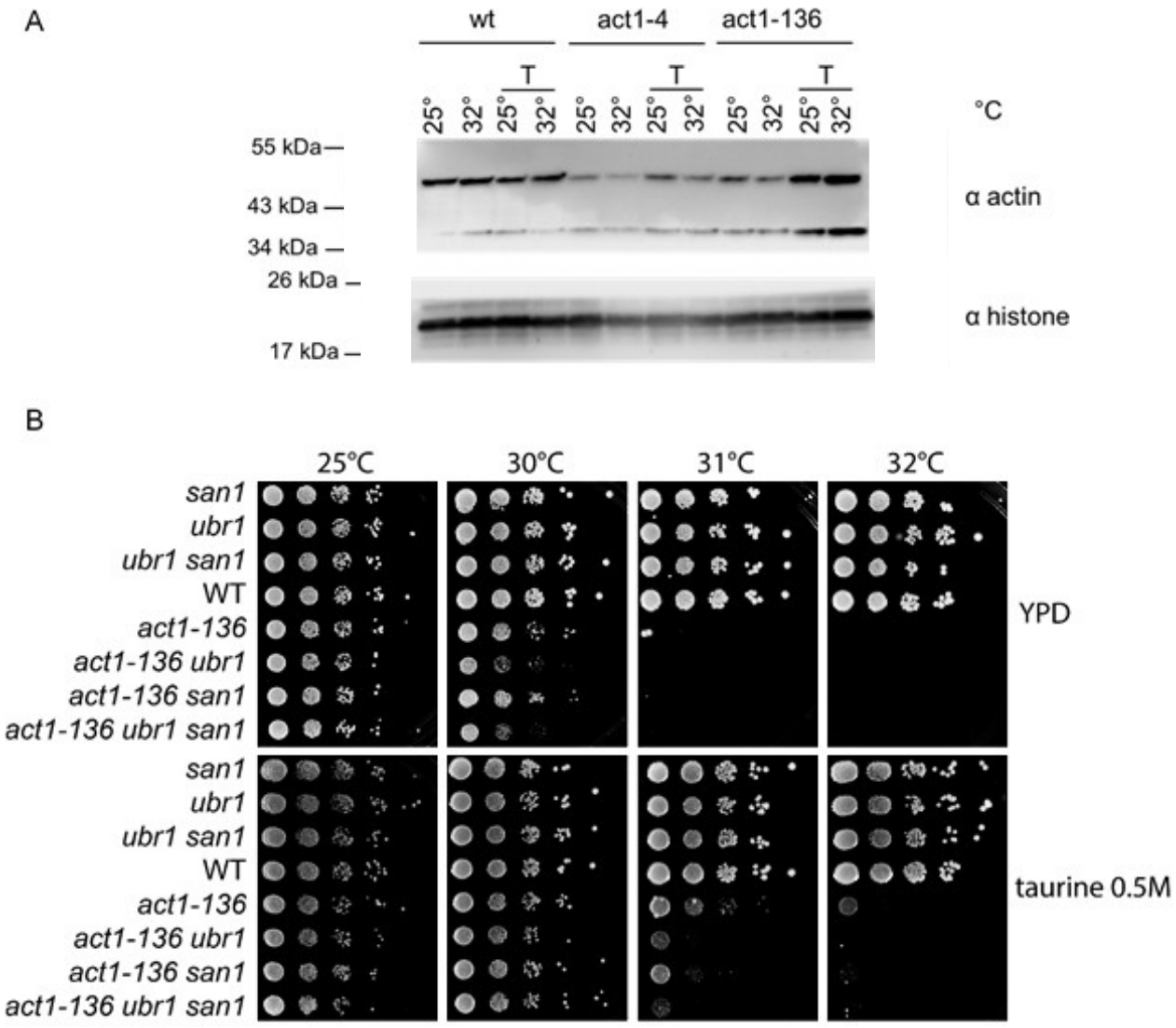

Figure 35: Spotting assay with TS actin mutants combined with in protein degradation impaired background. A. Western blot showing the abundancy of wt and TS actin in increased temperatures, degradation can further improve or match taurine results. Cells originate from a single tetrad to avoid artifacts and grown on YPD. Images were acquired 48h post spotting

3.2.5 Taurine screenings to identify determinants of protein stabilization and taurine import mechanisms

Upon showing that taurine benefits the cells via its osmolyte function, I further dissected the mechanism of action, aiming to understand what dictates whether a protein will be stabilized, or the degree of the stabilization. To this extent, the experiments described below indicate that it is the protein structure that dictates the susceptibility to osmolytes such as taurine, and the degree of the stabilization relies on the protein-osmolyte combination.

3.2.5.1 TS allele screening to identify patterns among rescuable mutants

We performed a large-scale, high-throughput screen to determine which TS mutants could be rescued by taurine. A library of 775 verified TS alleles (each representing a distinct protein or complex while also including different TS alleles for the same protein) was arrayed on 1536-well plates and spotted onto YPD plates supplemented with 500 mM taurine. After 24 h incubation at the semi-permissive temperature for each strain, colonies were photographed and image-analysis was performed by Eduardo Gameiro. Using very stringent criteria, as described in the methods section, 390 strains (~50%) were classified as “rescued” (Figure 36B). Spatial mapping of the rescued mutants onto subcellular localizations did not reveal any trends, while compartments such as endosomes or mitochondria were underrepresented (Figure 36C). These results suggest that the efficacy of taurine depends on the protein’s structure rather than its subcellular context.

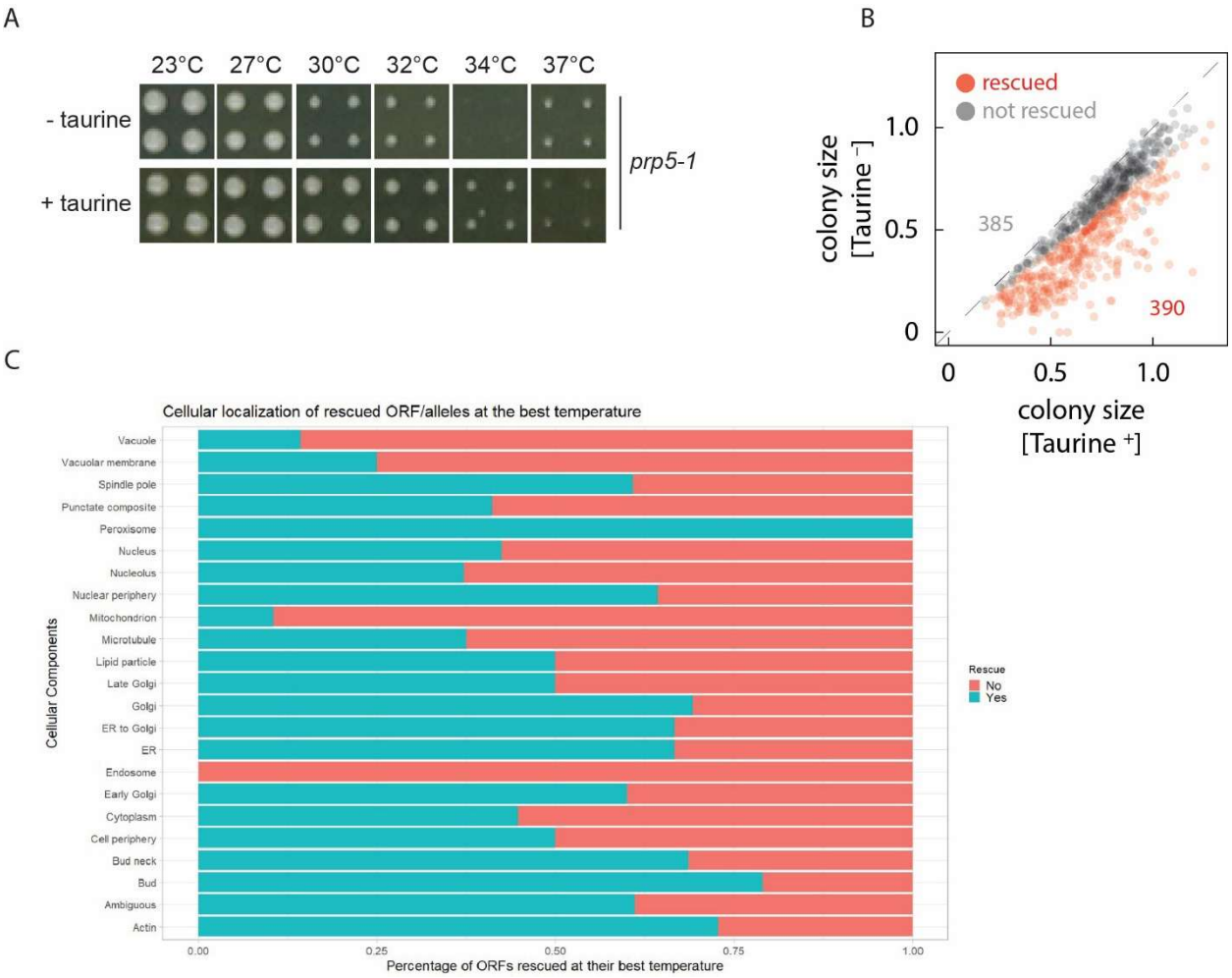

Figure 36: Identification of patterns among rescued TS mutants. A. Representative plates after 24 h at the semi-permissive temperature. *prp5-1* serves as an example of a mutant that fails to grow in higher temperatures the absence of taurine. B. Plot showing the number of strains (390 out of 775) classified as “rescued”. C. Bar graph showing the localization of rescued and non-rescued mutants categorized by cellular compartment. Analysis of the screening results and the figure were done by Eduardo Gameiro.

3.2.5.2 TS screening results are reproducible in low throughput

To validate the automated screen, 20 rescued and 20 non-significantly-rescued strains were manually spotted onto fresh YPD plates with or without 500 mM taurine. After 48 h at the strain-specific semi-permissive temperature, all rescued strains displayed a clear growth advantage, whereas only 1 of the 20 non-rescued strains grew appreciably in the presence of taurine (Figure 37). The discrepancy is attributable to the conservative cut-off used in the screen, which favored specificity over sensitivity.

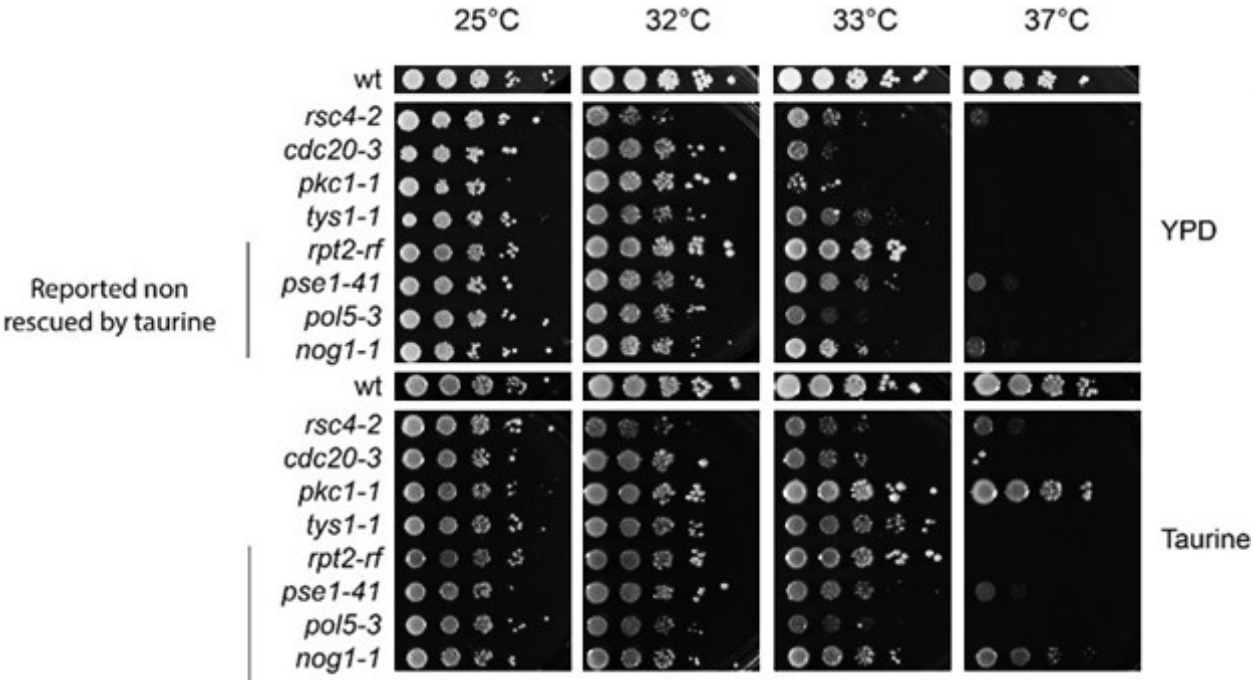

Figure 37: TS screening confirmation spotting. Example TS mutants were spotted and exposed to 0.5M taurine in a low throughput manner to confirm the screening results. Temperatures were selected to reflect semi- permissive temperatures of the alleles in the screening. Cells were cultured on YPD plates with or without supplementation of taurine. Plates were incubated at indicated temperatures to investigate both the rescue of TS mutants but also wt cells at high temperatures, images were acquired 48h post spotting. Full list of temperatures can be seen on figure A11.

3.2.5.3 Protein dictates osmolyte susceptibility, but stabilization degrees vary across osmolytes

We next asked whether alternative osmolytes could rescue TS mutants that were not rescued by taurine. A panel of 12 mutants (6 taurine-rescued, 6 non-rescued) was exposed to 500 mM of each of the following structurally distinct osmolytes: taurine, trehalose, proline, and glycine. In green are the mutants that taurine is able to rescue as discovered in previous experiments and in red are the mutants that taurine cannot rescue. None of the non-rescued mutants showed growth in any of the alternate osmolytes (Figure 38). In contrast, the rescued mutants responded to all osmolytes, albeit to varying degrees. These data imply that the intrinsic folding propensity of the protein determines osmolyte responsiveness in spite of the fact that most TS proteins lose their function as a result of missfolding, while the specific chemical nature of the osmolyte modulates the magnitude of rescue. This is in line with the observation that only the TS mutants taurine rescued are responding to the rest of the osmolytes, with the ones that taurine does not rescue remaining “immune” to all other osmolytes used.

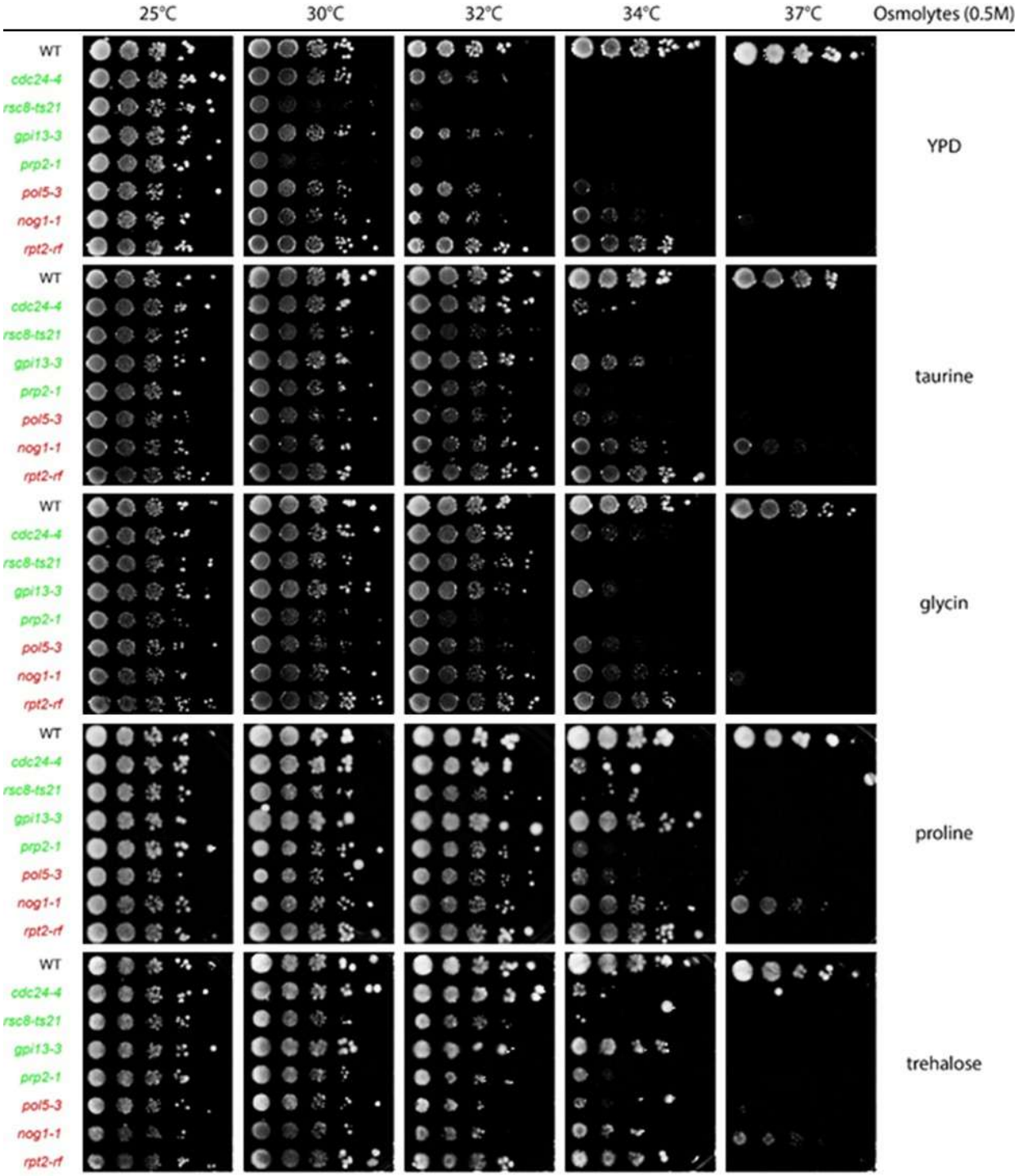

Figure 38: Spotting with rescuable and non- rescuable mutants, on different osmolytes. Spotting of TS mutants reported by the screening to be rescued by taurine (green) and not rescued (red). Cells were cultures on YPD plates supplemented with a diverse chemical compound selection. Plates were incubated at indicated temperatures.

3.2.5.4 Investigation of taurine's import mechanisms via genome wide KO screening

The observed phenotype of taurine suggests that it is somehow taken up by the cell, as other compounds achieving similar osmotic pressure do not exhibit the same effects (such as NaCl on Figure 31). To determine whether taurine indeed enters the cells, analysis of cell extracts using HPLC-MS could be performed. However, this would only confirm the presence of taurine within the cells and would not provide insight into how it is actually imported. *S. cerevisiae* lacks annotated taurine biosynthetic or import pathways. To identify genes required for taurine uptake, a genome-wide KO screen was performed. It was previously showed that taurine supplementation allows the growth of wt strains in higher temperatures. Hence, KO strains that do not have the ability to properly import taurine, will not be able to grow in high temperatures, indicating that the gene deleted is involved in taurine import. In Figure 39, an example of a screening plate is shown, where each tetrad is four technical replicates. Although the analysis of this screening however is still ongoing, it is shown below that most tetrads that cease growing the more temperature increases, are able to grow in the presence of taurine, implying that the gene deletion they harbor is not affecting the taurine import, however upon closer investigation there are also strains that are not benefited, implying a potential involvement of the gene deleted in the import mechanism.

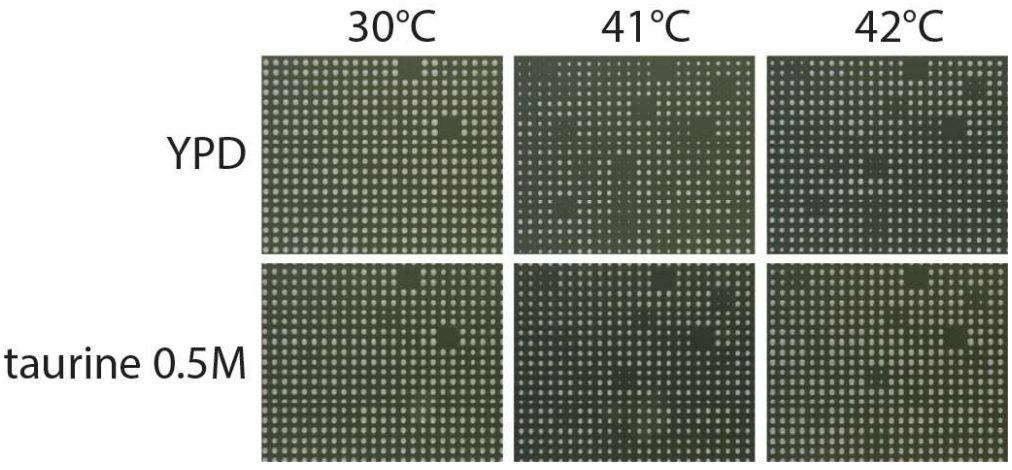

Figure 39: Pinning sample from the KO screening. The plates consist of tetrads of each genotype (technical replicates) with wt cells surrounding the KO mutants. The majority of the cells exhibit better growth at higher temperatures. KO collection was repined on new plates, incubated at designated temperatures in the presence or absence of taurine. Images were acquired in a Phenobooth station, after 24h of incubation.

3.2.6 Disease relevance

3.2.6.1 Taurine increases the viability of TDP43 expressing mutants, possibly through increased in vivo disaggregation rate

TDP-43 (TAR DNA-binding protein 43) is a RNA/DNA-binding protein involved in RNA processing and gene regulation. When dysfunctional in human, it has been linked to several neurodegenerative diseases, including amyotrophic lateral sclerosis (ALS), frontotemporal dementia (FTD), and Alzheimer's disease. In these conditions, TDP-43 miss localizes to the cytoplasm, forming toxic aggregates that disrupt cellular functions and contribute to disease progression. Attempts to degrade these aggregates, such as with PROTACs (proteolysis-targeting chimeras) have shown promise in reducing neurotoxicity and improving cellular health, making TDP-43 a promising therapeutic target. As previously demonstrated, taurine is a potent osmolyte, leading to protein stabilization. Building on this, we hypothesized that its capacity to improve protein interactions with the solvent could be leveraged to maintain protein solubility. Initially the potential of taurine to rescue mutants overexpressing *TDP43* was investigated, which does not exist in yeast endogenously, and can be lethal to *S. cerevisiae* cells as shown below.

However, the results showed that the lethality was not the complete picture, as decreasing the overexpression can lead to viable cells. It is therefore possible that the sheer amount of overexpression of the GALL promoter was too overwhelming for the cells to survive. To mitigate this issue, the GAL promoter was modified by removing the upstream activation sequence (UAS) to achieve weaker overexpression (GALS), resulting in cells more viable, but still unable to tolerate TDP43 overexpression for extensive time periods.

I show that indeed the lower overexpression of the GALS cells allows them to grow better compared to the GALL ones. Interestingly, taurine did not improve the viability of these cells, which either indicates that TDP43 is not susceptible to taurine, or that the damage is so severe that taurine is unable to reverse it (Figure 40A). Although no conclusions could be drown regarding any potential role of taurine in the TDP43 aggregation dynamics, taurine seems to have a role in the disruption of said aggregates, as indicated

in Figure 40B. Here, an overexpression of TDP43 tied to GFP leads to cell fluorescence, as cells form loci of TDP43 in variable sizes. Upon the halting of the overexpression, cells with taurine show a noticeable decrease in the fluorescence intensity.

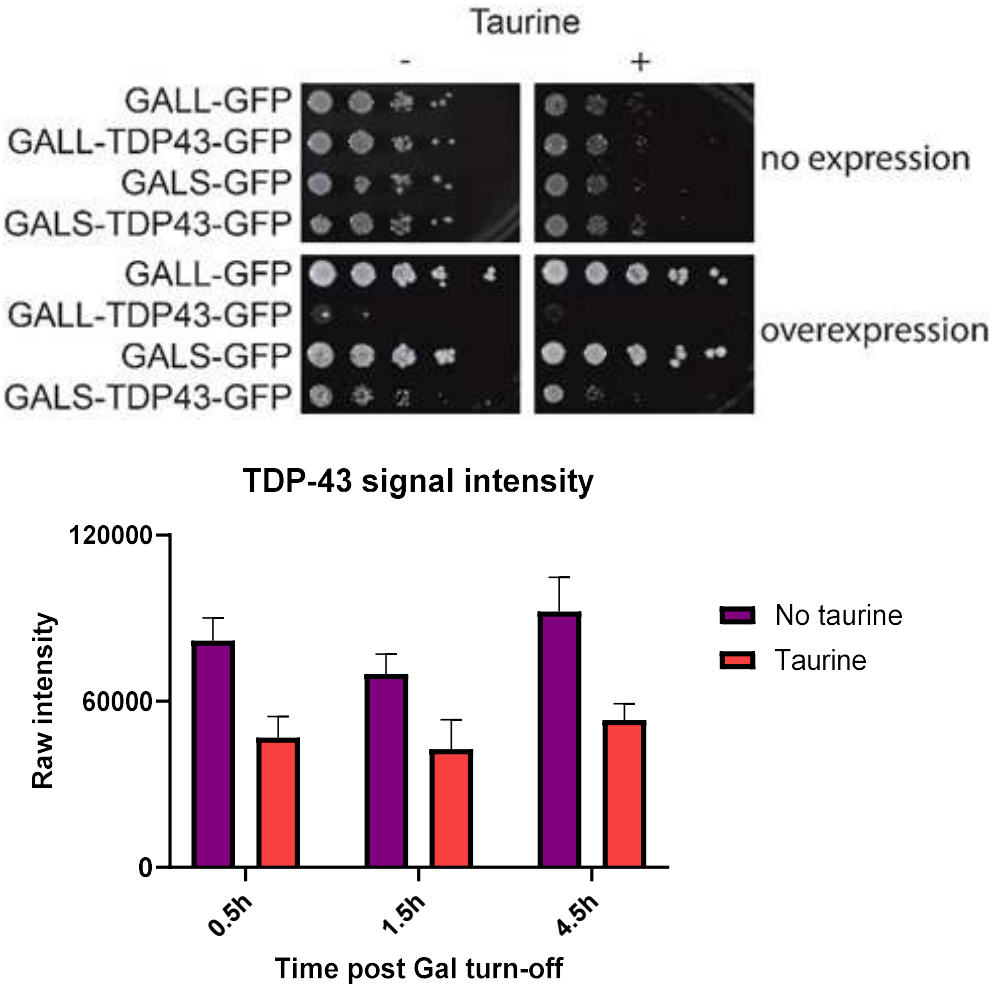

Figure 40: TDP43 aggregation alleviated upon taurine treatment. A. Spotting assay with TDP43-gfp overexpressing mutants of various intensities. Cells were cultures on YPD plates supplemented with taurine, incubated at designated temperatures, and images were acquired 48h post spotting. B. Plot showing signal intensity of TDP43-GFP in cells with and without taurine. Raw signal intensity reading as reported from the image analysis software for each detected cell, in medium with or without taurine, on different timepoints. Data are shown as mean ± SEM; n≥50 cells per sample.

3.2.6.2 Taurine rescues missfolding human senataxin disease alleles

Mutations in the senataxin (SETX) gene, which encodes a helicase protein, are linked to several neurodegenerative disorders, including ataxia with oculomotor apraxia type 2 (AOA2) and juvenile amyotrophic lateral sclerosis (ALS4). These mutations can lead to missfolding of the senataxin protein, disrupting its role in transcription regulation, RNA processing, and DNA damage response. Such dysfunctions contribute to motor neuron degeneration and other neurological impairments. Therapeutic strategies are being explored, focusing on restoring senataxin's normal function or compensating for its loss. The yeast homologue Sen1 has a lot of similarities to senataxin. These similarities have been leveraged to create Sen1 disease alleles mimicking the human ones, by replicating the same mutations in the conserved domains. In Figure 41, we tested several of these alleles that are known to missfold and we show that taurine successfully rescues them, but not the lethal Sen1 alleles. This is in agreement with the protein stabilization mechanism we suggest, and paves the way for potential applications of taurine in the treatment of these diseases.

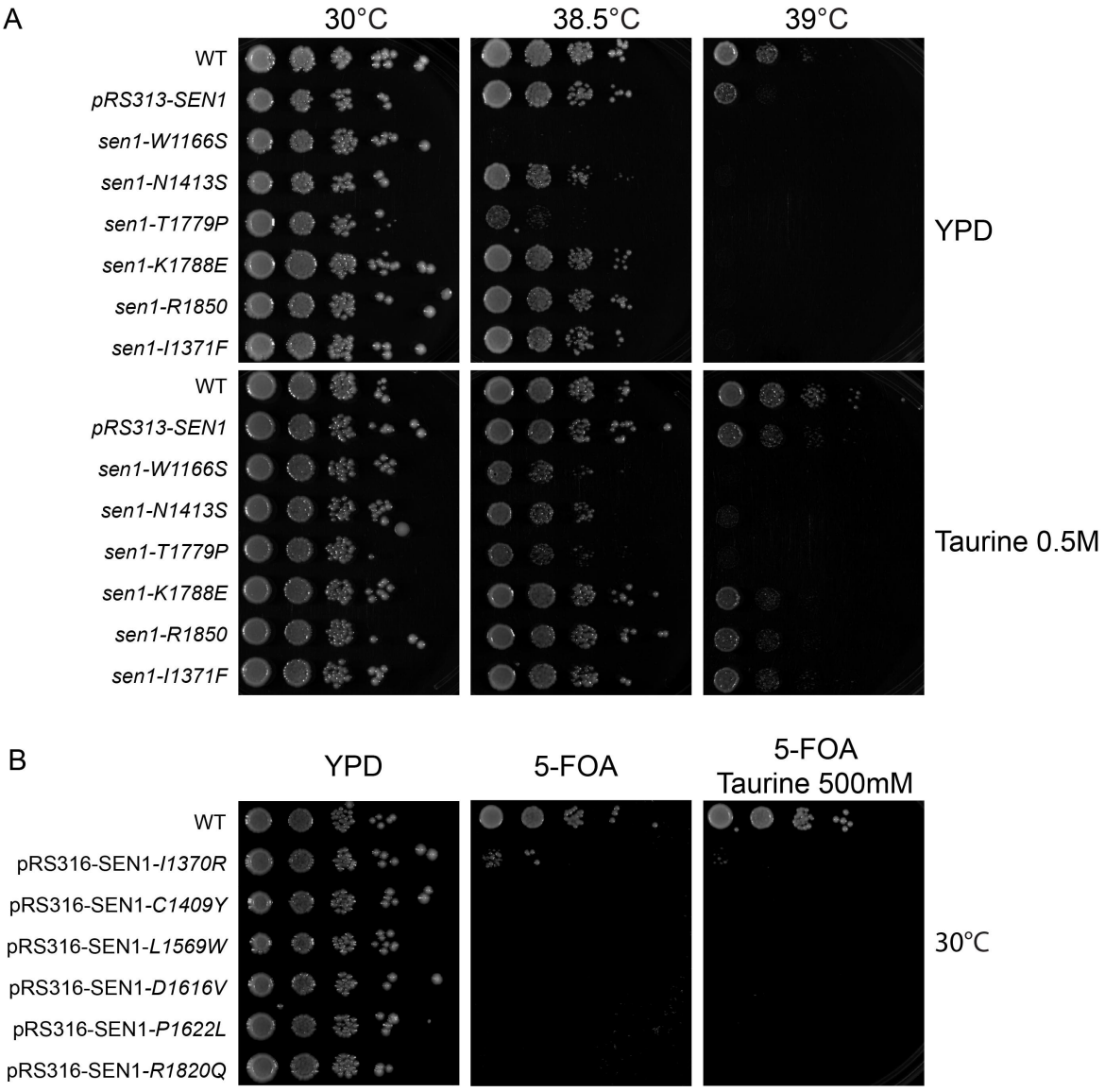

Figure 41: Spotting assays highlighting the difference in taurine rescue between missfolding and lethal SEN1 mutants. A. Spotting assay of sen1 TS alleles mimicking human senataxin disease mutations, in the absence and presence of taurine. Cells were cultures on YPD plates supplemented with taurine, incubated at designated temperatures, and images were acquired 72h post spotting. Full list of temperatures is displayed on A13. B. Spotting of lethal sen1 alleles, in YPD (expression covered by Sen1 plasmid), and 5-FOA plates (removal of covering plasmid) with and without taurine.

Discussion

4.1 AS signature

4.1.1 AS signature components are not individually sufficient to cause AS phenotype

As reported by Chang et al. 2011 among all non-essential genes in the *S. Cerevisiae* genome, deletion of approximately 200 genes leads to an accelerated entry into replicative senescence upon telomerase inactivation. To better understand the basis of this accelerated senescence, we first examined telomere length in the corresponding single-deletion mutants under telomerase-proficient conditions. If these single deletions lead to shorter telomeres to begin with, they will become critically short faster than if they were normal sized. However, this is not the case as among the tested mutants was no clear trend towards shorter telomeres, with some mutants even possessing telomeres longer than the ones of WT cells (Figure 6). To better understand the mechanisms underlying the AS (Accelerated Senescence) phenotype, we started the characterization of the AS mRNA signature. In order to do so, we utilized publicly available mRNA datasets of single KO mutants, in telomerase positive backgrounds. Although these cells do not senesce as their telomeres are properly maintained, we hypothesized that the deletions predispose these cells to senesce in an accelerated manner once telomerase is no longer active. Having acquired the mRNA expression profiles of single mutants that are reported to be associated with AS by Chang et al. 2011, we compared them to the expression profiles of mutants reported to senesce in a normal rate. In order to do so, an RF algorithm was developed in collaboration with the group of Prof. Zarnack, and the most important genes (features) were extracted using functionally diverse feature selection algorithms such as VSURF, BORUTA and TREESHAP. After finding the AS signature, we wanted to investigate whether any of the signature components is sufficient to lead to the manifestation of the AS phenotype by itself. Although for the majority of these genes it was their upregulation associated with the AS phenotype, we decided to also investigate the KO conditions in case we see an additional phenotype. To this extend, the senescence phenotype of KO mutants of a subset of the signature (features selected with VSURF) were analyzed using senescence curves in liquid media. As shown in figure 8, none of the deletions tested lead to an accelerated entry into senescence. However, this was again in line with the model's predictions. Naturally, we additionally tested

overexpression mutants of all the individual signature components, with a senescence-spotting assay. To achieve the overexpression we utilized a commercially available collection of overexpression plasmids (MoBy 2.0), which translates to an at least twofold overexpression, from the endogenous gene and the plasmid containing an additional gene copy under the endogenous promoter. Although the degree of overexpression might vary among the individual mutants, it ensures cell viability as in case the overexpression is harmful for the cells, they select for the optimal amount of plasmid (at least one per cell, which is needed for viability in selective media). As shown in Figure 9, although some mutants seem to be senescing in an accelerated manner, this was not observable among the biological replicates, therefore we concluded that none of the individual genes comprising the AS signature is sufficient to lead to AS.

4.1.2 Investigating the role of the AS signature in the AS phenotype manifestation

Since isolated signature components are not sufficient to lead to the AS phenotype manifestation, we hypothesized that maybe the signature as a whole is required to be present. This could in theory be tested via creating a multi-mutant with all signature components; however, it is not very feasible experimentally. Instead, we decided to use published mRNA expression databases and look for single KO mutants that seem to have an mRNA expression resembling the signature, ensuring that the mutants we find will at least have a percentage of the signature present. Initially, we identified a small set of mutants that seemed to possess the signature to varying degrees but were not reported to be associated with AS. Nevertheless, it was confirmed that they indeed possess at least parts of the signature using qPCR Figure 12A, and then proceeded to experimentally compare their senescence rates (Figure 12). As evident, *esc2, bim1* and *swi6* have a rapid decline in growth in the absence of telomerase, although they were not reported to be fast senescing in the original publication. Building on this success, we decided to incorporate an additional mRNA expression dataset and use it to expand the group we use to discover novel AS mutants, but also crosscheck the predictions based on the initial mRNA dataset. In Figure **7**, we show that now, area we can look for novel AS mutants (bordeaux) is bigger and we have access to more possible undiscovered AS mutants. Upon applying the model on the additional dataset as well, we plotted the predictions with their scores based on both mRNA datasets, and plotted them on a curve (figure 10). Here,

it is apparent that the predictions for most mutants align between the two datasets, and to confirm the functionality of the method I proceeded with the experimental confirmation of the most certain predictions, 12 mutants from the most certainly AS, and 12 from the bottom of the curve where the chances of them being AS are very low. These results are shown on figure 13, and it is evident that from the 12 strains predicted to be AS, five were indeed (*ptc1, pho85, fab1, sit4, cla4*). However, as mentioned in the introduction, the predictions are not necessarily for mutants exhibiting the AS phenotype rather than *rad52* like phenotypes. A characteristic example is the *elm1* mutant that was predicted to be the most *rad52* like but did not exhibit AS. However, it did not form survivors, which is a characteristic of *rad52* mutants. This collectively shows that our model is capable of predicting novel AS mutants, based only on the mRNA expression profiles of the respective non-senescing telomerase positive mutants, and to take it one-step further, it seems that these gene deletions predispose these cells to have a rapid entry into senescence upon telomerase inactivation. Additionally, when the 12 normal senescing predictions were tested, they were indeed senescing with a normal senescence rate, with the only exception being *yak1*. Upon further investigation though, it became apparent that the mRNA expression profile of *yak1* was distinct from the ones of the rest of the mutants (both AS and not) and there were not many other mutants in the mRNA databases having a similar mRNA expression profile. This could indicate that this was a result of underrepresentation of this mRNA expression cluster, rather than a false positive and it may suggest an additional mechanism of senescence predisposition or initiation.

In summary, we found an mRNA signature of telomerase proficient cells that can be used to predict whether a strain will senesce in an accelerated manner upon telomerase deletion. Furthermore, this system can be adapted to function with phenotypes different of AS, or with mRNA data from cells that have undergone any treatment with drugs or altered growth conditions. This paves the way to new discoveries based on machine learning rather than conventional phenotype observation.

4.1.3 Investigation of the AS phenotype

Upon discovering several novel AS mutants, we were interested in the mechanisms underlying this AS phenotype. A preliminary GO-term analysis did not yield any results, and no commonalities between these genes could be found. In the original publication, all KO mutants were categorized in three archetypes. The AS one was termed *rad52* archetype, due to *rad52* cells having a very rapid senescence phenotype. In order to determine whether the AS phenotype these novel AS mutants exhibit is Rad52 related, the senescence curves were repeated in a *rad52* background. As shown in Figure 16, nearly all of them, with the exception of *sit4* are additive to *rad52*, indicating a separate mode of function. To see if these gene deletions hinder the cells' capacity to deal with DNA damage, spotting assays were conducted with and without *rad52* in the presence of MMS, a general DNA damaging agent, and the results are shown on figure 15. Although there is high variability in some samples, possibly due to background mutations, it is interesting that none of the single mutants showed measurable sensitivity to MMS, however when combined with *rad52*, *cla4, esc2* and *bim1* double mutants were even more sensitive to MMS than *rad52* cells alone. Due to the qualitative character of the assays used and the variability among the replicates, no quantitative data can be extrapolated to confirm or reject the independence of these mechanisms to HR, however the consistency of the qualitative observations supports the conclusion of Rad52 independence. Adding to that, to see if there is any difference in their phenotype upon induction of telomere specific DNA damage in the form of telomere deprotection, spotting assays were performed in the *cdc13-1* background. Here (figure 16), there was no difference in the way *cdc13-1* cells become sick at semi permissive temperatures, with the exception of *pho85*, where a slight but reproducible rescue was observed.

Finally, in order to investigate whether they are senescing faster due to telomere shortening, a telomere shortening rate analysis was done. To this extend, samples were acquired along the progress of the individual senescence curves, and the telomere length of the 1L telomere were measured. As shown in Figure 15, in some samples the telomere-shortening rate is a bit steeper compared to the *tlc1* single mutants, however the SD of the samples did not allow for a solid answer. Overall, these results suggest that the reason these mutants senesce in such an accelerated manner is not because of recombination

issues or a role in telomeres. In addition, they do not have any major decline in telomere lengths, indicating that the senescence reason might be something not relevant. Upon further literature search, it became apparent that most of these genes however, are partially involved in cell cycle progression and specifically the Mitotic Exit Network, whose involvement in senescence is still under investigation.

4.1.4 Possible implication of the Mitotic Exit Network (MEN)

Despite the lack of strong functional commonalities among the newly identified AS mutants, literature analysis revealed that several of these genes have reported roles in the Mitotic Exit Network (MEN) or in processes related to mitotic progression (Figure 42). The Mitotic Exit Network (MEN) in budding yeast is a highly conserved signaling cascade that ensures the proper transition from mitosis into the G1 phase of the cell cycle. It coordinates the inactivation of the mitotic Cdks (cyclin-dependent kinases) to ensure proper chromosome segregation, spindle assembly and the cells' advancement into mitosis. Accordingly, perturbations in MEN signaling have the potential to exacerbate age-associated cellular decline. Aberrations in the cascade may lead to improper inactivation of mitotic Cdks or delayed cytokinesis, resulting in mitotic errors or prolonged cell cycle arrests. Such defects may promote genomic instability, a well-recognized hallmark of ageing and cellular senescence. Additionally, premature mitosis leads to aneuploidy and in mammalian cells can translate to senescence or malignant transformation and aberrant cell proliferation. In budding yeast, the MEN is composed of several key components, including the small GTPase Tem1, protein kinases such as Cdc15 and Dbf2 in complex with Mob1, and the effector phosphatase Cdc14. The activation of the network typically begins with Tem1, which initiates a kinase cascade that ultimately leads to the release and activation of Cdc14 from the nucleolus, which is the point of irreversible commitment to mitotic exit. Cdc14 then dephosphorylates numerous substrates to reverse Cdk-dependent phosphorylations, thereby promoting exit from mitosis. With respect to their reported positions within or adjacent to MEN signaling, Cla4 functions upstream of Tem1, while both Cla4 and Sit4 have been implicated in pathways leading to Dbf2 activation. Pho85 acts both upstream of Cdc14 and Dbf2 as well, while

Ptc1 inactivates the HOG pathway by dephosphorylating Hog1, and allowing the exit of Cdc14 from the nucleus. Notably, Bim1 has been reported to bind microtubules and to modulate the timing of mitotic exit.

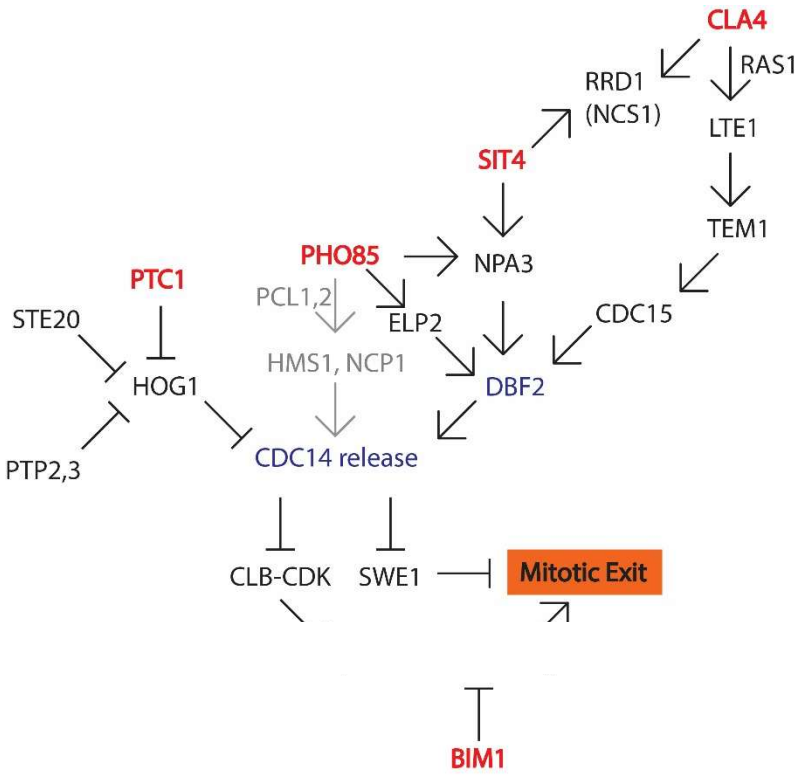

Figure 42: Schematic representation of the Mitotic Exit Network. Simplified depiction of relevant pathways involved in mitotic exit. Core MEN members are in blue, genes whose deletion was found to lead to AS are in red.

The spatial and temporal regulation of the events in MEN is critical, ensuring that cytokinesis occurs only after proper chromosome segregation in a timely manner. Another interesting aspect of MEN regulation is its contribution to cellular ageing, particularly in the context of asymmetric cell division, a process that central to yeast chronological lifespan. In *S. cerevisiae*, cell division is inherently asymmetric: the mother cell accumulates age-associated damage while producing a rejuvenated daughter cell. The MEN, through its regulation of the mitotic exit, indirectly influences this asymmetry. By precisely controlling the timing of mitotic exit, the MEN helps ensure that old or damaged cellular components remain with the mother cell, such as the old Spindle Pole Bodies that

are always inherited with the bud. This selective segregation is crucial for rejuvenating the daughter cell, essentially granting it a reset in terms of chronological and replicative age. With respect to MEN's potential involvement in the AS phenotype, defects in mitotic progression or delayed cell-cycle transitions could provide an explanation for the rapid decline in proliferative capacity observed, despite the absence of pronounced changes in telomere shortening rates. Additionally, impaired MEN function could lead to the gradual accumulation of DNA damage across successive cell divisions, potentially lowering the threshold at which cells undergo permanent cell-cycle arrest and senescence, however direct experimental evidence linking MEN dysfunction to the observed AS phenotype is currently lacking and will require further investigation.

4.1.5 MEN in senescence

The MEN is essential for proper mitotis exit, and ensures timely cell cycle progression. Dysfunction of core MEN components typically results in mitotic arrest, which is mechanistically distinct from the stable G1 arrest characteristic of replicative senescence. However, delayed or failed mitotic exit can cause age-associated catastrophic mitotic failures, genomic instability which intersect with age-related phenotypes and possibly limit replicative lifespan. In mammalian cells it has been shown that in the case of premature mitosic exit to the G1 phase of the cell cycle, regardless of the cells having the replicated DNA and centrosomal phenotype of a cell that has entered mitosis and failed to divide. A key modulator of MEN is the Cdc14 release from the nucleolus as part of the RENT complex (Regulator of Nucleolar silencing and Telophase exit), which includes also Net1 and Sir2. In addition to this however, Cdc14 is required for the proper segregation of highly repetitive regions, such as the telomeres. Senescent cells frequently display altered Cdc14 regulation, increased segregation defects, and elevated chromosomal instability, which may reflect age-associated deterioration and, potentially, impaired MEN function. Timely Cdc14 release is essential for untangling and physically segregating the long rDNA array before spindle disassembly, as well as decrease Dna2 mediated resection. cells defective in MEN-driven Cdc14 mobilization show over-resection, rDNA

bridges formation, rDNA recombination and anaphase delays, and even Extrachromosomal rDNA Circles (ERCs)[7].

Several of the genes whose deletion leads to AS are implicated in MEN-related pathways, and their loss may compromise aspects of mitotic exit regulation. Taken together, these observations suggest that the accelerated senescence observed in these knockout mutants is unlikely to be driven by accelerated telomere shortening, and may instead be influenced by the accumulation of telomere-independent DNA damage. This interpretation is supported by the observation that several of these mutants display reduced proliferative capacity even in the presence of telomerase, implying a possible delay in the cell cycle progression, likely due to DNA damage and subsequent repair, which however needs to be experimentally confirmed. Notably, the accelerated senescence phenotype becomes apparent primarily upon telomerase removal. A possible explanation is that in the presence of telomerase, telomeres are maintained and therefore remain capped, leading to an inactive DNA damage checkpoint, and even in the absence of these MEN genes, the damage is not extensive enough to trigger cellular arrest. In the case of telomerase deficient cells, telomeres get shorter until they get recognized as DNA damage. If these cells already experience elevated basal levels of DNA damage due to impaired mitotic regulation, the threshold of damage tolerated before checkpoint activation and permanent arrest may be reduced. Hence, when telomerase is deleted and the cells start experiening shortening telomeres, the checkpoint is triggered earlier. This model is consistent with telomere-length analyses showing that, although these cultures enter senescence at approximately 40 population doublings, their telomere lengths are comparable to those of tlc1 mutants at earlier stages of senescence. Then, the rate in which cell cultures will halt their growth will assumedly depend on the extend of MEN miss regulation that results from the deletion of the individual genes.

When telomerase is present, however, critically short telomeres never arise and Mec1 remains largely inactive. Under these circumstances, MEN deletion still causes cytokinesis defects, spindle checkpoint activation, and modest genomic instability, but cells retain sufficient repair capacity and nucleolar integrity to continue dividing, even in a reduced rate. Thus telomerase may act as a buffering factor that uncouples MEN-

associated mitotic perturbations from telomere-dependent DNA-damage signaling pathways that ultimately enforce permanent G1 arrest. It would therefore be interesting to investigate whether the critical telomere length of these KO mutants is the same as with the normal senescing ones, or whether there is a correlation between this critical length and the amount of DNA damage a cell has accumulated.

4.2 Investigation of taurine supplementation benefits in yeast

4.2.1 The effect of taurine on yeast cells

It has been reported recently that taurine extends the lifespan of multiple organisms, however, these results were not recapitulated in *S. Cerevisiae*. We initially considered whether the absence of a lifespan extension in S. cerevisiae could be attributed to its telomerase-positive status, in contrast to the predominantly telomerase-negative organisms examined in the original study. Therefore although *S. Cerevisiae* is an excellent model to study senescence and ageing, telomerase has to be knocked out to allow for telomere shortening. However, even in a telomerase-negative background, taurine supplementation did not increase replicative lifespan (*Figure 19*). This suggests that telomerase activity alone cannot account for the lack of a lifespan phenotype in yeast, and that taurine's reported effects in mammalian systems may arise through mechanisms that are not readily captured within yeast replicative lifespan assays. A major difference is the time each cell needs to complete a cell cycle, and in mammalian cells, the lifespan extension may only be an indirect outcome of taurine's effects, rather than its direct effect. To identify any direct effects of taurine supplementation on yeast, the growth of wt yeast challenged by different DNA damaging agents was observed. In

Figure 21 it became evident that taurine benefits the growth of these cells in all conditions, but not in MMS. Upon closer examination, the MMS phenotype is biphasic as although in the beginning taurine seems to decrease the growth of cells exposed to MMS in lower concentrations, but once taurine concentration is 500mM, the growth of cells is almost normal. A possible explanation is that these deleterious effects of low concentration taurine are masked by taurine's growth improvement and the overall growth seems similar to the ones with just MMS and no taurine. Taurine has been shown to increase the uptake

of small molecules, like peptides although experiments are needed to confirm or decline this hypothesis, MMS uptake could therefore be increased in the presence of taurine. However, once taurine concentration gets higher, taurine exerts its beneficial effects on cells and improve their viability in MMS, back to the pre-taurine levels. This interpretation however, remains speculative, as MMS uptake was not directly measured in this study. Another type of damage investigated in this thesis is telomere deprotection. For this purpose, the *cdc13-1* tool was used and showed that taurine enables *cdc13-1* cells to grow better at semi-permissive temperatures (Figure 22).

In order to understand how this is achieved, I had to investigate whether taurine is epistatic with deletions that are known to rescue the *cdc13-1* phenotype. Several KO mutants were tested in a *cdc13-1* background, and taurine was found to be additive to the majority of these interventions. This suggests that taurine-mediated rescue is largely independent of the pathways previously reported to suppress the *cdc13-1* phenotype, and that taurine may not manifest its effects through interactions at the telomeres.

4.2.2 Taurine does not act *via* specific pathways and has a global effect

Taurine is not commonly binding directly onto proteins, and the concentration range used in this thesis to see rescuing effects and the physiological concentration in our bodies is orders of magnitude higher for a traditional small molecule mechanism of action, as these are usually in a nM scale (such as rapamycin at 3nM). Interestingly, taurine was also able to rescue additional mutants apart from *cdc13*-1 such as the ones on

Figure 28. Additionally, taurine supplementation can raise the maximum temperature in which wt cells can grow. These findings collectively suggest a more global mode of action for taurine rather than binding onto specific proteins. This conclusion is based on the breadth of genetic backgrounds and stress conditions under which taurine exerted a rescuing effect. Following this line of thought, I started experimenting with different parameters to find any information about taurine's underlying mechanism. One such experiment was the comparison between taurine and rapamycin, or taurine and antioxidants, which have been shown to rescue *cdc13-1* cells, but not many other mutants. In order to confirm that taurine does not have a common mechanism with rapamycin, more experiments were conducted with different TS mutants that taurine was shown to rescue, whereas rapamycin did not. Although taurine has some minor antioxidant capabilities, it is unlikely that this is the main mechanism of action, as taurine also rescued several other TS mutants that designated antioxidants failed to. Taking all the points above into consideration, and since taurine has a global effect and is not contained to just *cdc13-1* or just TS mutants. Given that osmolytes are well established to modulate protein folding equilibria without requiring specific binding interactions, my hypothesis was that taurine stabilizes proteins. Thorough literature research reveals that taurine has been implicated in protein stabilization *in vitro*, due to its activity as an osmolyte. Similarly, small molecules such as guanidine or trimethylamine-N-oxide (TMAO) can rescue Temperature Sensitive (TS) mutants. To confirm that this is the mechanism behind taurine's profound effects, I designed a study with different commonly used osmolytes, and other molecules that although not so common, resemble taurine's structure (Figure 31B) and thus should share some of its activity. Such examples are D-alanine, which is structurally similar to taurine, and it is also not proteinogenic due to its D conformation, and TMT (N,N,N trimethyltaurine), which discriminates from taurine by its loss the capability to form hydrogen bonds with its amino-moiety, as it is protected. Additionally, I wanted to investigate whether different osmolytes stabilize different proteins, depending on the protein and the osmolyte chemistry, however this did not seem to be the case. As shown in Figure 31, taurine is the most potent of all the osmolytes, along with trimethylglycine, a known protein stabilizer. Urea is a destabilizing osmolyte and it diminishes the growth of the tested TS mutants, showing that their viability is

inherently tied to the folding status of the protein, and depends on the osmolyte. TMT, is a stabilizer even if it has been reported to have destabilizing capabilities *in vitro*, however it is evident that taurine is more potent, suggesting that the amino-moiety is important for the stabilization but not necessary.

Although we did not observe and improvement in the growth of wt strains at 40°C with the addition of trehalose, a growth improvement was present with other osmolytes. This is interesting as trehalose is the preferred osmolyte of budding yeast, however it seems to not aid it in higher temperatures, despite it improving the viability of TS alleles in their corresponding semi-permissive temperature. From an evolutionary perspective this can be attributed to the lack of the need for budding yeast cells to survive these temperatures naturally, but how does trehalose improve the viability of TS strains but not wt? The reason wt cells cannot survive the 40°C is similar to the TS alleles at the non-permissive temperatures, one essential protein (or a group) are missfolding and stop functioning. In the case of other osmolytes such as taurine, they can stabilize these misfolded proteins, whereas trehalose might have a lower affinity, hence the wt cells do not grow.

Overall, it is showed here that taurine's effects are not strictly taurine's, as they are common among a category of molecules termed osmolytes. Other molecules belonging in this group exhibited the same effect, in various degrees, and interestingly different proteins were affected differently by the individual osmolytes. The concept of osmolyte induced protein stabilization is no news, but this study bridges the gap between the profound effects of taurine in the cells, with the protein stabilization theory *in vivo.*

4.2.3 Exploring the Mechanisms of Osmolyte-Induced Protein Stabilization: Insights from Screening TS Mutants

Although all data suggests that taurine acts *via* protein stabilization, it is not known what determines if a protein is susceptible to stabilization or not. In order to shed light there, a screening with taurine was conducted, using the TS collection on various temperatures, to collect data on which alleles are rescued and what commonalities they might have that non-rescuable ones do not. So far, there was no enrichment of rescuable mutants in any cellular compartment, no pathway enrichment and not a temperature where taurine rescues the best. Our data suggest that more than half of the TS mutants are rescued by

taurine allowing to study factors that do not affect the degree of rescue, such as cellular compartment or semi-permissive temperature. To assess the quality of the screening and of its analysis (performed by Eduardo Gameiro), I proceeded to manually spot 12 of the most and 12 of the least rescued mutants, in the presence of taurine, to confirm their characterization. As shown in Figure 37, all mutants reported to be rescued were in fact rescued, and not all of the reported as non-rescued were actually correct. This however, is in line with our predictions as for the characterization of strains to rescued or not, very stringent cutoffs were set. With the screening's quality confirmed, I wanted to investigate how different osmolytes work, and whether their difference extends further from having different affinities for different proteins to whether one osmolyte can stabilize protein another cannot. To get a closer look into this, a small-scale experiment with four osmolytes that vary in their structure was performed, and as for proteins, four mutants that taurine rescues and three that it does not lead to an observable rescue were chosen. The results of this experiment (figure 33) suggest that different osmolytes have varying affinities for different proteins, but whether a protein is rescuable or not depends on the protein itself. There are several characteristics of a protein that could dictate whether it is rescued or not.

One hypothesis aiming to explain how osmolytes can rescue these TS alleles is by alignment of the osmolytes along the mutated amino acid and mimicking the WT amino acid, restoring the folded conformation of the TS protein. Although this could potentially explain the different affinity osmolytes have with varying proteins, direct structural data supporting this hypothesis is very scarce, and require heavy cheminformatics simulations. Although this would be a wonderful addition to the taurine mechanism of action puzzle, it is unfortunately slipping away from the scope of this study. Alternatively determining factors could be the PI of the protein, or the aminoacid ratio it has which in the end affects the PI, although upon careful investigation it is unlikely due to the fact that even different TS alleles of the same protein seem to have different rescue potential, hence suggesting that it most likely the important factor has to do with the geometry of the unfolded state, which is in line with my hypothesis is that it is not about the protein characteristics only, but mostly the misfolded form. These TS proteins are in an equilibrium with their unfolded state. As introduced earlier, an osmolyte can stabilize a protein by reinforcing its hydration

sphere in the folded form, or directly interact with the misfolded form in an unfavorable manner, so that it shifts the equilibrium towards the proper folded one. What happens though if a protein has similar aminoacid ratios or numbers in its exposed chains between its folded and unfolded form? What if the SASA (solvent accessible surface area) between the two forms is the same? Then the osmolyte might have the same or very similar interactions in either sides of the equilibrium and hence be unable to “tip” it towards the folded state (Figure 5).

The answer to this might come from the Solvent Accessible Surface Area (SASA). The solvent accessible surface area (SASA) of a protein is defined as the area of the molecular surface that is in contact with the solvent. This parameter is crucial when analyzing how osmolytes modulate protein stability because it provides a quantitative measure of which regions of the protein are available for interactions with solvent molecules and small added solutes. SASA allows not only for the easier visualization of the protein’s three-dimensional arrangement but also guides our interpretation of how different osmolytes influence the native state of proteins, by providing a metric to be used for comparing different protein states or osmolytes. Using SASA, we can distinguish between proteins or protein segments that are inherently prone to destabilizing interactions and segments that contribute to overall resilience. Recent studies have employed SASA assessments to predict the effects of different osmolytes on protein stability by monitoring the surface exposure of amino acid side chains and the protein backbone. Advanced molecular dynamics simulations have increasingly employed SASA calculations to map transient interactions between the protein and its surrounding solvent environment. These computational studies have demonstrated that even minor modifications in SASA can produce significant shifts in stability, directly influencing the equilibrium between the unfolded and folded states. Moreover, SASA-based models offer a parameter-free approach that is coherent with the electrostatic potential of the interacting surfaces, providing a broad and robust framework for predicting the impact of various osmolytes on protein stability. Thus tracking the changes in SASA upon osmolyte addition, but also between the folded and misfolded protein structures helps in dissecting the dual role of water and osmolytes in mediating protein-folding dynamics. In summary, solvent accessible surface area offers a powerful tool through which we can understand

and predict osmolyte-protein interactions. By integrating SASA measurements with the well-established concepts of hydration and preferential exclusion, we are better equipped to understand the balance of protein stability and how osmolytes can tip it.

4.2.4 Taurine can act synergistically with other osmolytes, and mitigate the effects of denaturants

In this study, I argue that taurine harbors its effects *via* protein stabilization. To support this argument, we designed an experiment where taurine is supplemented to actin TS mutants which have impaired proteasome degradation machinery. In theory, TS actin mutants could have a slight rescue phenotype when combined with mutations that impede protein degradation, by tipping the balance towards the folded protein state. Specifically, the folded protein state is in equilibrium with the misfolded state, by raising the amount of misfolded actin we would also increase the amounts of properly folded one. This rescue phenotype was not observed in figure Figure 35, while taurine showed a rescue phenotype regardless of the genetic background. Importantly, this negative result does not argue against protein stabilization, as impaired degradation of a highly abundant protein such as actin is expected to exacerbate proteotoxic stress.

Although this might imply taurine might act in an ubr1 or san1 pathway, a more plausible explanation is that since actin is so highly expressed, interfering with the degradation might lead to massive amounts of misfolded proteins, which impairs the cells further instead of allowing them to function better. This is in agreement with the fact that the TS mutants contained these deletions, are growing even worse than the single mutant in high temperatures, but grow perfectly well at permissive temperatures. The failure of *ubr1* and *san1* to rescue TS growth suggests that the removal of misfolded actin was not enough to restore viability to the TS mutants, possibly due to an unfavorable K constant in the folded/misfolded equilibrium. Taurine likely stabilizes the folded state of actin directly, bypassing the need for degradation of misfolded species, however the results of this experiment could not confirm nor decline the activity of taurine through protein stabilization. In order to show that taurine stabilizes proteins by acting as an osmolyte, a combination of taurine and a second common protein stabilizer, betaine (trimethylglycine)

was used. As shown on figure 34, betaine rescues the two TS mutants to the same extend if not slightly better than taurine. The condition with the highest effect is 0.5M of betaine. When used taurine and betaine in combination, at 0.25M each, the effects are similar to either of the osmolytes at 0.5M. Ideally, the experiment would have been performed with 0.5M of each osmolyte to show that they are not additive, but there would be several problems with this setup as we are not certain that the stabilization is happening at osmolyte concentrations above 0.5M, the solubility of the osmolytes at a combined molarity of 1 M is not guaranteed at these temperatures, and these high concentrations would eventually initiate the cell's response to osmotic stress, introducing more parameters to the experiment. Another way to approach the same question is by using urea instead of betaine. Urea is a broadly known agent that denatures proteins as a destabilizing osmolyte. In order to show that taurine but also other osmolytes mitigate urea's deleterious effects on TS mutants, TS mutants were cultured on plates with a combination of taurine and urea and as shown in

Figure 34, taurine and all osmolytes used can reverse the effects of urea. Moreover, the growth at 29 °C for the combination of osmolyte and urea looks similar to the YPD control, if not better, depending on the osmolyte. Finally, it is shown that different proteins react differently to osmolytes such as the case or *rsp5-3* where regardless of the taurine supplementation; it is too sensitive to urea to be rescued, which further highlights the importance of the protein structure in the osmolyte susceptibility. These results highlight how much of an effect osmolytes have in cells, how they can ensure proper protein function under stress, and further indicate how broad of an application field they have.

It is by now evident then that taurine in fact harbors its immediate effects in yeast as well, as shown by the protein thermal stability experiments. Building on that, I hypothesize that since budding yeast is shorter lived than mammalian cells, they might not accumulate as many misfolded proteins so that it would affect their replicative lifespan, and that could be the reason we do not see an effect on the 10 days timespan of a senescence curve. In order to confirm or reject this however, additional experiments should be performed, studying yeast cells in a longer timespan to allow for the accumulation of misfolded

proteins. Such experiments could be either mutants prone to quick accumulation of misfolded constructs, or a chronological lifespan assay focusing on mother cells. Yeast cells divide in an asymmetrical way, with the daughter cells being “reset” while the old mother cells tend to accumulate the organelles and old proteins of the cell. Therefore this experiment ought to be closer to the lifespan measurements done in the original study as the mother cells would have enough time to accumulate misfolded proteins that taurine can act on, and lead to an observable increase in lifespan.

4.2.5 Investigating the Mechanisms of Taurine Import into Yeast Cells

S. cerevisiae does not rely on taurine for its osmolyte needs. To date, no study has been published on how taurine enters yeast cells, and since taurine is a polar compound, it is more difficult to be passively imported through the membrane. It is also not unlikely that taurine uses the transporters of similarly structured aminoacids to get inside the cell; however, we also do not know the efficiency of that route. In order to identify the importing mechanisms of taurine, we designed a screening of the KO collection, cultured in high temperatures with and without taurine supplementation. We suggest that upon the deletion of a taurine transporter, endogenous taurine levels will decrease. We have shown that taurine supplementation increases the viability of non-TS strains at high temperatures. When intracellular taurine levels drop, we expect to not see this consistent rescue that taurine has, and therefore highlight these non-rescued strains as potential taurine import mutants. Although the analysis of the screening is still pending, it will offer valuable insights on how taurine is imported in yeast and potentially answer some of the questions as to why the yeast results differ that much from the ones of other organisms. However, I strongly believe that the efficiency of the import still has to be evaluated with quantitative techniques such as HPLC-MS, in order to provide concrete support for its importing mechanisms. Apart from the supportive role this screening has in the research of taurine in yeast, it has the potential to highlight novel ways taurine enters cells in human, besides its canonical importers. Finally, it will allow the development of mutants that facilitate further investigations into taurine biology.

4.2.6 Modelling ataxia in yeast

Ataxia with Oculomotor Apraxia type 2 (AOA2) is a disease caused by improper SETX function. Senataxin (SETX) is a critical DNA/RNA helicase that ensures proper RNA processing by resolving R-loop structures during transcription. The helicase domain of SETX is highly conserved, and is similar to the Sen1 helicase domain in budding yeast. It has been published that missense mutations in the SETX gene can be replicated in yeast Sen1 and lead to improper folding of the sen1 protein. This missfolding compromises its helicase function, resulting in inefficient resolution of R-loops and subsequent transcriptional dysregulation. In human, the resulting neuronal dysfunction and loss manifest clinically as ataxia, highlighting how the structural instability of senataxin leads to the disease pathology. These *SEN1* alleles are TS and in *S. cerevisiae* TS alleles are powerful tools for studying essential genes and their functions. In permissive temperatures the proteins are folded normally, mimicking the WT counterpart and remain functional. Once the temperature reaches and surpasses a threshold, they missfold, drastically become less functional and since they are essential, they lead to observable phenotypic changes, in most cases decreased growth. In Figure 41 it is shown that all TS Sen1 mutants are rescued by taurine, whereas mutations that abolish the functionality of the protein altogether are not. This not only reinforces the notion that taurine is a very potent protein stabilizer, but also highlights potential uses of taurine as a drug against diseases of nature similar to the ones we modelled.

4.2.7 Potential taurine applications

As shown in the results section, taurine was also able to rescue all non-lethal *SEN1* TS mutants, which in combination with the fact that these mutations were inspired by real senataxin mutations, and the fact that the helicase domain of senataxin and *SEN1* are highly conserved, raises the possibility that taurine supplementation could be explored as a modifier of protein stability in disease contexts such as ataxia.

However, ataxia is not the only disease that can stem from improper protein folding. Genetic mutations, environmental stresses, and age-related declines in proteostasis also compromise folding fidelity, leading to the formation of toxic oligomers or protein aggregates.

These aggregates disrupt cellular homeostasis by impairing mitochondrial function, triggering endoplasmic reticulum stress, and activating the unfolded protein response (UPR) as cells attempt to cope with the accumulating load of aberrant proteins. These misfolded proteins are the culprits behind several neurodegenerative diseases such as Alzheimer's disease, Parkinson's disease or amyotrophic lateral sclerosis (ALS). Neurons are especially vulnerable to proteostasis failure given their limited regenerative capacity. The persistent accumulation of misfolded proteins not only overwhelms cellular quality control systems such as molecular chaperones and degradation pathways like autophagy and proteasomal clearance, but also sets the stage for chronic inflammation and eventual cell arrest or death. Current therapeutic approaches often explore ways to enhance these intrinsic protective mechanisms, either by upregulating chaperones or by pharmacologically activating clearance processes.

In this thesis I have touched the surface of potential taurine applications in such aggregation prone proteins by showing a trend of taurine to decrease the presence of TDP43 aggregates, however the mechanism is still not confirmed. Subsequently, additional experiments are required, such as FRAP to measure and quantify the impact of taurine in the de-aggregation and confirm the hypothesis that it also acts in the prevention of said aggregates, when supplemented in advance. Additionally, taking into consideration the fact that different osmolytes exhibit different affinities on specific proteins, hence it is highly plausible that although an osmolyte might not be applicable to a specific disease or protein aggregate, another might very well be. In order to test for this either experiments need to be conducted, similar to the ones shown here, or we can also leverage the technological leaps characterizing our times and conduct cheminformatic simulations with different protein and osmolyte on platforms such as Gromacs, uncover structural patterns of proteins that predefine the most compatible osmolyte and then advance to the translation of these into the lab using cells.

Taurine and other osmolytes maintain the protein hydration shell and promotes a favorable folding environment, indirectly supporting the proper functioning of chaperone proteins and the UPR, ultimately mitigating the cytotoxic effects of aggregated proteins. These qualify taurine as a promising candidate in addressing neurodegenerative

diseases associated with protein missfolding. In fact, considering how broad taurine's activity is I firmly believe it can find applications in the treatment of several diseases in addition to neurodegrading ones, including diseases of ageing and proteinopathies in general.

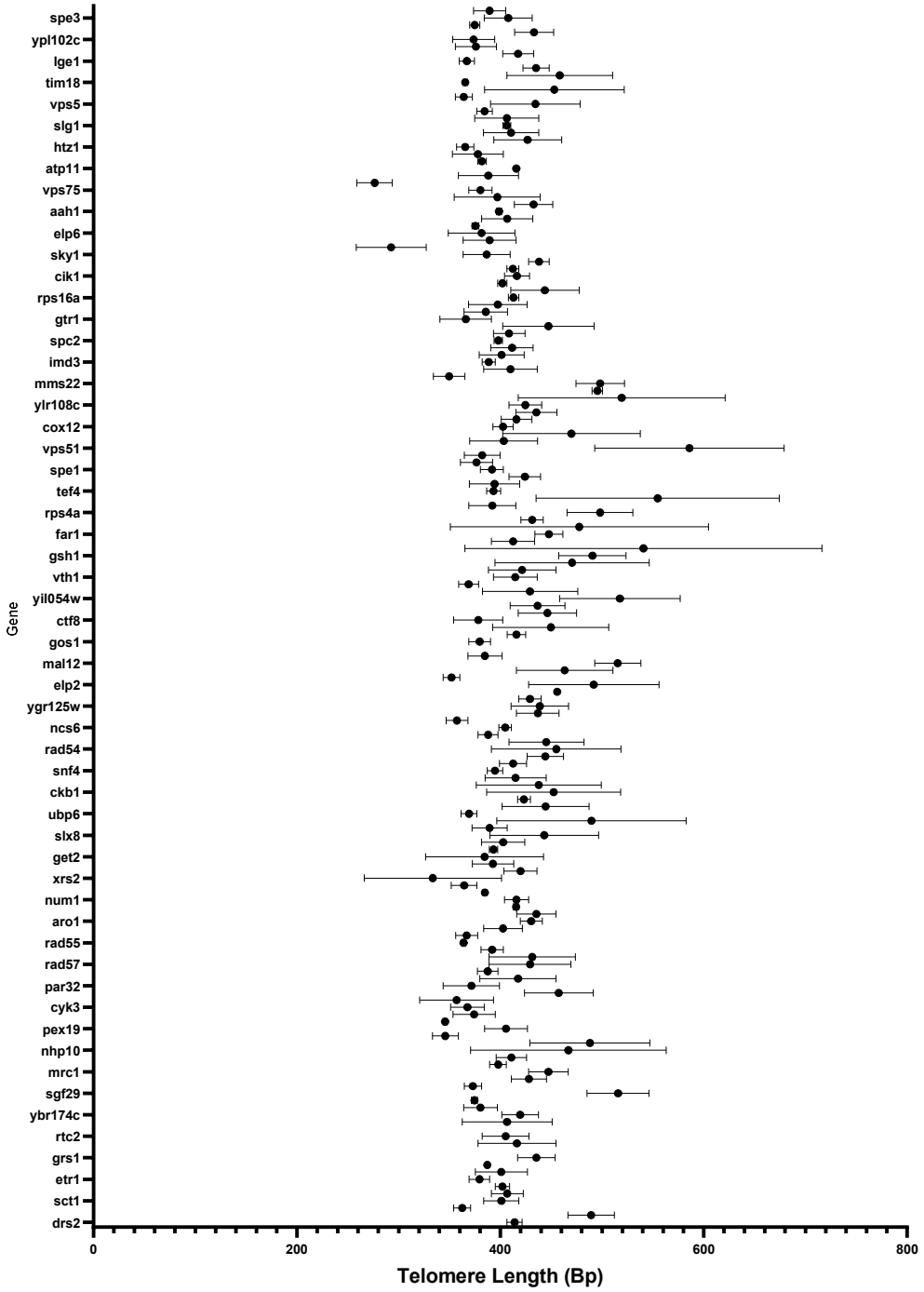

Appendix figure 1: Telomere length measurements of single mutants. Mutants have variable telomere lengths, with some of them even having longer telomeres than those of wild-type cells. X-axis is telomere length in base pairs, Y-axis the individual gene KO mutant tested. Data are shown as mean ± SD; n≥3 biological replicates per genotype.

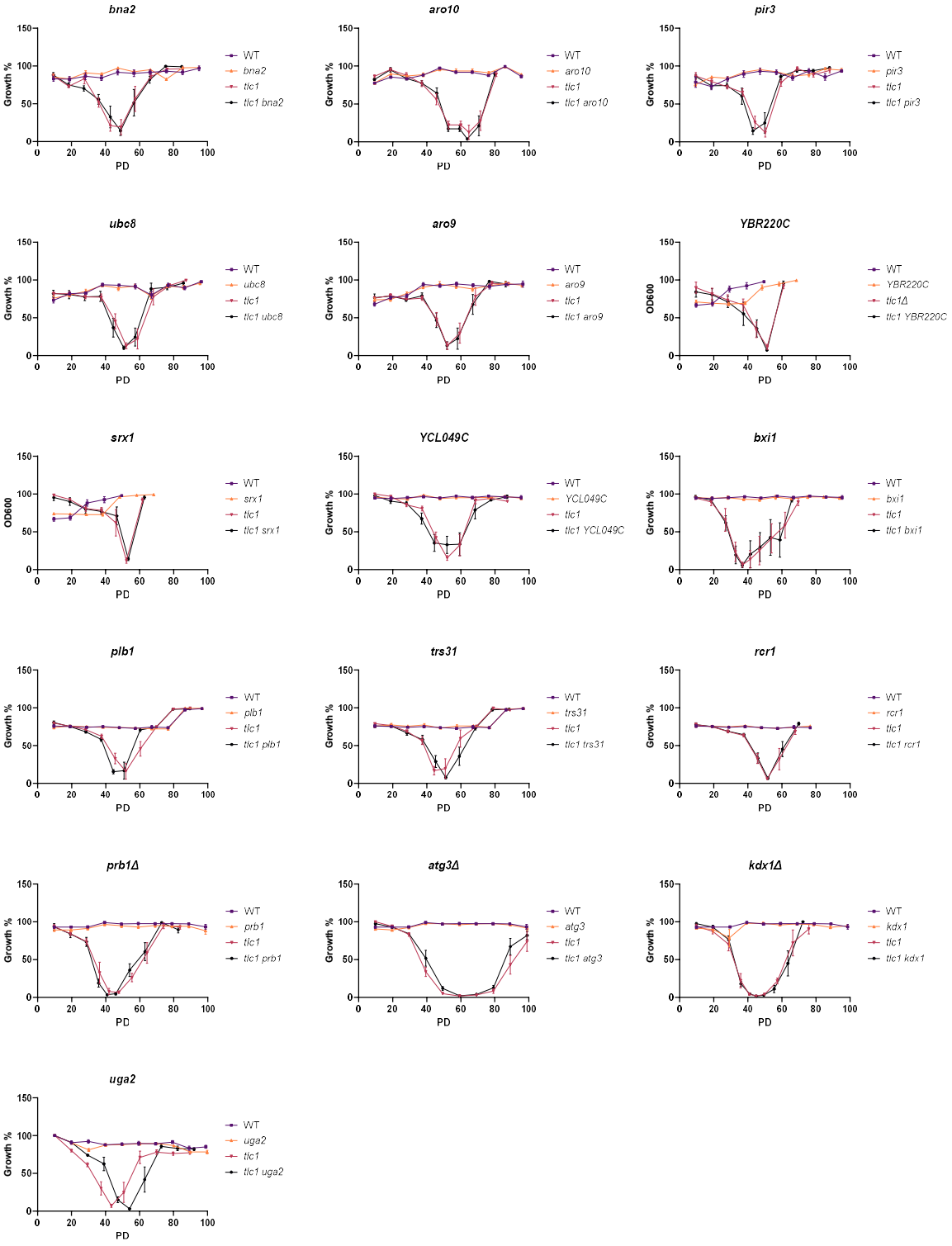

Appendix figure 2: Senescence curves of KO mutants of genes in the VSURF prediction package. All cells were cultured in YPD and were measured and diluted to a fixed OD_{600} every 24h.

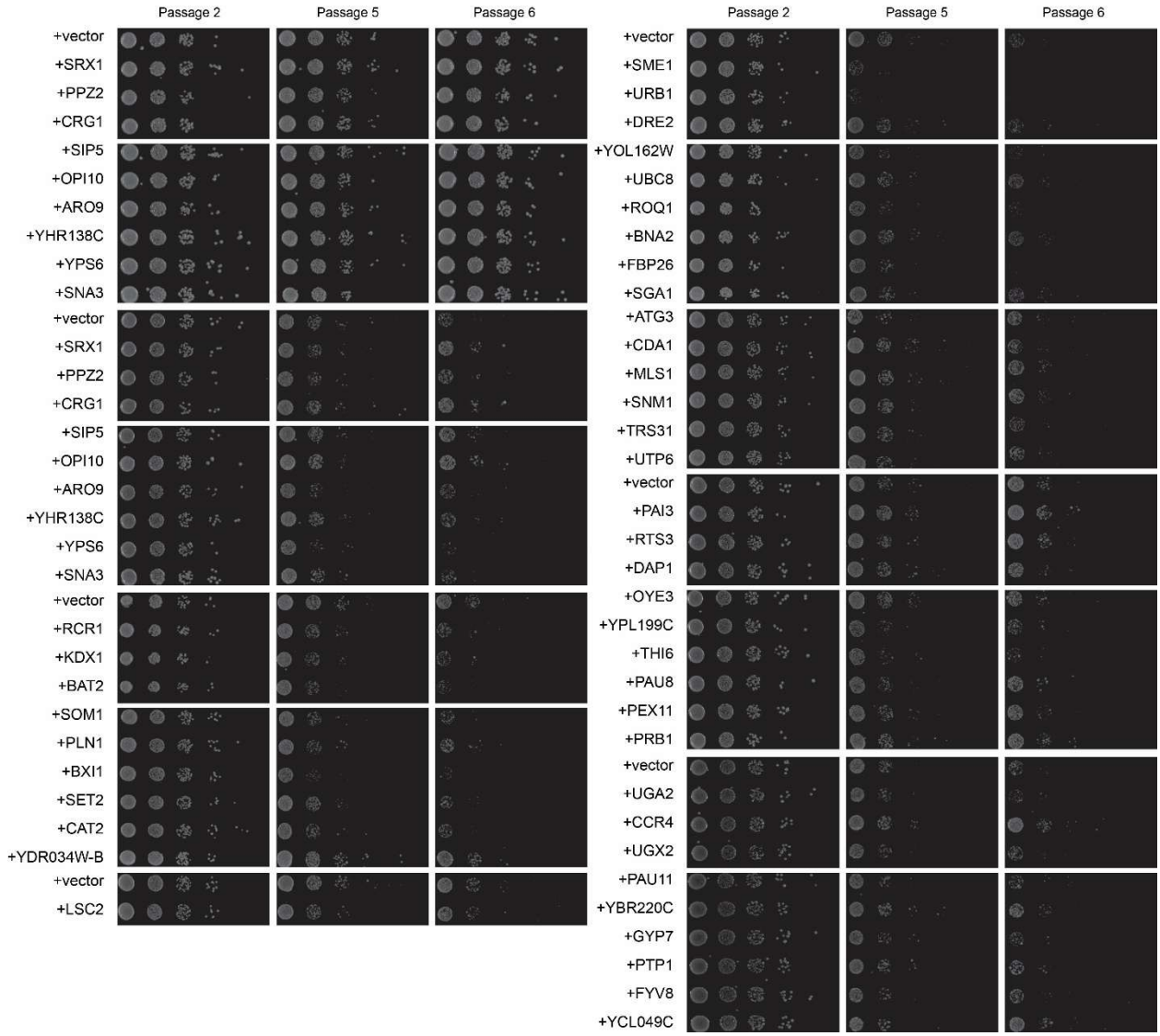

Appendix figure 3: Overexpression mutant spotting assays. Spottings of mutants having an at least twofold overexpression of the genes in the AS signature. All cells were cultured on –Leu plates to select for cells having at least one copy of the respective overexpression plasmid. After 48h, samples were taken from each genotype (same column) and was re- spotted on fresh plates. Images were acquired after 48h.

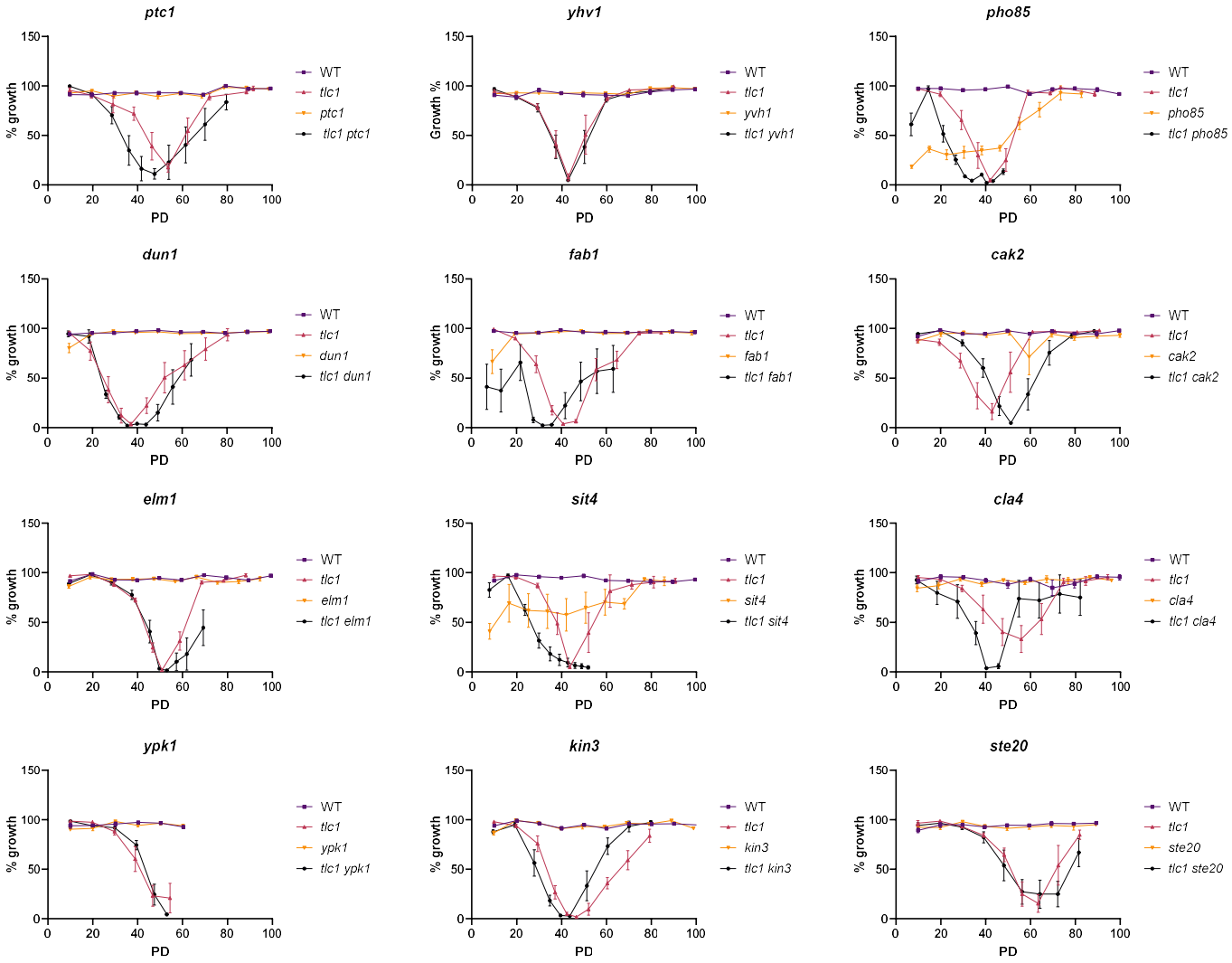

Appendix figure 4: Senescence curves of all KO mutants predicted to be AS. KO mutants exhibiting the AS signature in telomerase positive conditions, have telomerase removed and have gone through senescence curves in YPD. All cell cultures were measured and diluted to a fixed OD_{600} every 24h.

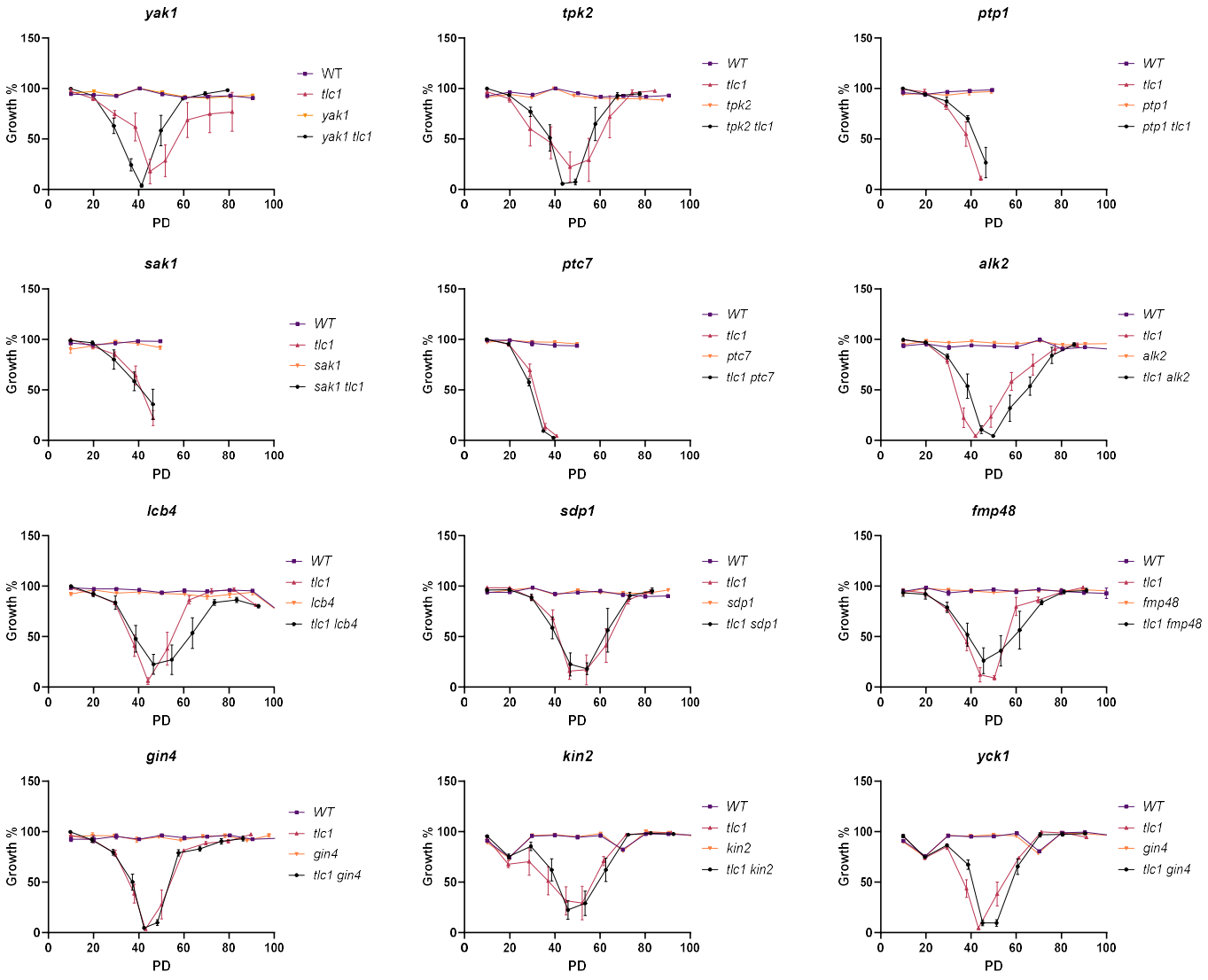

Appendix figure 5: Senescence curves of strains predicted to be senescing in a normal rate. KO mutants not exhibiting the AS signature in telomerase positive conditions, have telomerase removed and have gone through senescence curves in YPD. All cell cultures were measured and diluted to a fixed OD_{600} every 24h.

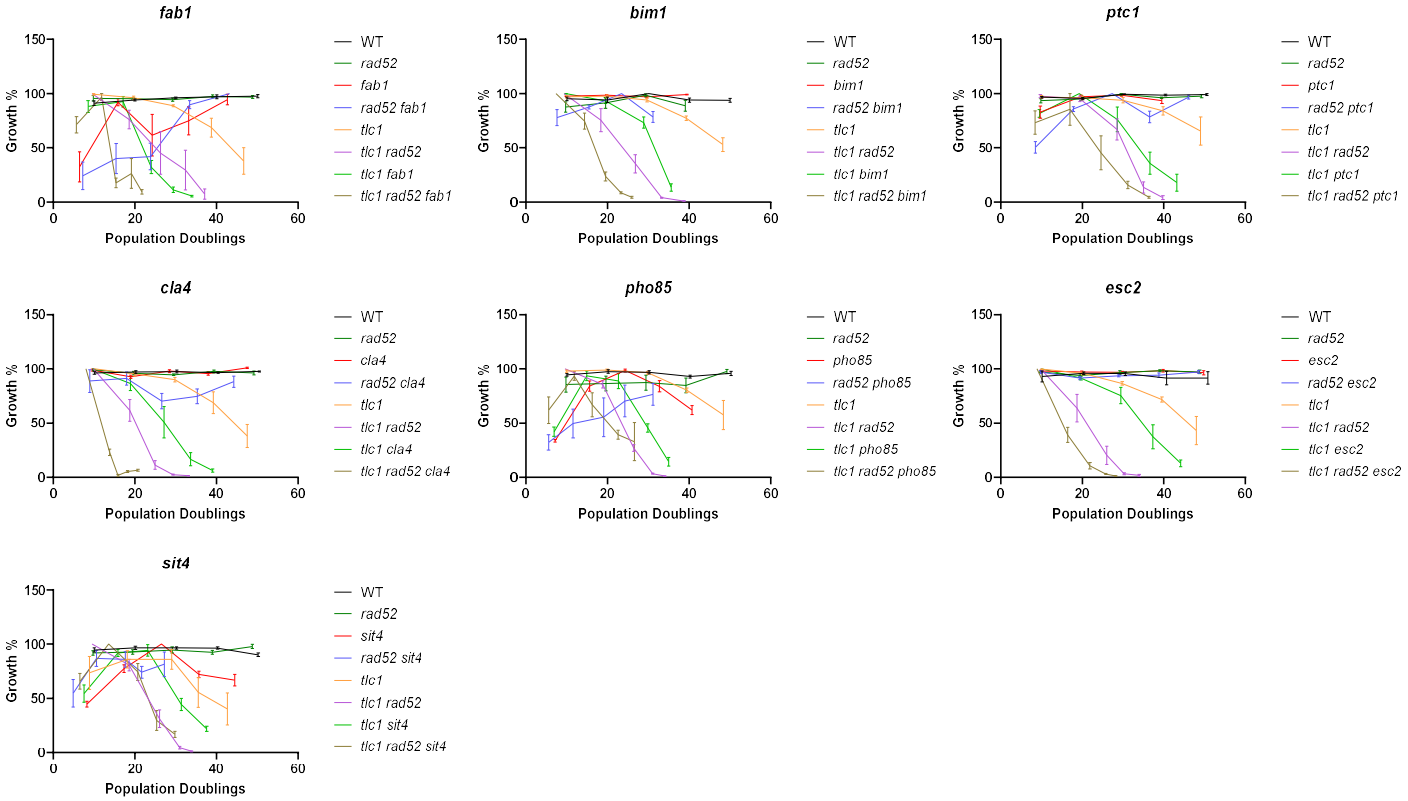

Appendix figure 6: Senescence curves of novel AS strains in *rad52* background. Confirmed AS mutants have been studied in *rad52* conditions to investigate whether the AS phenotype is *RAD52* dependent. All genotypes were isolated from the same diploid cells to avoid differences in the background.

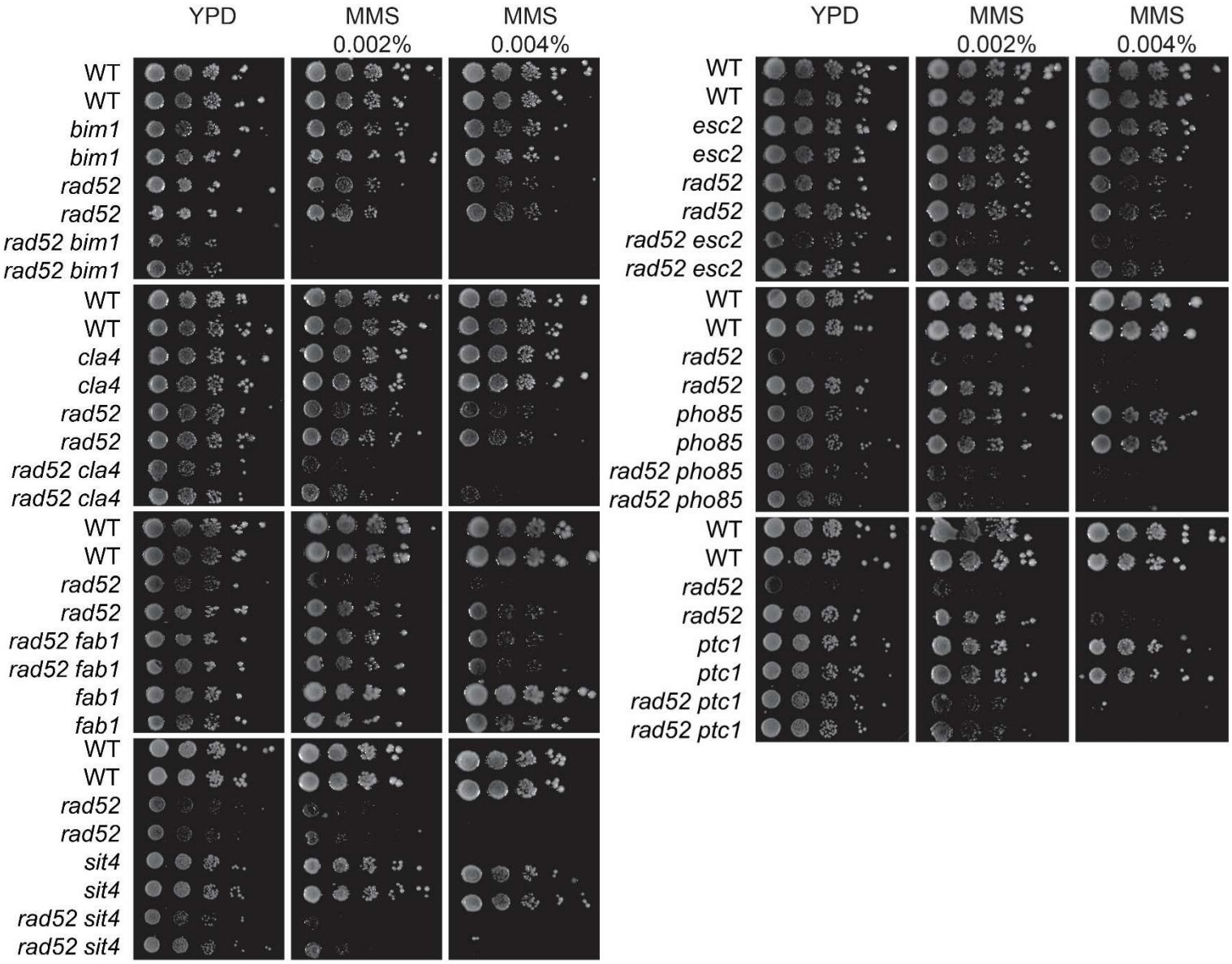

Appendix figure 7: Complete list of spottings in *rad52* and MMS exposure. KO mutants shown to be AS in telomerase negative conditions, were paired with *rad52* and cultured in MMS to investigate whether they are sensitive to DNA damage. All cultures were done in YPD supplemented with MMS according to the description.

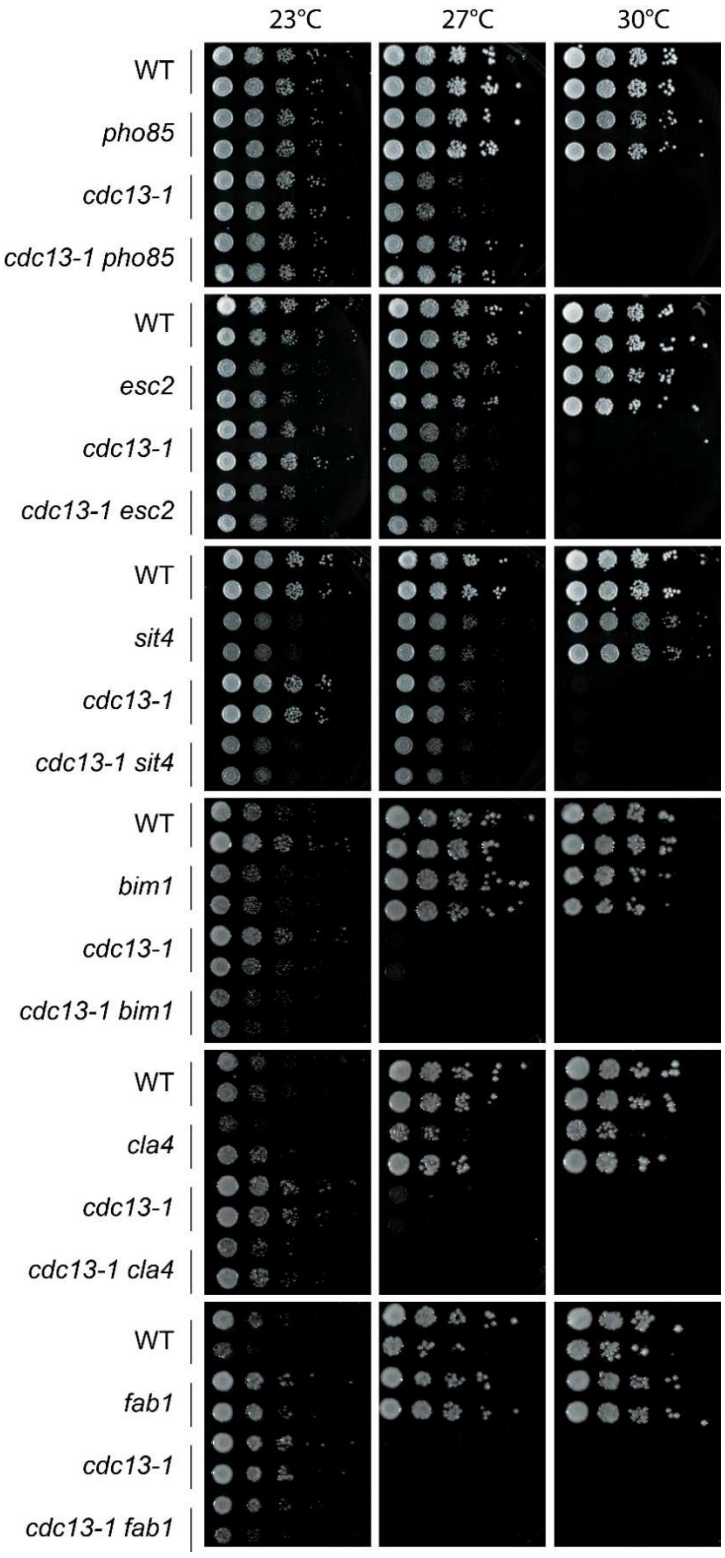

Appendix figure 8: complete list of AS mutants in *cdc13-1* background. KO mutants leading to AS were combined with *cdc13-1*. All cells were cultured in YPD and in the indicated temperatures.

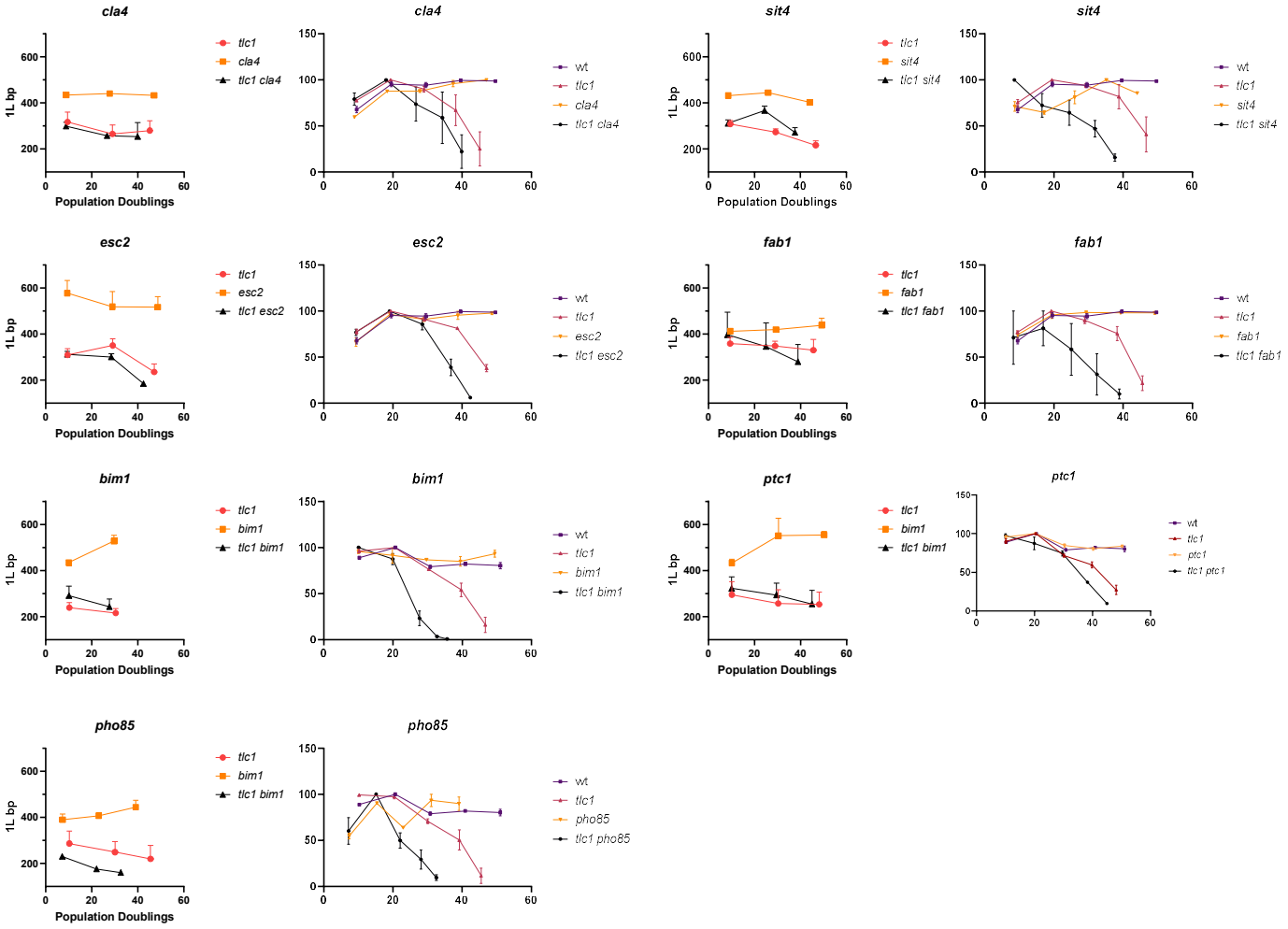

Appendix figure 9: Telomere shortening rate measurements of all tested mutants. Senescence curves of confirmed AS mutants were repeated and cell samples were acquired with each dilution. Telomere length of 1L telomere was measured with telomere-PCR and the results were displayed next to the respective senescence curve.

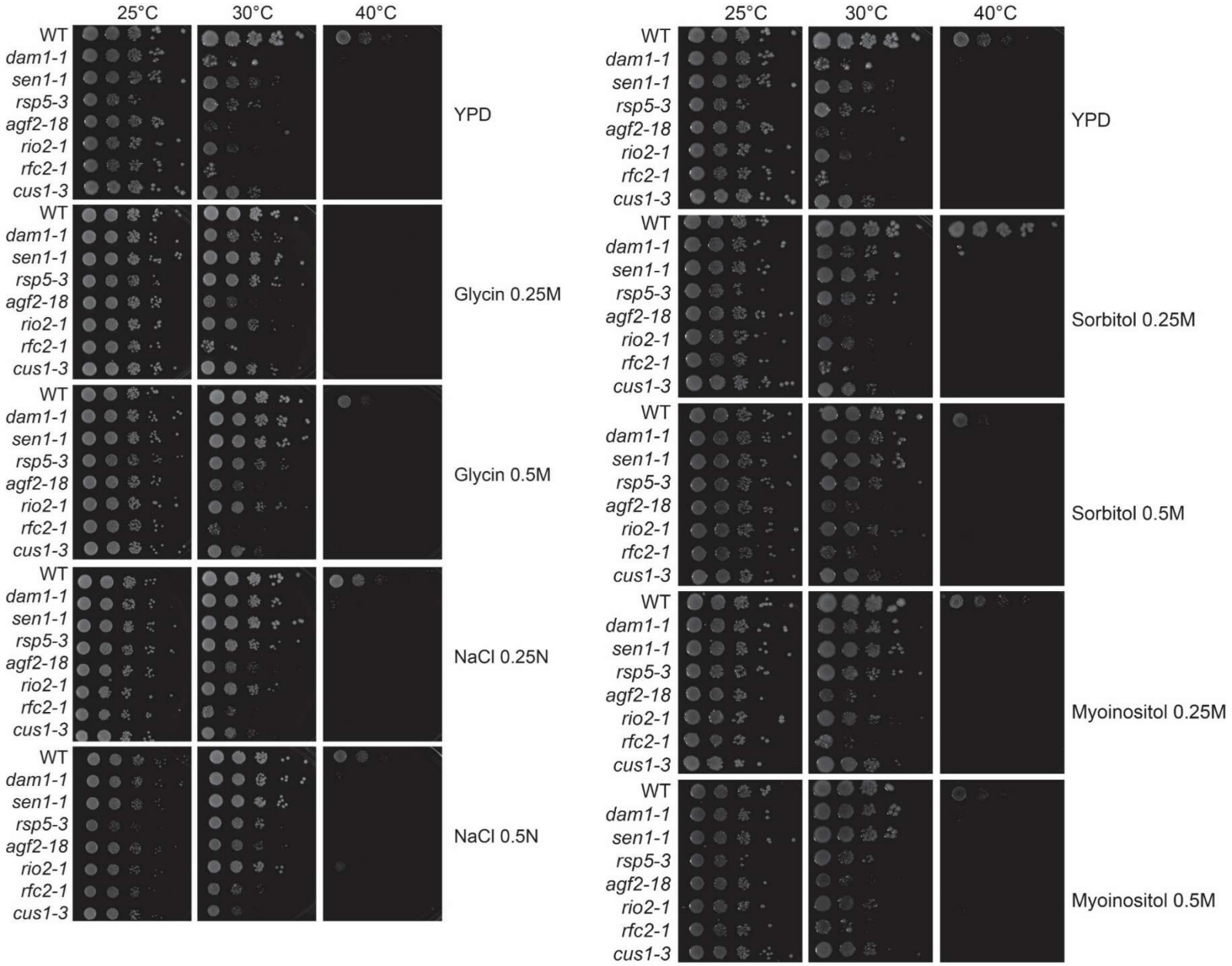
25°C
30°C
40°C
WT
dam1-1
sen1-1
rsp5-3
agf2-18
rio2-1
rfc2-1
cus1-3
YPD
Glycin 0.25M
Glycin 0.5M
NaCl 0.25N
NaCl 0.5N
Sorbitol 0.25M
Sorbitol 0.5M
Myoinositol 0.25M
Myoinositol 0.5M

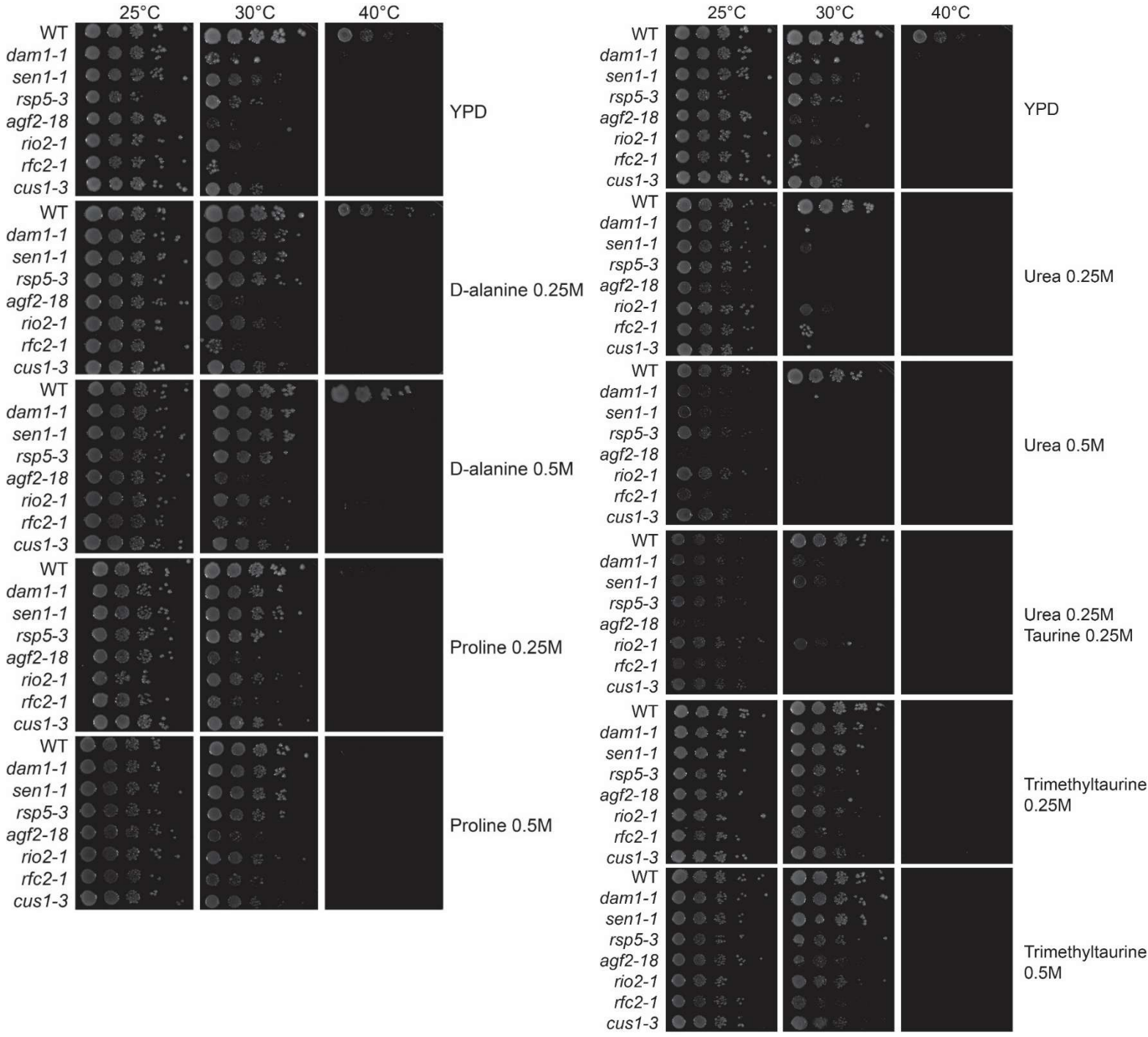

Appendix figure 10: Spotting assays with all the osmolytes tested. Osmolytes were dissolved in YPD and cells were cultured in the respective media. Images were acquired after 48h.

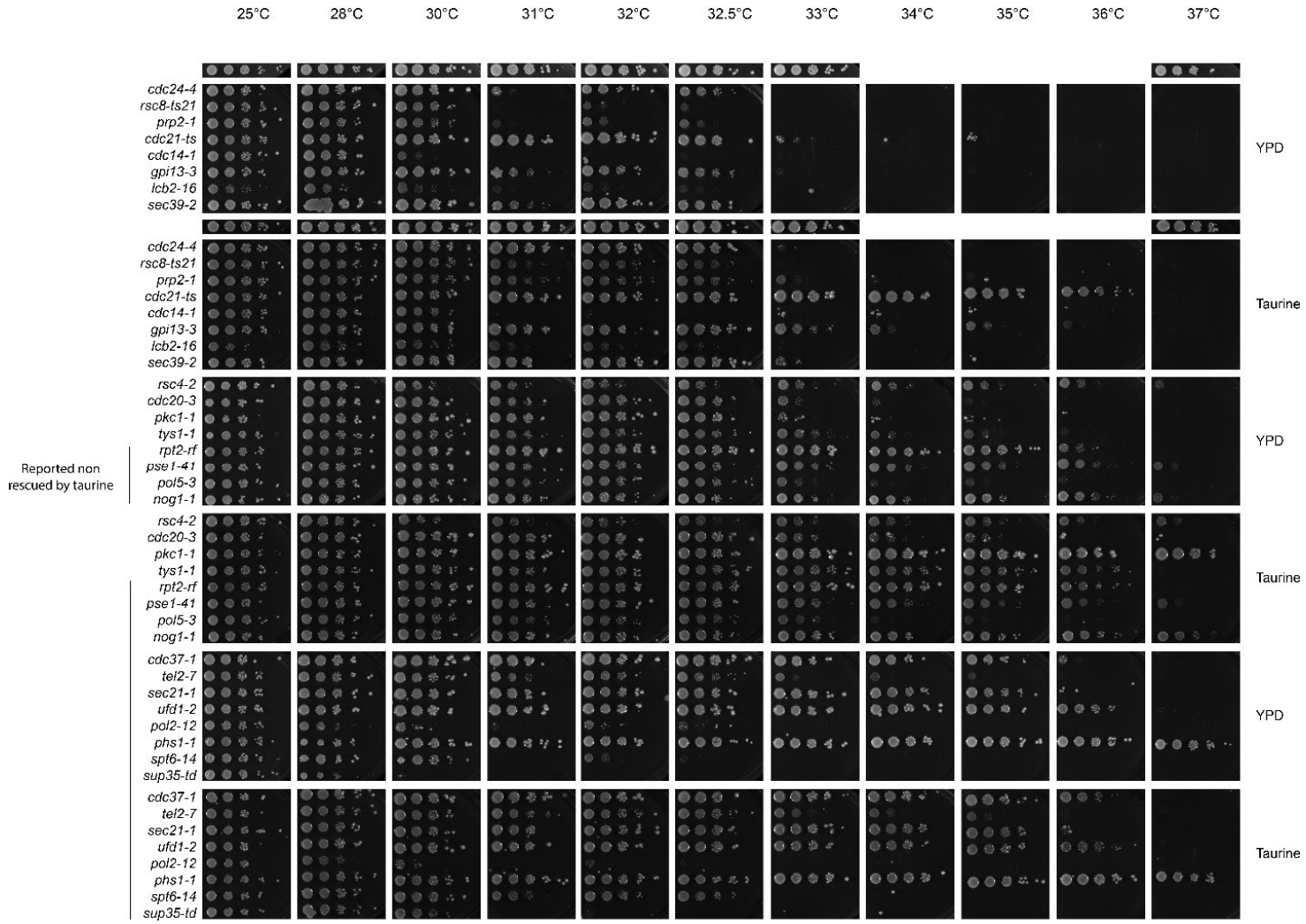

Appendix figure 11: Complete figure of the TS screening confirmations, including all intermediate temperatures. All cells were cultured on YPD, and images were taken after 48h.

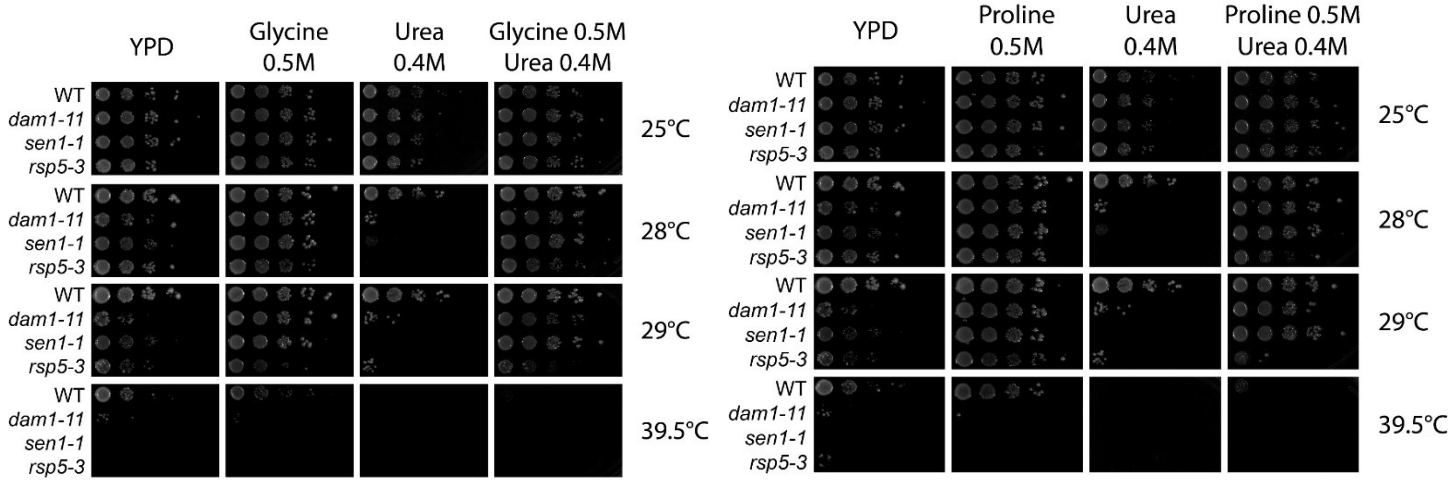

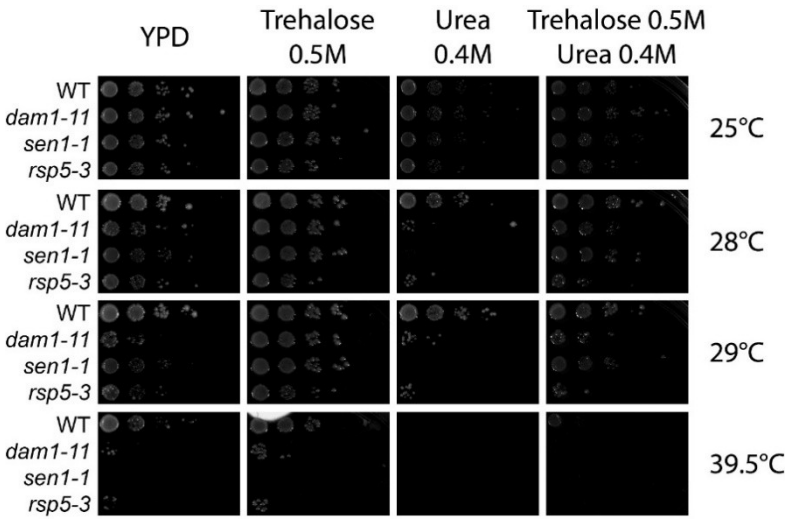

Appendix figure 12: Spotting assays with different osmolyte combinations with urea. The osmolytes (including urea) were diluted in the YPD and cells were cultured on the indicated plates and temperatures for 48h before image acquisition.

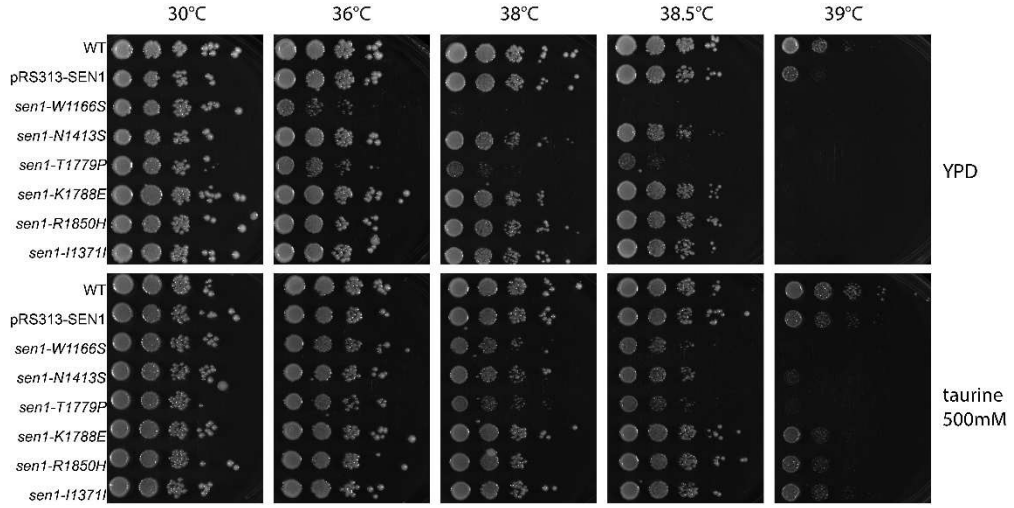

Appendix figure 13: SEN1 TS alleles are rescued by taurine in different temperatures. Cells were cultured in YPD and images were acquired after 72h.

References

1. Hayflick L, Moorhead PS. The serial cultivation of human diploid cell strains. *Exp Cell Res*. 1961;25(3):585-621. doi:10.1016/0014-4827(61)90192-6

2. Kumari R, Jat P. Mechanisms of Cellular Senescence: Cell Cycle Arrest and Senescence Associated Secretory Phenotype. *Front Cell Dev Biol*. 2021;9. doi:10.3389/fcell.2021.645593

3. Mylonas A, O'Loghlen A. Cellular Senescence and Ageing: Mechanisms and Interventions. *Front Aging*. 2022;3:866718. doi:10.3389/fragi.2022.866718

4. López-Otín C, Blasco MA, Partridge L, Serrano M, Kroemer G. Hallmarks of aging: An expanding universe. *Cell*. 2023;186(2):243-278. doi:10.1016/j.cell.2022.11.001

5. Yousefzadeh MJ, Zhu Y, McGowan SJ, et al. Fisetin is a senotherapeutic that extends health and lifespan. *eBioMedicine*. 2018;36:18-28. doi:10.1016/j.ebiom.2018.09.015

6. Huang W, Hickson LJ, Eirin A, Kirkland JL, Lerman LO. Cellular senescence: the good, the bad and the unknown. *Nat Rev Nephrol*. 2022;18(10):611-627. doi:10.1038/s41581-022-00601-z

7. Schosserer M, Grillari J, Breitenbach M. The Dual Role of Cellular Senescence in Developing Tumors and Their Response to Cancer Therapy. *Front Oncol*. 2017;7. doi:10.3389/fonc.2017.00278

8. Nakano Y, Johmura Y. Functional diversity of senescent cells in driving ageing phenotypes and facilitating tissue regeneration. *J Biochem (Tokyo)*. 2025;177(3):189-195. doi:10.1093/jb/mvae098

9. Eppard M, Passos JF, Victorelli S. Telomeres, cellular senescence, and aging: past and future. *Biogerontology*. 2024;25(2):329-339. doi:10.1007/s10522-023-10085-4

10. Krisko A, Kennedy BK. Chapter 8 - Yeast as a model organism for aging research. In: Musi N, Hornsby PJ, eds. *Handbook of the Biology of Aging (Ninth Edition)*. Handbooks of Aging. Academic Press; 2021:183-197. doi:10.1016/B978-0-12-815962-0.00008-1

11. Mavrogonatou E, Papadopoulou A, Pratsinis H, Kletsas D. Senescence-associated alterations in the extracellular matrix: deciphering their role in the regulation of cellular function. *Am J Physiol-Cell Physiol*. 2023;325(3):C633-C647. doi:10.1152/ajpcell.00178.2023

12. Claussin C, Chang M. The many facets of homologous recombination at telomeres. *Microb Cell*. 2015;2(9):308-321. doi:10.15698/mic2015.09.224

13. Shi T, Bunker RD, Mattarocci S, et al. Rif1 and Rif2 Shape Telomere Function and Architecture through Multivalent Rap1 Interactions. *Cell*. 2013;153(6):1340-1353. doi:10.1016/j.cell.2013.05.007

14. Balk B, Maicher A, Dees M, et al. Telomeric RNA-DNA hybrids affect telomere-length dynamics and senescence. *Nat Struct Mol Biol*. 2013;20(10):1199-1205. doi:10.1038/nsmb.2662

15. Graf M, Bonetti D, Lockhart A, et al. Telomere Length Determines TERRA and R-Loop Regulation through the Cell Cycle. *Cell*. 2017;170(1):72-85.e14. doi:10.1016/j.cell.2017.06.006

16. Wellinger RJ, Zakian VA. Everything You Ever Wanted to Know About Saccharomyces cerevisiae Telomeres: Beginning to End. *Genetics*. 2012;191(4):1073-1105. doi:10.1534/genetics.111.137851

17. Misino S, Busch A, Wagner CB, Bento F, Luke B. TERRA increases at short telomeres in yeast survivors and regulates survivor associated senescence (SAS). *Nucleic Acids Res*. 2022;50(22):12829-12843. doi:10.1093/nar/gkac1125

18. Lu M, Guo Q, Kallenbach NR. Thermodynamics of G-tetraplex formation by telomeric DNAs. *Biochemistry*. 1993;32(2):598-601. doi:10.1021/bi00053a027

19. Lu R, Pickett HA. Telomeric replication stress: the beginning and the end for alternative lengthening of telomeres cancers. *Open Biol*. 12(3):220011. doi:10.1098/rsob.220011

20. Lingner J, Cooper JP, Cech TR. Telomerase and DNA End Replication: No Longer a Lagging Strand Problem? *Science*. 1995;269(5230):1533-1534. doi:10.1126/science.7545310

21. Dionne I, Wellinger RJ. Processing of telomeric DNA ends requires the passage of a replication fork. *Nucleic Acids Res*. 1998;26(23):5365-5371. doi:10.1093/nar/26.23.5365

22. Gobbini E, Cassani C, Vertemara J, et al. The MRX complex regulates Exo1 resection activity by altering DNA end structure. *EMBO J*. 2018;37(16):e98588. doi:10.15252/embj.201798588

23. Mimitou EP, Symington LS. Sae2, Exo1 and Sgs1 collaborate in DNA double-strand break processing. *Nature*. 2008;455(7214):770-774. doi:10.1038/nature07312

24. Bertuch AA, Lundblad V. EXO1 contributes to telomere maintenance in both telomerase-proficient and telomerase-deficient Saccharomyces cerevisiae. *Genetics*. 2004;166(4):1651-1659. doi:10.1534/genetics.166.4.1651

25. Westmoreland JW, Mihalevic MJ, Bernstein KA, Resnick MA. The global role for Cdc13 and Yku70 in preventing telomere resection across the genome. *DNA Repair*. 2018;62:8-17. doi:10.1016/j.dnarep.2017.11.010

26. Bonetti D, Martina M, Clerici M, Lucchini G, Longhese MP. Multiple Pathways Regulate 3′ Overhang Generation at S. cerevisiae Telomeres. *Mol Cell*. 2009;35(1):70-81. doi:10.1016/j.molcel.2009.05.015

27. Tuzon CT, Wu Y, Chan A, Zakian VA. The Saccharomyces cerevisiae Telomerase Subunit Est3 Binds Telomeres in a Cell Cycle– and Est1–Dependent Manner and Interacts Directly with Est1 In Vitro. *PLOS Genet*. 2011;7(5):e1002060. doi:10.1371/journal.pgen.1002060

28. Blackburn H. An Alternative Pathway for Yeast Telomere Maintenance Rescues estl-Senescence.

29. Teng SC, Zakian VA. Telomere-telomere recombination is an efficient bypass pathway for telomere maintenance in Saccharomyces cerevisiae. *Mol Cell Biol*. 1999;19(12):8083-8093. doi:10.1128/MCB.19.12.8083

30. O'Sullivan RJ, Greenberg RA. Mechanisms of Alternative Lengthening of Telomeres. *Cold Spring Harb Perspect Biol*. 2025;17(1):a041690. doi:10.1101/cshperspect.a041690

31. Xu Z, Duc KD, Holcman D, Teixeira MT. The Length of the Shortest Telomere as the Major Determinant of the Onset of Replicative Senescence. *Genetics*. 2013;194(4):847-857. doi:10.1534/genetics.113.152322

32. Kupiec M. Biology of telomeres: lessons from budding yeast. *FEMS Microbiol Rev*. 2014;38(2):144-171. doi:10.1111/1574-6976.12054

33. Enomoto S, Glowczewski L, Berman J. *MEC3* , *MEC1,* and *DDC2* Are Essential Components of a Telomere Checkpoint Pathway Required for Cell Cycle Arrest during Senescence in *Saccharomyces cerevisiae*. Koshland D, ed. *Mol Biol Cell*. 2002;13(8):2626-2638. doi:10.1091/mbc.02-02-0012

34. Pardo B, Crabbé L, Pasero P. Signaling pathways of replication stress in yeast. *FEMS Yeast Res*. 2017;17(2):fow101. doi:10.1093/femsyr/fow101

35. Rufini A, Tucci P, Celardo I, Melino G. Senescence and aging: the critical roles of p53. *Oncogene*. 2013;32(43):5129-5143. doi:10.1038/onc.2012.640

36. Chang HY, Lawless C, Addinall SG, et al. Genome-wide analysis to identify pathways affecting telomere-initiated senescence in budding yeast. *G3 Bethesda Md*. 2011;1(3):197-208. doi:10.1534/g3.111.000216

37. Sinclair DA, Guarente L. Extrachromosomal rDNA Circles— A Cause of Aging in Yeast. *Cell*. 1997;91(7):1033-1042. doi:10.1016/S0092-8674(00)80493-6

38. Erjavec N, Larsson L, Grantham J, Nyström T. Accelerated aging and failure to segregate damaged proteins in Sir2 mutants can be suppressed by overproducing the protein aggregation-remodeling factor Hsp104p. *Genes Dev*. 2007;21(19):2410-2421. doi:10.1101/gad.439307

39. Yi DG, Hong S, Huh WK. Mitochondrial dysfunction reduces yeast replicative lifespan by elevating RAS-dependent ROS production by the ER-localized NADPH oxidase Yno1. *PLOS ONE*. 2018;13(6):e0198619. doi:10.1371/journal.pone.0198619

40. Jay KA, Smith DL, Blackburn EH. Early Loss of Telomerase Action in Yeast Creates a Dependence on the DNA Damage Response Adaptor Proteins. *Mol Cell Biol*. 2016;36(14):1908-1919. doi:10.1128/MCB.00943-15

41. Li Y, Daniel M, Tollefsbol TO. Epigenetic regulation of caloric restriction in aging. *BMC Med*. 2011;9(1):98. doi:10.1186/1741-7015-9-98

42. Kaeberlein M, Andalis AA, Fink GR, Guarente L. High osmolarity extends life span in Saccharomyces cerevisiae by a mechanism related to calorie restriction. *Mol Cell Biol*. 2002;22(22):8056-8066. doi:10.1128/MCB.22.22.8056-8066.2002

43. Singh P, Gollapalli K, Mangiola S, et al. Taurine deficiency as a driver of aging. *Science*. 2023;380(6649):eabn9257. doi:10.1126/science.abn9257

44. Fernandez ME, Bernier M, Price NL, et al. Is taurine an aging biomarker? *Science*. 2025;388(6751):eadl2116. doi:10.1126/science.adl2116

45. Miyazaki T, Ito T, Conrado AB, Murakami S. Regulation and Effect of Taurine on Metabolism.

46. Santulli G, Kansakar U, Varzideh F, Mone P, Jankauskas SS, Lombardi A. Functional Role of Taurine in Aging and Cardiovascular Health: An Updated Overview. *Nutrients*. 2023;15(19):4236. doi:10.3390/nu15194236

47. Jong CJ, Sandal P, Schaffer SW. The Role of Taurine in Mitochondria Health: More Than Just an Antioxidant. *Molecules*. 2021;26(16):4913. doi:10.3390/molecules26164913

48. Bhat MA, Ahmad K, Khan MSA, et al. Expedition into Taurine Biology: Structural Insights and Therapeutic Perspective of Taurine in Neurodegenerative Diseases. *Biomolecules*. 2020;10(6):6. doi:10.3390/biom10060863

49. Bianchi F, Klooster JS van't, Ruiz SJ, Poolman B. Regulation of Amino Acid Transport in Saccharomyces cerevisiae. *Microbiol Mol Biol Rev*. Published online October 16, 2019. doi:10.1128/mmbr.00024-19

50. Gaull GE. Taurine in Pediatric Nutrition: Review and Update. *Pediatrics*. 1989;83(3):433-442. doi:10.1542/peds.83.3.433

51. Thirupathi A, Pinho RA, Baker JS, István B, Gu Y. Taurine Reverses Oxidative Damages and Restores the Muscle Function in Overuse of Exercised Muscle. *Front Physiol*. 2020;11. doi:10.3389/fphys.2020.582449

52. Böhles H, Michalk D, Wagner-Thiessen E. Taurine Concentrations in Human Heart — A Retrospective Analysis. In: Huxtable RJ, Franconi F, Giotti A, eds. *The Biology of Taurine: Methods and Mechanisms*. Springer US; 1987:135-138. doi:10.1007/978-1-4899-0405-8_13

53. Wójcik OP, Koenig KL, Zeleniuch-Jacquotte A, Costa M, Chen Y. The potential protective effects of taurine on coronary heart disease. *Atherosclerosis*. 2010;208(1):19-25. doi:10.1016/j.atherosclerosis.2009.06.002

54. Toyoda A, Koike H, Nishihata K, Iio W, Goto T. Effects of Chronic Taurine Administration on Gene Expression, Protein Translation and Phosphorylation in the Rat Hippocampus. In: Marcinkiewicz J, Schaffer SW, eds. *Taurine 9*. Springer International Publishing; 2015:473-480. doi:10.1007/978-3-319-15126-7_37

55. Wang B, Wang Z, Yang Y, et al. Taurine Alleviates Pancreatic β-Cell Senescence by Inhibition of p53 Pathway. *J Diabetes*. 2025;17(6):e70100. doi:10.1111/1753-0407.70100

56. De Luca A, Pierno S, Camerino DC. Taurine: the appeal of a safe amino acid for skeletal muscle disorders. *J Transl Med*. 2015;13(1):243. doi:10.1186/s12967-015-0610-1

57. Cheong SH, Moon SH, Lee SJ, Kim SH, Chang KJ. Antioxidant and DNA Protection Effects of Taurine by Electron Spin Resonance Spectroscopy. In: El Idrissi A, L'Amoreaux WJ, eds. *Taurine 8*. Springer; 2013:167-177. doi:10.1007/978-1-4614-6093-0_17

58. Surai PF, Earle-Payne K, Kidd MT. Taurine as a Natural Antioxidant: From Direct Antioxidant Effects to Protective Action in Various Toxicological Models. *Antioxidants*. 2021;10(12):1876. doi:10.3390/antiox10121876

59. Aruoma OI, Halliwell B, Hoey BM, Butler J. The antioxidant action of taurine, hypotaurine and their metabolic precursors. *Biochem J*. 1988;256(1):251-255. doi:10.1042/bj2560251

60. Shimada K, Jong CJ, Takahashi K, Schaffer SW. Role of ROS Production and Turnover in the Antioxidant Activity of Taurine. In: Marcinkiewicz J, Schaffer SW, eds. *Taurine 9*. Springer International Publishing; 2015:581-596. doi:10.1007/978-3-319-15126-7_47

61. Surai PF, Earle-Payne K, Kidd MT. Taurine as a Natural Antioxidant: From Direct Antioxidant Effects to Protective Action in Various Toxicological Models. *Antioxidants*. 2021;10(12):12. doi:10.3390/antiox10121876

62. Adhish M, Manjubala I. Integrative in-silico and in-vitro analysis of taurine and vitamin B12 in modulating PPARγ and Wnt signaling in hyperhomocysteinemia-induced osteoporosis. *Biol Direct*. 2024;19(1):141. doi:10.1186/s13062-024-00581-z

63. Olson MT, Yergey AL, Mukherjee K, et al. Taurine Is Covalently Incorporated into Alpha-Tubulin. *J Proteome Res*. 2020;19(8):3184-3190. doi:10.1021/acs.jproteome.0c00147

64. Suzuki T, Suzuki T, Wada T, Saigo K, Watanabe K. Taurine as a constituent of mitochondrial tRNAs: new insights into the functions of taurine and human mitochondrial diseases. *EMBO J*. 2002;21(23):6581-6589. doi:10.1093/emboj/cdf656

65. Cuanalo-Contreras K, Schulz J, Mukherjee A, Park KW, Armijo E, Soto C. Extensive accumulation of misfolded protein aggregates during natural aging and senescence. *Front Aging Neurosci*. 2022;14:1090109. doi:10.3389/fnagi.2022.1090109

66. Chesney RW, Han X, Patters AB. Taurine and the renal system. *J Biomed Sci*. 2010;17(Suppl 1):S4. doi:10.1186/1423-0127-17-S1-S4

67. Hardy J, Selkoe DJ. The Amyloid Hypothesis of Alzheimer's Disease: Progress and Problems on the Road to Therapeutics. *Science*. 2002;297(5580):353-356. doi:10.1126/science.1072994

68. Toader C, Tataru CP, Munteanu O, et al. Decoding Neurodegeneration: A Review of Molecular Mechanisms and Therapeutic Advances in Alzheimer's, Parkinson's, and ALS. *Int J Mol Sci*. 2024;25(23):12613. doi:10.3390/ijms252312613

69. Soares TR, Reis SD, Pinho BR, Duchen MR, Oliveira JMA. Targeting the proteostasis network in Huntington's disease. *Ageing Res Rev*. 2019;49:92-103. doi:10.1016/j.arr.2018.11.006

70. Lee H, Hossain MK, Lee HY, et al. Taurine suppresses Aβ aggregation and attenuates Alzheimer's disease pathologies in 5XFAD mice and patient-derived cerebral organoids. *Biomed Pharmacother*. 2025;191:118527. doi:10.1016/j.biopha.2025.118527

71. Tadros MG, Khalifa AE, Abdel-Naim AB, Arafa HMM. Neuroprotective effect of taurine in 3-nitropropionic acid-induced experimental animal model of Huntington's disease phenotype. *Pharmacol Biochem Behav*. 2005;82(3):574-582. doi:10.1016/j.pbb.2005.10.018

72. Spink CH, Garbett N, Chaires JB. Enthalpies of DNA melting in the presence of osmolytes. *Biophys Chem*. 2007;126(1):176-185. doi:10.1016/j.bpc.2006.07.013

73. Yancey PH, Blake WR, Conley J. Unusual organic osmolytes in deep-sea animals: adaptations to hydrostatic pressure and other perturbants. *Comp Biochem Physiol A Mol Integr Physiol*. 2002;133(3):667-676. doi:10.1016/s1095-6433(02)00182-4

74. Yancey PH. Organic osmolytes as compatible, metabolic and counteracting cytoprotectants in high osmolarity and other stresses. *J Exp Biol*. 2005;208(15):2819-2830. doi:10.1242/jeb.01730

75. Burg MB, Ferraris JD. Intracellular Organic Osmolytes: Function and Regulation *. *J Biol Chem*. 2008;283(12):7309-7313. doi:10.1074/jbc.R700042200

76. Hohmann S. Osmotic Stress Signaling and Osmoadaptation in Yeasts. *Microbiol Mol Biol Rev*. 2002;66(2):300-372. doi:10.1128/MMBR.66.2.300-372.2002

77. Diamant S, Eliahu N, Rosenthal D, Goloubinoff P. Chemical Chaperones Regulate Molecular Chaperones in Vitro and in Cells under Combined Salt and Heat Stresses. *J Biol Chem*. 2001;276(43):39586-39591. doi:10.1074/jbc.M103081200

78. Wu H, Jin Y, Wei J, Jin H, Sha D, Wu JY. Mode of action of taurine as a neuroprotector. *Brain Res*. 2005;1038(2):123-131. doi:10.1016/j.brainres.2005.01.058

79. Duveau F, Cordier C, Chiron L, et al. Yeast cell responses and survival during periodic osmotic stress are controlled by glucose availability. *eLife*. 12:RP88750. doi:10.7554/eLife.88750

80. Kuczyńska-Wiśnik D, Stojowska-Swędrzyńska K, Laskowska E. Intracellular Protective Functions and Therapeutical Potential of Trehalose. *Molecules*. 2024;29(9):2088. doi:10.3390/molecules29092088

81. Timasheff SN. Protein-solvent preferential interactions, protein hydration, and the modulation of biochemical reactions by solvent components. *Proc Natl Acad Sci*. 2002;99(15):9721-9726. doi:10.1073/pnas.122225399

82. Auton M, Bolen DW. Additive Transfer Free Energies of the Peptide Backbone Unit That Are Independent of the Model Compound and the Choice of Concentration Scale. *Biochemistry*. 2004;43(5):1329-1342. doi:10.1021/bi035908r

83. Street TO, Bolen DW, Rose GD. A molecular mechanism for osmolyte-induced protein stability. *Proc Natl Acad Sci*. 2006;103(38):13997-14002. doi:10.1073/pnas.0606236103

84. Bolen DW, Rose GD. Structure and energetics of the hydrogen-bonded backbone in protein folding. *Annu Rev Biochem*. 2008;77:339-362. doi:10.1146/annurev.biochem.77.061306.131357

85. Panuszko A, Bruździak P, Kaczkowska E, Stangret J. General Mechanism of Osmolytes' Influence on Protein Stability Irrespective of the Type of Osmolyte Cosolvent. *J Phys Chem B*. 2016;120(43):11159-11169. doi:10.1021/acs.jpcb.6b10119

86. Bruździak P, Panuszko A, Kaczkowska E, et al. Taurine as a water structure breaker and protein stabilizer. *Amino Acids*. 2018;50(1):125-140. doi:10.1007/s00726-017-2499-x

87. Liu J, Wang L, Wang Z, Liu JP. Roles of Telomere Biology in Cell Senescence, Replicative and Chronological Ageing. *Cells*. 2019;8(1):54. doi:10.3390/cells8010054

88. Holstein EM, Clark KRM, Lydall D. Interplay between Nonsense-Mediated mRNA Decay and DNA Damage Response Pathways Reveals that Stn1 and Ten1 Are the Key CST Telomere-Cap Components. *Cell Rep*. 2014;7(4):1259-1269. doi:10.1016/j.celrep.2014.04.017

89. Lundin C, North M, Erixon K, et al. Methyl methanesulfonate (MMS) produces heat-labile DNA damage but no detectable in vivo DNA double-strand breaks. *Nucleic Acids Res*. 2005;33(12):3799-3811. doi:10.1093/nar/gki681

90. Ovejero S, Soulet C, Moriel-Carretero M. The Alkylating Agent Methyl Methanesulfonate Triggers Lipid Alterations at the Inner Nuclear Membrane That Are Independent from Its DNA-Damaging Ability. *Int J Mol Sci*. 2021;22(14):14. doi:10.3390/ijms22147461

91. Chankova SG, Dimova E, Dimitrova M, Bryant PE. Induction of DNA double-strand breaks by zeocin in Chlamydomonas reinhardtii and the role of increased DNA double-strand breaks rejoining in the formation of an adaptive response. *Radiat Environ Biophys*. 2007;46(4):409-416. doi:10.1007/s00411-007-0123-2

92. Singh A, Xu YJ. The Cell Killing Mechanisms of Hydroxyurea. *Genes*. 2016;7(11):11. doi:10.3390/genes7110099

93. R: The R Project for Statistical Computing. Accessed December 15, 2025. https://www.r-project.org/

94. Wagih O, Parts L. gitter: A Robust and Accurate Method for Quantification of Colony Sizes From Plate Images. *G3 GenesGenomesGenetics*. 2014;4(3):547-552. doi:10.1534/g3.113.009431

95. Kemmeren P, Sameith K, van de Pasch LAL, et al. Large-scale genetic perturbations reveal regulatory networks and an abundance of gene-specific repressors. *Cell*. 2014;157(3):740-752. doi:10.1016/j.cell.2014.02.054

96. van Wageningen S, Kemmeren P, Lijnzaad P, et al. Functional Overlap and Regulatory Links Shape Genetic Interactions between Signaling Pathways. *Cell*. 2010;143(6):991-1004. doi:10.1016/j.cell.2010.11.021

97. Addinall SG, Downey M, Yu M, et al. A Genomewide Suppressor and Enhancer Analysis of cdc13-1 Reveals Varied Cellular Processes Influencing Telomere Capping in Saccharomyces cerevisiae. *Genetics*. 2008;180(4):2251. doi:10.1534/genetics.108.092577

98. Zubko MK, Guillard S, Lydall D. Exo1 and Rad24 Differentially Regulate Generation of ssDNA at Telomeres of Saccharomyces cerevisiae cdc13-1 Mutants. *Genetics*. 2004;168(1):103-115. doi:10.1534/genetics.104.027904

99. Addinall SG, Downey M, Yu M, et al. A Genomewide Suppressor and Enhancer Analysis of cdc13-1 Reveals Varied Cellular Processes Influencing Telomere Capping in Saccharomyces cerevisiae. *Genetics*. 2008;180(4):2251-2266. doi:10.1534/genetics.108.092577

100. Klermund J, Bender K, Luke B. High Nutrient Levels and TORC1 Activity Reduce Cell Viability following Prolonged Telomere Dysfunction and Cell Cycle Arrest. *Cell Rep*. 2014;9(1):324-335. doi:10.1016/j.celrep.2014.08.053

101. Vydzhak O, Bender K, Klermund J, Busch A, Reimann S, Luke B. Checkpoint adaptation in repair-deficient cells drives aneuploidy and resistance to genotoxic agents. *bioRxiv*. Preprint posted online July 30, 2019:464685. doi:10.1101/464685

102. Pif1- and Exo1-dependent nucleases coordinate checkpoint activation following telomere uncapping. doi:10.1038/emboj.2010.267

103. Langston RE, Palazzola D, Bonnell E, Wellinger RJ, Weinert T. Loss of Cdc13 causes genome instability by a deficiency in replication-dependent telomere capping. *PLoS Genet*. 2020;16(4):e1008733. doi:10.1371/journal.pgen.1008733

104. Yao Y, Fekete-Szücs E, Rosas Bringas FR, Chang M. Deletion of MEC1 suppresses the replicative senescence of the cdc13-2 mutant in Saccharomyces cerevisiae. *G3 GenesGenomesGenetics*. 2023;13(5):jkad065. doi:10.1093/g3journal/jkad065

105. Yu H. Cdc20: A WD40 Activator for a Cell Cycle Degradation Machine. *Mol Cell*. 2007;27(1):3-16. doi:10.1016/j.molcel.2007.06.009

106. Vannini M, Mingione VR, Meyer A, Sniffen C, Whalen J, Seshan A. A Novel Hyperactive Nud1 Mitotic Exit Network Scaffold Causes Spindle Position Checkpoint Bypass in Budding Yeast. *Cells*. 2021;11(1):46. doi:10.3390/cells11010046

107. Reed SI. Ratchets and clocks: the cell cycle, ubiquitylation and protein turnover. *Nat Rev Mol Cell Biol*. 2003;4(11):855-864. doi:10.1038/nrm1246

108. Gaglione R, Caradonna J, MacQueen AJ, Luk E, Hollingsworth NM. The conserved SEN1 DNA:RNA helicase has multiple functions during yeast meiosis. *bioRxiv*. Preprint posted online April 12, 2025:2025.04.10.648140. doi:10.1101/2025.04.10.648140

109. Bento F, Longaretti M, Pires VB, Lockhart A, Luke B. RNase H1 and Sen1 ensure that transient TERRA R-loops promote the repair of short telomeres. *EMBO Rep*. Published online May 22, 2025:1-13. doi:10.1038/s44319-025-00469-7

110. Qi H, Chen Y, Fu X, Lin CP, Zheng XFS, Liu LF. TOR Regulates Cell Death Induced by Telomere Dysfunction in Budding Yeast. *PLoS ONE*. 2008;3(10):e3520. doi:10.1371/journal.pone.0003520

111. Quantifying why urea is a protein denaturant, whereas glycine betaine is a protein stabilizer. *Proc Natl Acad Sci U S A*. 2011;108(41):16932-16937. doi:10.1073/PNAS.1109372108

112. Atkins PW, Paula JD, Keeler J. *Atkins' Physical Chemistry*. Oxford University Press; 2018.

113. BARNHURST JD. Dipolar Ions Related to Taurine. *J Org Chem*. 1961;26(11):4520-4522. doi:10.1021/jo01069a077

114. Yang AS, Honig B. On the pH Dependence of Protein Stability. *J Mol Biol*. 1993;231(2):459-474. doi:10.1006/jmbi.1993.1294

115. Yin M, Palmer HR, Fyfe-Johnson AL, Bedford JJ, Smith RAJ, Yancey PH. Hypotaurine, N-Methyltaurine, Taurine, and Glycine Betaine as Dominant Osmolytes of Vestimentiferan Tubeworms from Hydrothermal Vents and Cold Seeps. *Physiol Biochem Zool*. Published online September 2000. doi:10.1086/317749

116. Khosrow-Khavar F, Fang NN, Ng AHM, Winget JM, Comyn SA, Mayor T. The Yeast Ubr1 Ubiquitin Ligase Participates in a Prominent Pathway That Targets Cytosolic Thermosensitive Mutants for Degradation. *G3 GenesGenomesGenetics*. 2012;2(5):619-628. doi:10.1534/g3.111.001933

117. Tomala K, Zrebiec P, Hartl DL. Limits to Compensatory Mutations: Insights from Temperature-Sensitive Alleles. *Mol Biol Evol*. 2019;36(9):1874-1883. doi:10.1093/molbev/msz110

118. Jo M, Lee S, Jeon YM, Kim S, Kwon Y, Kim HJ. The role of TDP-43 propagation in neurodegenerative diseases: integrating insights from clinical and experimental studies. *Exp Mol Med*. 2020;52(10):1652-1662. doi:10.1038/s12276-020-00513-7

119. Tseng YL, Lu PC, Lee CC, et al. Degradation of neurodegenerative disease-associated TDP-43 aggregates and oligomers via a proteolysis-targeting chimera. *J Biomed Sci*. 2023;30(1):27. doi:10.1186/s12929-023-00921-7

120. Tsui A, Kouznetsova VL, Kesari S, Fiala M, Tsigelny IF. Role of Senataxin in Amyotrophic Lateral Sclerosis. *J Mol Neurosci*. 2023;73(11):996-1009. doi:10.1007/s12031-023-02169-0

121. Chen X, Müller U, Sundling KE, Brow DA. Saccharomyces cerevisiae Sen1 as a Model for the Study of Mutations in Human Senataxin That Elicit Cerebellar Ataxia. *Genetics*. 2014;198(2):577-590. doi:10.1534/genetics.114.167585

122. Monje-Casas F, Queralt E, eds. *The Mitotic Exit Network: Methods and Protocols*. Vol 1505. Springer New York; 2017. doi:10.1007/978-1-4939-6502-1

123. Matellán L, Monje-Casas F. Regulation of Mitotic Exit by Cell Cycle Checkpoints: Lessons From Saccharomyces cerevisiae. *Genes*. 2020;11(2):195. doi:10.3390/genes11020195

124. Higuchi-Sanabria R, Pernice WMA, Vevea JD, Alessi Wolken DM, Boldogh IR, Pon LA. Role of asymmetric cell division in lifespan control in Saccharomyces cerevisiae. *FEMS Yeast Res*. 2014;14(8):1133-1146. doi:10.1111/1567-1364.12216

125. Restall IJ, Parolin DAE, Daneshmand M, et al. PKCι depletion initiates mitotic slippage-induced senescence in glioblastoma. *Cell Cycle*. 2015;14(18):2938-2948. doi:10.1080/15384101.2015.1071744

126. Clemente-Blanco A, Sen N, Mayan-Santos M, et al. Cdc14 phosphatase promotes segregation of telomeres through repression of RNA polymerase II transcription. *Nat Cell Biol*. 2011;13(12):1450-1456. doi:10.1038/ncb2365

127. Crane MM, Russell AE, Schafer BJ, et al. DNA damage checkpoint activation impairs chromatin homeostasis and promotes mitotic catastrophe during aging. Tyler JK, Hao N, eds. *eLife*. 2019;8:e50778. doi:10.7554/eLife.50778

128. Budd ME, Campbell JL. Dna2 is involved in CA strand resection and nascent lagging strand completion at native yeast telomeres. *J Biol Chem*. 2013;288(41):29414-29429. doi:10.1074/jbc.M113.472456

129. Campos A, Ramos F, Iglesias L, et al. Cdc14 phosphatase counteracts Cdk-dependent Dna2 phosphorylation to inhibit resection during recombinational DNA repair. *Nat Commun*. 2023;14(1):2738. doi:10.1038/s41467-023-38417-5

130. Zhou J, Du X, Li J, Yamagata N, Xu B. Taurine Boosts Cellular Uptake of Small d-Peptides for Enzyme-Instructed Intracellular Molecular Self-Assembly. *J Am Chem Soc*. 2015;137(32):10040-10043. doi:10.1021/jacs.5b06181

131. Leuenberger P, Ganscha S, Kahraman A, et al. Cell-wide analysis of protein thermal unfolding reveals determinants of thermostability. *Science*. 2017;355(6327):eaai7825. doi:10.1126/science.aai7825

132. Hassell DS, Steingesser MG, Denney AS, Johnson CR, McMurray MA. Chemical rescue of mutant proteins in living *Saccharomyces cerevisiae* cells by naturally occurring small molecules. Andrews B, ed. *G3 GenesGenomesGenetics*. 2021;11(9):jkab252. doi:10.1093/g3journal/jkab252

133. Dobson CM. Principles of protein folding, misfolding and aggregation. *Semin Cell Dev Biol*. 2004;15(1):3-16. doi:10.1016/j.semcdb.2003.12.008

134. Raghunathan S. Solvent accessible surface area-assessed molecular basis of osmolyte-induced protein stability. *RSC Adv*. 2024;14(34):25031-25041. doi:10.1039/D4RA02576H

135. Fogel BL, Cho E, Wahnich A, et al. Mutation of senataxin alters disease-specific transcriptional networks in patients with ataxia with oculomotor apraxia type 2. *Hum Mol Genet*. 2014;23(18):4758-4769. doi:10.1093/hmg/ddu190

136. Bennett CL, La Spada AR. Senataxin, A Novel Helicase at the Interface of RNA Transcriptome Regulation and Neurobiology: From Normal Function to Pathological Roles in Motor Neuron Disease and Cerebellar Degeneration. *Adv Neurobiol*. 2018;20:265-281. doi:10.1007/978-3-319-89689-2_10

137. Sweeney P, Park H, Baumann M, et al. Protein misfolding in neurodegenerative diseases: implications and strategies. *Transl Neurodegener*. 2017;6:6. doi:10.1186/s40035-017-0077-5

138. Koszła O, Sołek P. Misfolding and aggregation in neurodegenerative diseases: protein quality control machinery as potential therapeutic clearance pathways. *Cell Commun Signal CCS*. 2024;22(1):421. doi:10.1186/s12964-024-01791-8